



This is a repository copy of *A singular vorticity wave packet within a rapidly rotating vortex : spiralling versus oscillating motions.*

White Rose Research Online URL for this paper:
<https://eprints.whiterose.ac.uk/180588/>

Version: Accepted Version

Article:

Caillol, P. (2019) A singular vorticity wave packet within a rapidly rotating vortex : spiralling versus oscillating motions. *Journal of Fluid Mechanics*, 873. pp. 688-741. ISSN 0022-1120

<https://doi.org/10.1017/jfm.2019.374>

This article has been published in a revised form in *Journal of Fluid Mechanics*
<https://doi.org/10.1017/jfm.2019.374>. © Cambridge University Press. Article available under the terms of the CC-BY-NC-ND license (<https://creativecommons.org/licenses/by-nc-nd/4.0/>).

Reuse

This article is distributed under the terms of the Creative Commons Attribution-NonCommercial-NoDerivs (CC BY-NC-ND) licence. This licence only allows you to download this work and share it with others as long as you credit the authors, but you can't change the article in any way or use it commercially. More information and the full terms of the licence here: <https://creativecommons.org/licenses/>

Takedown

If you consider content in White Rose Research Online to be in breach of UK law, please notify us by emailing eprints@whiterose.ac.uk including the URL of the record and the reason for the withdrawal request.



eprints@whiterose.ac.uk
<https://eprints.whiterose.ac.uk/>

A singular vorticity wave packet within a rapidly rotating vortex: spiraling vs oscillating motions

Philippe Caillol¹†

¹Department of Fundamental Sciences, University of Bío-Bío, Chillán, Chile

(Received xx; revised xx; accepted xx)

This paper considers a free vorticity wave packet propagating within a rapidly rotating vortex in the quasi-steady régime, a long time after the wave packet strongly and unsteadily interacted with the vortex. We study a singular, nonlinear, helical and asymmetric shear mode inside a linearly stable, columnar and axisymmetric vortex on the f -plane. The amplitude modulated mode enters resonance with the vortex at a certain radius r_c , where the phase angular speed is equal to the rotation frequency. The singularity in the modal equation at r_c strongly modifies the flow in the 3D helical critical layer, the region around r_c where the wave/vortex interaction occurs. This interaction generates a vertically sheared 3D mean flow of higher amplitude than the wave packet. The chosen envelope régime assumes the formation of a mean radial velocity of the same order as the wave packet amplitude, leading to that the streamlines experience a spiral motion in the neighborhood of the critical layer. Radar images frequently show such spiral bands in tropical cyclones or tornadoes. Through matched asymptotic expansions, we find an analytical solution of the leading-order equations inside the critical layer. The generalized Batchelor integral condition applied to the quasi-steady 3D motion inside the separatrices yields a leading-order non-uniform 3D vorticity. The critical layer pattern, strongly deformed by the mean radial velocity, loses its symmetries with respect to the azimuthal and radial directions, which makes the leading-order mean radial wave fluxes non zero. Finally, a stronger wave/vortex interaction occurs with respect to the previous studies where a steady neutral vortical mode or a larger-extent envelope was involved.

1. Introduction

Large-scale intense vortices are impressive and devastating coherent structures. They intrigue researchers because they have not yet revealed their secrets regarding their formation and evolution. The presence of asymmetric disturbances inside such vortices is a possible intensification mechanism driven by the differential rotation. A set of spiral rainbands for instance, is frequently observed in most of the tropical cyclones. The evolutions of the eyewall and rainbands as well as their mutual interactions are believed to play an important role in the vortex dynamics and its intensification (Houze *et al.* (2006)). According to wave analysis, spiral bands could be partly explained by vorticity wave dynamics (Guinn & Schubert (1993); Reasor *et al.* (2000); Wang (2002*b*); Chen *et al.* (2003); Corbosiero *et al.* (2006); Judt & Chen (2010)).

In geophysical vortices, potential vorticity (PV) wave packets are emitted by PV anomalies generated for instance, by latent heat release. These waves are stretched by the radial rotational-wind shear into spiral bands and have been recently coined

† Email address for correspondence: pcaillol@ubiobio.cl

vortex Rossby waves (Montgomery & Kallenbach (1997); Chen & Yau (2001)). These inwardly spiraling structures are localized areas of deep clouds in the lower and middle atmosphere, providing heavy rains, strong winds and thunderstorms. Like eyewalls, they are associated with local maxima of absolute vorticity, potential vorticity, convection, upward and sometimes rotational winds, encountered in the vortex. Some rainbands are likely to evolve into a secondary eyewall (Qiu *et al.* (2010); Didlake *et al.* (2018)); conversely, an eyewall can generate spiral bands (Corbosiero *et al.* (2006)).

Wave activity analysis in numerical hurricane-like vortex models shows that vortices only interact with vorticity waves and that the related modes are continuous (Chen *et al.* (2003)). Basic-state vortex radial shear increases their radial wavenumbers, which slows down wave packet radial propagation. The latter ceases at the stagnation radius where the radial group velocity vanishes. In the WKB approximation, this radius coincides with the phase-velocity critical radius where the phase angular speed is equal to the basic-vortex rotation frequency (Montgomery & Kallenbach 1997; Gao & Zhu 2016). These waves are thus confined to the near-vortex region and cannot propagate to infinity. They locally exchange kinetic energy and angular momentum with the vortex around the stagnation radius. They can nevertheless transport energy out of the vortex core whereas wave momentum fluxes can cause an inward transport of angular momentum, intensifying the basic vortex (Montgomery & Enagonio 1998; Corbosiero *et al.* 2006; Houze *et al.* 2006).

This article focuses on the nonlinear dynamics of continuous vorticity modes embedded in rapidly rotating vortices. Continuous modes are singular and neutral modes related to resonating and propagating waves. The paper wishes to make progress in the understanding of such waves in relation to vortex intensification. In particular, we wish to study the wave packet/vortex interaction and the subsequent breaking through the nonlinear critical layer (CL) theory. The vortical mode singularity is removed by introducing nonlinearity in the CL motion equations, which is relevant to large Reynolds number large-scale atmospheric motions. This theory also sounds relevant for tropical cyclone or tornado intensification, firstly because the nonlinear CL development time scale is faster than the intensification duration. Secondly, this weakly nonlinear approach may give the right order of intensification magnitude; it indeed yields a higher intensification than the traditional non-resonant interaction quadratic order obtained in the numerical simulations that do not resolve the critical layer (Montgomery & Kallenbach 1997; Qiu *et al.* 2010; Caillol 2015). When an asymmetric neutral mode is superimposed onto the basic vortex, provided resonance occurs, a first linear stage starts characterized by the CL formation and the beginning of the wave/mean-flow interaction (WMFI). Then, the nonlinear critical layer settles down in a transition stage where the WMFI continues in an unsteady but decelerated way. We assume the existence of a quasi-steady state when the wave packet has become weakly singular; it keeps on interacting with the vortex but in a more slowly way so that perturbation theory may be handled. The emergence of a final quasi-steady state is related to the smoothness of the radial eigenfunction. The weakly singular mode radial structure is indeed sufficiently smooth to enable it to resist shear and store part of the basic-vortex angular momentum and subsequently to weaken the vortex in this asymptotic stage (Nolan & Farrell 1999).

Caillol (2017) described a slowly space-time evolving asymmetric, singular, helical and vorticity mode in a circular vortex with the same CL theory. This previous paper will be referred to as C17. This amplitude modulated wave modeled a wave train whose envelope had a $O(\epsilon^{-1})$ vertical extent for a dimensionless wave amplitude ϵ . He derived the system of evolution equations governing the wave packet amplitude and the wave/vortex interaction induced mean flow a long time after the interaction started. He observed that the wave packet always broke and noticed that considering a wave packet

instead of a single steady mode enhanced the wave/vortex interaction. The vortex was however weakening in the long time asymptotic stage. We here consider a more compact wave packet. The vertical envelope wavenumber is of order $O(\epsilon^{1/2})$, and we expect to obtain a faster and stronger interaction in the quasi-steady stage. This regime usually corresponds to a balance between nonlinear effects and dispersion characterized by a coherent-structure (Leibovich 1970; Kivshar & Malomed 1989; Derzho & Grimshaw 2002; Shagalov *et al.* 2009).

In a cylindrical geometry, the modulated amplitude slowly evolves over height and time. Through the critical layer coupling, we assume the same space-time scales for the CL induced mean flow around r_c . This mean flow cannot be neglected because it is of higher amplitude than the wave packet. Owing to the divergenceless-flow condition, the presence of a mean radial velocity is necessary, which makes the flow asymmetric and even more distorted in the CL neighborhood than in the steady-state assumption. The stagnation line is not here axisymmetric any longer but is given by a spiral located near r_c that slowly varies in height and time in the same way as the wave modulation. To perform the analysis, we use a stressed radius-like coordinate which uniquely parameterizes each streamline (Davis 1969; Caillol & Grimshaw 2004). This variable takes into account the deformed motion that streamlines experience in the CL neighborhood. Streamlines deviate from the critical radius with a spiraling departure proportional to the mean radial velocity. As a result, a secular azimuthal variable naturally arises to describe this spiraling motion. Secularity is required to deal with the CL induced varying mean flow that thus evolves over the rotational direction as well. The preceding wave packet study in C17 involved a secular time scale, which did not have a true physical sense. In the present study, we argue that the existence of a 3D mean flow coupled with the wave packet strongly affects the nonlinear wave dynamics. In the past quasi-steady 3D critical-layer analytical studies, the induced mean flow was not however taken into account (Voronovich *et al.* 1998*a,b*).

We assume that the critical layer forms in the outer vortex core where the mean absolute axial vorticity is smaller than the absolute inertial frequency of the circular vortex, which is relevant to large-scale rapidly rotating vortices (Caillol 2015). An azimuthal-wavenumber m weakly singular vortical mode generates a CL pattern characterized by m intersecting helical cylinders winding and spiraling along the vortex axis. These cylinders are three-dimensional separatrices which bound two qualitatively distinct CL flows: the flow outside them spans a 2π azimuthal range whereas the flow inside them spans a $2\pi/m$ range (cf. figures 1-3). At each vortex height, a “cat’s-eye” pattern thus appears within these cylindrical cavities exhibiting a recirculating flow.

The extended 3D Prandtl-Batchelor theorem predicts in the steady-state assumption a leading-order uniform axial vorticity inside the separatrices (Caillol 2014); this result is no longer valid here. A Galerkin method is required to integrate the motion equations within the cat’s eye. A unique inviscid CL solution is found out at the non-trivial expansion order by firstly, applying secularity conditions on both inviscid and viscous inner flows, secondly matching both outer and inner flows on the CL edges, then matching the inner flow on the separatrices (cf. figure 2). The second part of the study will be presented in a separate paper. We will derive the system of the leading-order nonlinear PDEs that governs the slowly evolving amplitudes of the wave packet and CL induced mean flow. The numerical system resolution will bring about a lot of information on the wave packet + vortex evolution in the quasi-steady stage.

The paper is hence organized as follows. Section 2 displays the general outer-flow perturbation and phase-averaged equations. Section 3 gives the low-order outer flow asymptotic solutions through Frobenius series. Section 4 formulates the CL motion and

gives the two first inner-flow orders. Section 5 examines the low-order CL induced mean flow. Section 6 describes the first non-trivial inner-flow order strongly altered by the presence of the leading-order mean radial velocity. Section 7 presents the CL numerical results. At last, Section 8 offers the conclusion.

2. Formulation and main assumptions

We consider the motion of an unbounded, axisymmetric, columnar and linearly stable vortex on the f -plane in a slightly viscous, incompressible and dry atmosphere. We use the cylindrical coordinates (r, θ, z) , the variable z being related to the height of the vortex along its rotation axis, (u, v, w) being the velocity vector in these coordinates. Quantities have been made dimensionless through characteristic velocity and length scales: the maximum rotational wind of the vortex V_{mw} and the maximum wind radius R_{mw} . The related Reynolds number is $Re = V_{mw}R_{mw}/\nu$, where ν is the kinematic viscosity. The inertial force \mathbf{f}_i due to the rotating framework is $\mathbf{f}_i = v/r(v\mathbf{e}_r - u\mathbf{e}_\theta)$. The geopotential (Earth's rotation driven centrifugal force and gravity) with pressure p is inserted into the gradient force to form the variable Γ defined by $\Gamma = p + gz - Co^2/8r^2$ and erroneously called geopotential. A constant value of the Coriolis parameter $Co = (fR_{mw})/V_{mw}$ is used throughout the study. The dimensionless equations governing this motion are the momentum and mass conservation equations in the ground-based frame of reference

$$\partial_t \mathbf{u} + \mathbf{u} \cdot \nabla \mathbf{u} + Co \mathbf{z} \times \mathbf{u} = \mathbf{f}_i - \nabla \Gamma + \frac{1}{Re} \Delta \mathbf{u} + \mathbf{F}, \quad (2.1)$$

$$D^* u + \frac{1}{r} \partial_\theta v + \partial_z w = 0, \quad D^* \bullet = \partial_r \bullet + \frac{1}{r} \bullet \cdot$$

The velocities and geopotential are decomposed between the wave phase averaged flow and the asymmetric perturbations under the following form

$$\begin{aligned} u &= \bar{U}(r, \Theta, \Phi) + \epsilon U_r(\xi, r, \Theta, \Phi), & v &= \bar{V}(r, \Theta, \Phi) + \epsilon U_\theta(\xi, r, \Theta, \Phi), \\ w &= \bar{W}(r, \Theta, \Phi) + \epsilon U_z(\xi, r, \Theta, \Phi), & \Gamma &= \bar{\Gamma}(r, \Theta, \Phi) + \epsilon P(\xi, r, \Theta, \Phi), \end{aligned} \quad (2.2)$$

where the wave phase is $\xi = kz + m\theta - \omega t$, with k and m respectively the axial and azimuthal wavenumbers. The overbar notation defines the phase-averaged quantity \bar{q} , $\bar{q} = 1/(2\pi) \int_0^{2\pi} q d\xi$. The secular variable $\Theta = m\theta$ characterizes the spiral motion. The leading-order perturbation is namely an amplitude modulated, free vortical mode whose small dimensionless amplitude is ϵ and whose real and slowly evolving frequency is ω . The dimensionless wave phase tilt is denoted by $\varpi = kr_c/m$ and is taken $O(1)$ or smaller. The mode is neutral and singular in the nonlinear theory while it is assumed stable in the linear theory provided certain conditions are satisfied in the basic-state vorticity profile (Caillol 2015). We consider that wave packets propagate episodically in the vortex when they are excited by convective pulses. The mode is then supposed to be generated by an initial, localized and short-time forcing: for examples an impulse or a step-like condition. We assume a quasi-steady asymptotic state, so the fast time t only appears in the phase ξ , the WMFI evolving at the slow time scales $T_i = \epsilon^{i/2}t$, $i = 1, 2$, that are omitted in the notations. The quasi-steady state assumption is not restrictive since it is often observed among large-scale vortices due to a balance between the friction in the boundary layer and sea-air exchanges (Emanuel (1985)). For the sake of simplicity, these effects will not be however modeled in the following equations. We will study the WMFI above the surface boundary layer in order to neglect the effects of the latter on the interaction and to neglect the mean radial flow of the inflow layer (Zhang *et al.* 2011). We will simply

introduce the body force \mathbf{F} that permits to discard the viscous diffusion effect on the basic-state vortex evolution without altering the inner flow, to the profit of the WMFI.

The critical layer imposes its proper scalings. The wave packet must be advected by the leading-order $O(\epsilon^{1/2})$ CL induced mean vertical velocity, which leads to a time scale T_2 faster than the usual time T_3 for the Korteweg-de-Vries equation (Leibovich 1970). The amplitude modulation space and time variables are hence

$$\Phi = \epsilon^{\frac{1}{2}} \frac{m}{r_c} z, \quad \text{and} \quad \tau_2 \equiv T_2.$$

Note that for the larger wave envelope in C17, the scalings were slower ($\Phi \equiv \epsilon z, \tau_3 \equiv T_3$). In this multiple-scale approach, the various partial derivatives are computed in this way

$$\partial_\theta \bullet = m(\partial_\xi \bullet + \partial_\Theta \bullet), \quad \partial_z \bullet = \epsilon^{\frac{1}{2}} \frac{m}{r_c} \partial_\Phi \bullet + \tilde{k} \partial_\xi \bullet, \quad \partial_t \bullet = \epsilon^{\frac{1}{2}} \partial_{T_1} \bullet + \epsilon \partial_{T_2} \bullet - \tilde{\omega} \partial_\xi \bullet.$$

The modulation-modified wave number and frequency are: $\tilde{k} = k - m/r_c \omega_\Phi T_1$ and $\tilde{\omega} = \omega + \epsilon^{1/2} \omega_{T_2} T_1$. In spite of the smaller wave envelope vertical scale with respect to C17, the chosen régime is still the nonlinear critical layer, the wave packet linear effects like dispersion do not prevail (Mallier & Maslowe 1999; Campbell 2004).

The system of equations (2.1) after the decomposition (2.2) yields two subsystems of equations: the first describing the evolution of the perturbations, Eqs. (2.3:a-d) and the second the evolution of the mean flow, Eqs. (2.4:a-d).

$$\frac{DU_r}{Dt} = \varrho(r)U_\theta - D[P + \overline{U}U_r] - \left(\frac{U_\theta}{r}\partial_\theta + U_z\partial_z\right)\overline{U} + \frac{\epsilon}{r}(U_\theta^2 - \overline{U}_\theta^2) \quad (2.3a)$$

$$+ \epsilon D^*[\overline{U}_r^2] + \epsilon \partial_z \overline{U}_z \overline{U}_r + \frac{1}{Re} \left[\Delta U_r - \frac{U_r}{r^2} - \frac{2}{r^2} \partial_\theta U_\theta \right],$$

$$\frac{DU_\theta}{Dt} = -Q_z(r)U_r - \overline{U}D^*[U_\theta] - \frac{\partial_\theta P}{r} - \left(\frac{U_\theta}{r}\partial_\theta + U_z\partial_z\right)\overline{V} + \frac{\epsilon}{r^2}D[r^2\overline{U}_r\overline{U}_\theta] \quad (2.3b)$$

$$- \epsilon \frac{U_\theta}{r}U_r + \epsilon \partial_z \overline{U}_z \overline{U}_\theta + \frac{1}{Re} \left[\Delta U_\theta - \frac{U_\theta}{r^2} + \frac{2}{r^2} \partial_\theta U_r \right],$$

$$\frac{DU_z}{Dt} = Q_\theta(r)U_r - \overline{U}D[U_z] - \partial_z P - \left(\frac{U_\theta}{r}\partial_\theta + U_z\partial_z\right)\overline{W} + \epsilon D^*[\overline{U}_r\overline{U}_z] \quad (2.3c)$$

$$+ \epsilon \partial_z \overline{U}_z^2 + \frac{1}{Re} \Delta U_z,$$

$$D^*U_r + \frac{1}{r}\partial_\theta U_\theta + \partial_z U_z = 0. \quad (2.3d)$$

As for the mean flow, we have the set of equations

$$\frac{D\overline{U}}{Dt} = \overline{V}(Co + \Omega) - D[\overline{I} + \frac{1}{2}\overline{U}^2] + \epsilon^2 \left(\frac{\overline{U}_\theta^2}{r} - D^*[\overline{U}_r^2]\right) - \epsilon^{\frac{5}{2}} \frac{m}{r_c} \partial_\Phi \overline{U}_z \overline{U}_r + \frac{\Delta_r}{Re} \overline{U} \quad (2.4a)$$

$$\frac{D\overline{V}}{Dt} = -Q_z \overline{U} - \frac{m}{r} \partial_\Theta \overline{I} - \frac{\epsilon^2}{r^2} D[r^2 \overline{U}_r \overline{U}_\theta] - \epsilon^{\frac{5}{2}} \frac{m}{r_c} \partial_\Phi \overline{U}_z \overline{U}_\theta + \frac{\Delta_r}{Re} \overline{V} + F_\theta, \quad (2.4b)$$

$$\frac{D\overline{W}}{Dt} = Q_\theta \overline{U} - \epsilon^{\frac{1}{2}} \frac{m}{r_c} \partial_\Phi [\overline{I} + \epsilon^2 \overline{U}_z^2] - \epsilon^2 D^*[\overline{U}_r \overline{U}_z] + \frac{1}{Re} (\Delta_r \overline{W}(r) + \frac{\overline{W}}{r^2}), \quad (2.4c)$$

$$D^*\overline{U} + m \frac{\partial_\Theta \overline{V}}{r} + \epsilon^{\frac{1}{2}} \frac{m}{r_c} \partial_\Phi \overline{W} = 0. \quad (2.4d)$$

The azimuthal gradients related to the diffusion terms and to the mean rotational wave momentum fluxes $\partial_\Theta \overline{U}_\theta \overline{U}_r, \partial_\Theta \overline{U}_\theta^2, \dots$ have been omitted in (2.3) and (2.4) because they appear at high orders and they are negligible in this study. The system (2.3) is coupled

with the following boundary conditions

$$\begin{aligned} r \rightarrow \infty, \quad (U_r, U_\theta, U_z, P) &\rightarrow (0, 0, 0, 0); \\ r \rightarrow 0, \quad U_\theta &\rightarrow 0, \quad \text{and if } |m| \neq 1, \quad U_r \rightarrow 0. \end{aligned} \quad (2.5)$$

The CL induced mean flow expands in two spiraling helical diffusion boundary layers at either CL side, and far from r_c vanishes. No boundary condition is specified in the vertical direction. The circular vortex is characterized by the mean angular rotation $\Omega(r) = \overline{V}(r)/r$, the absolute mean axial vorticity $Q_z(r) = 1/rD[r\overline{V}(r)] + Co$, the mean azimuthal vorticity $Q_\theta(r) = -\overline{W}'(r)$ and the absolute inertial frequency $\varrho(r) = 2\Omega(r) + Co$. The prime denotes the radial derivative of the phase-averaged quantities when it is not precised, otherwise D denotes the radial differential operator. We also have the different notations

$$\frac{D}{Dt} \bullet = \partial_t \bullet + \epsilon [U_r \partial_r + \frac{U_\theta}{r} \partial_\theta + U_z \partial_z] \bullet + \Omega \partial_\theta \bullet + \overline{W} \partial_z \bullet, \quad \Delta_r \bullet = D[D^*[\bullet]] + \epsilon \frac{m^2}{r_c^2} \partial_\Phi^2 \bullet,$$

$$\frac{D}{Dt} \bullet = \epsilon \partial_{T_2} \bullet + m \Omega \partial_\theta \bullet + \epsilon \frac{1}{2} \frac{m}{r_c} \overline{W} \partial_\Phi \bullet, \quad \Delta \bullet = D^*[D[\bullet]] + \frac{1}{r^2} \partial_\theta^2 \bullet + \partial_z^2 \bullet, \quad \text{and} \quad \frac{1}{Re} = \lambda \epsilon^{\frac{3}{2}}.$$

Here, the nonlinear CL theory shall be used, so we will assume that the Haberman parameter λ , the cubic ratio of the viscous CL thickness to the nonlinear CL thickness, is small: $\lambda \ll 1$ when it is not indicated, which allows for a λ -expansion of the flow, dividing it into an inviscid part and a smaller viscous part, e.g. for the radial velocity $U = U_{r,i} + \lambda U_{r,v} + o(\lambda)$. The perturbations of velocity, geopotential and vorticity are expanded according to the square root of the wave packet amplitude, for instance for the radial velocity

$$U_r = U_r^{(0)} + \epsilon^{\frac{1}{2}} U_r^{(1)} + \epsilon U_r^{(2)} + \dots, \quad (2.6)$$

with the zeroth order characterizing the amplitude-modulated non-normal vorticity mode. Although large vertical and radial velocities may occur in tropical cyclones above the inflow layer, these are always smaller than the rotational velocities (Reasor *et al.* 2000), we will then assume that the basic-state vortex only contains a field of mean azimuthal velocity. The WMF interaction will nevertheless yield induced mean vertical and radial velocity fields. As a result, the mean radial, azimuthal and axial shear flows are $\epsilon^{1/2}$ -expanded in the same way, like the frequency $\omega(\Phi) = \omega_0 + \epsilon^{1/2} \omega_1(\Phi) + \epsilon \omega_2(\Phi) + \dots$

$$\overline{U} = \epsilon \overline{U}_2(r, \theta, \Phi) + \epsilon^{\frac{3}{2}} \overline{U}_3(r, \theta, \Phi) + \dots, \quad (2.7a)$$

$$\overline{V} = \overline{V}_0(r) + \epsilon^{\frac{1}{2}} \overline{V}_1(r, \theta, \Phi) + \epsilon \overline{V}_2(r, \theta, \Phi) + \epsilon^{\frac{3}{2}} \overline{V}_3(r, \theta, \Phi) + \dots, \quad (2.7b)$$

$$\overline{W} = \epsilon^{\frac{1}{2}} \overline{W}_1(r, \theta, \Phi) + \epsilon \overline{W}_2(r, \theta, \Phi) + \epsilon^{\frac{3}{2}} \overline{W}_3(r, \theta, \Phi) + \dots, \quad (2.7c)$$

$$Q_z = Q_0(r) + \epsilon^{\frac{1}{2}} Q_{z,1}(r, \theta, \Phi) + \epsilon Q_{z,2}(r, \theta, \Phi) + \dots, \quad (2.7d)$$

$$Q_\theta = \epsilon^{\frac{1}{2}} Q_{\theta,1}(r, \theta, \Phi) + \epsilon Q_{\theta,2}(r, \theta, \Phi) + \dots \quad (2.7e)$$

The subscript 0 characterizes the $O(1)$ phase averaged rotational flow at the end of the transition stage, result from the strong interaction between the basic vortex and the wave packet. As $|r - r_c| \rightarrow \infty$, the zeroth-order mean flow tends to the basic vortex. The body force is thus $F_\theta(r) = -Q'_0(r)/Re$. We also assume that Co expansion is restricted to the first order: $Co = Co_0 + \epsilon^{1/2} Co_1$. The mean geopotential is determined by Eq. (2.4a) and

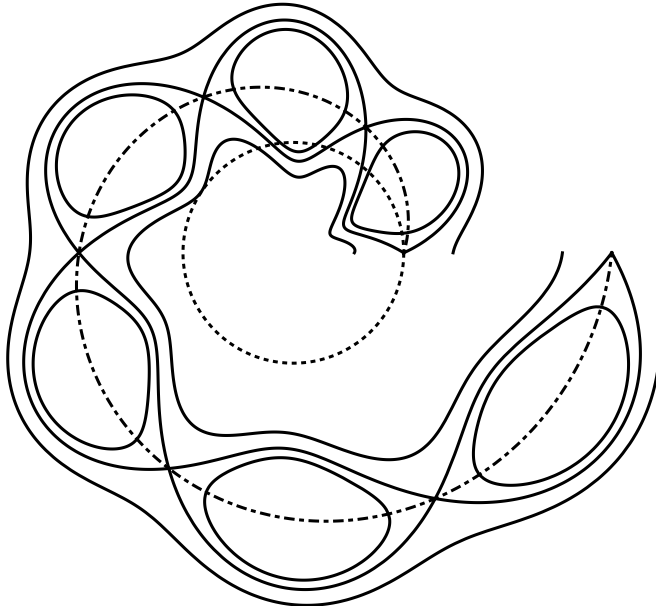


FIGURE 1. Sketch of a few streamline envelopes projected on a horizontal plane, spiraling around the critical radius r_c (dotted line) at either side of the CL axis $r = r_a(\xi, \Phi, \Theta)$ (dotdashed line), $m = 6$.

to the first orders, it is defined by the gradient wind balance

$$\bar{T}_0 = \frac{1}{8}(\varrho_{0,c}^2 - Co_0^2)r_c^2 + \frac{1}{4} \int_{r_c}^r \varrho_0^2(r) - Co_0^2 r dr, \quad (2.8a)$$

$$\bar{T}_1 = \bar{T}_1(r_c) + \frac{1}{2} \int_{r_c}^r \varrho_0 \varrho_1 - Co_0 Co_1 r dr, \quad (2.8b)$$

$$\bar{T}_2 = \bar{T}_2(r_c) + \frac{1}{2} \int_{r_c}^r \varrho_0 \varrho_2 + \frac{1}{2}(\varrho_1^2 - Co_1^2) r dr. \quad (2.8c)$$

3. The outer flow

In this Section, we give the outer-flow asymptotic solution near r_c , which will be useful to determine the CL flow in a unique way through matchings with the outer flow.

The spiraling motion shifts the CL symmetry axis from the critical radius; this difficulty is overcome here by introducing a coordinate η which is constant along a streamline (Davis 1969). As a result, the representation, in cylindrical coordinates, of a streamline is

$$r = r_c + \eta + h(\eta, \xi, \Theta, \Phi),$$

where the deviation h from axisymmetry is assumed to be of order ϵ (cf. figures 1 and 2). Owing to the vorticity erosion inside the CL occurring during the WMFI, we assume that the basic-vortex axial vorticity becomes zero on the CL axis $r_a = r(\eta = 0)$ a long time after the beginning of the interaction but before the quasi-steady stage starts:

$$Q_0 = 0 \quad \text{at} \quad r = r_a(\xi, \Theta, \Phi) = r_c + h(0, \xi, \Theta, \Phi).$$

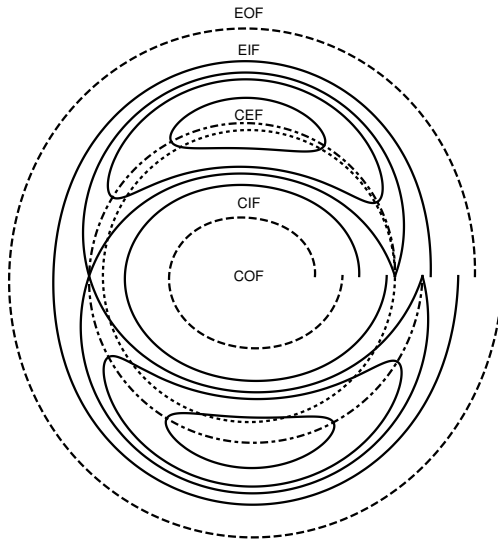


FIGURE 2. The vortex + the wave packet $m = 2$ and the various regions (bounded by dashed lines) in a horizontal plane: COF the core outer flow characterized by $\eta < 0$, CIF the core inner flow defined by $s = -$, CEF the cat's eye flow defined by $Z \leq A$, EIF the external inner flow defined by $s = +$ and EOF the external outer flow defined by $\eta > 0$. The CL involves the CIF + CEF + EIF. The dotted line represents the critical radius r_c and the dotdashed line is the CL symmetry radius r_a .

3.1. The amplitude-modulated singular mode

The linearized, inviscid and stationary system (2.3) can be reduced to a single equation, the Howard-Gupta modal equation generalized to the f -plane and related to the modal radial velocity $U_r^{(0)}$ (Howard & Gupta (1962)). This is expressed as $\mathcal{L}_0(U_r^{(0)}) = 0$, namely

$$D[S(r)D^*U_r^{(0)}] + \partial_\xi^2 U_r^{(0)} + \left((rD - 2)[S(r)Q_0(r)] + \frac{k^2 r^2 \varrho_0(r)}{m\omega_0^D(r)} S(r)Q_0(r) \right) \frac{m U_r^{(0)}}{\omega_0^D(r)r^2} = 0. \quad (3.1)$$

The superscript D defines the Doppler-shifted frequency

$$\omega^D(r) = \tilde{\omega} - m\Omega(r) - \tilde{k}\overline{W}(r), \quad S(r) = \frac{r^2}{m^2 + k^2 r^2}.$$

The equation (3.1) is singular at the critical radius r_c where the Doppler-shifted frequency $\omega_0^D(r)$ vanishes, that is $\omega_0 = m\Omega_{0,c}$. But the solution is weakly singular around r_c , at the end of the strong vortex/wave packet interaction, since the local equivalent Richardson number $J(r) = (kr/m)^2 \varrho_0(r)Q_0(r)/[Q_0(r) - \varrho_0(r)]^2$ becomes small near the CL symmetry axis r_a , as the zeroth-order mean axial vorticity vanishes at r_a . The connection of this number with the linear stability of a rotating sheared flow is evoked in Caillol (2014, 2015). The subscript c characterizes the critical radius.

The neutral-mode radial velocity evaluated on the streamline η is expressed by two Frobenius series of the variable $r - r_c = \eta + h(\eta)$

$$U_r^{(0)} = \left(\frac{a}{r_c} \phi_a[\eta + h(\eta)] + \phi_b[\eta + h(\eta)] \right) U_0(\Phi) \sin \xi + \frac{C}{r_c} \phi_a[\eta + h(\eta)] U_0(\Phi) \cos \xi, \quad (3.2)$$

where both Frobenius series ϕ_a and ϕ_b are expanded around r_c in this way

$$\phi_a(\eta) = \eta + \sum_{n=2}^{\infty} a_{0,n} \eta^n, \quad \phi_b(\eta) = 1 + \sum_{n=2}^{\infty} b_{0,n} \eta^n + b_0 \phi_a(\eta) \ln \eta^*. \quad (3.3)$$

The radius η inside the logarithm is normalized by $\eta^* = \eta/\eta_0$, where $\eta_0 = r_c/\sqrt{2}$. The complex logarithmic function in (3.3) induces an additional and in phase quadrature term in (3.2) as $r < r_c$, caused by the logarithmic phase shift ϕ defining C as follows:

$$r > r_c, \quad C^+ = 0, \quad \text{and} \quad r < r_c, \quad C^- = b_0 r_c \phi(\lambda). \quad (3.4)$$

The superscript $s = -$ shall be used to characterize the vortex core where $r < r_c$ and the superscript $s = +$ the outer core where $r > r_c$.

3.2. Order $\epsilon^{\frac{3}{2}}$ outer flow

The first-order inviscid disturbance is decomposed in five contributions. The radial velocity $U_{r,i}^{(1)}$ can be then written

$$U_{r,i}^{(1)} = U_{r,h}^{(1)} + U_{r,l}^{(1)} + U_{r,d}^{(1)} + U_{r,ad}^{(1)} + U_{r,\omega d}^{(1)}.$$

The first term constitutes a CL feedback into the outer flow. It is required while matching the inner flow on the separatrices. The second term $U_{r,l}^{(1)}$ is generated by the advection of the mode by the first-order mean flow, the three next terms $U_{r,d}^{(1)}$, $U_{r,ad}^{(1)}$ and $U_{r,\omega d}^{(1)}$ are respectively created by the vertical gradients of the modal amplitude U_0 , the phase jump a and the frequency ω_1 . The velocities $U_{r,h}^{(1)}$ and $U_{r,\omega d}^{(1)}$ are not Θ -secular at the lowest expansion order near $\eta = 0$. So their secularity can be neglected in the study. The differentiation with respect to Θ in the system (2.3) leads to the presence of coupled sine and cosine eigenfunctions. The $U_{r,i}^{(1)}$ dependence on the phase ξ is hence as follows

$$U_{r,i}^{(1)}(r, \xi) = \{[\phi_l^{(1,1)}(r) + \omega_{1,\Phi} T_1 \phi_{\omega d}^{(1,1)}(r) + a_{\Phi} \phi_{ad}^{(1,1)}(r)] U_0 + \phi_d^{(1,1)} U_{0,\Phi}\} \sin \xi \\ + \{[\phi_l^{(1,2)}(r) + a_{\Phi} \phi_{ad}^{(1,2)}(r)] U_0 + \phi_d^{(1,2)}(r) U_{0,\Phi}\} \cos \xi + \phi_h^{(1)}(r) U_0 \cos(2\xi).$$

The feedback flow satisfies the homogeneous equation

$$\mathcal{L}_0(U_{r,h}^{(1)}) = 0, \quad \text{with} \quad \phi_h^{(1)}(\eta) = \frac{\gamma_{h,1}}{r_c} \phi_a(\eta) + \kappa_{h,1} \phi_b(\eta). \quad (3.5)$$

The other terms satisfy non-homogeneous linear equations. The second contribution $U_{r,l}^{(1)}$ satisfies the equation

$$\mathcal{L}_0(U_{r,l}^{(1,1)}) = -\mathcal{L}_{1,1}(U_r^{(0)}) - \mathcal{L}_{1,\theta}(\mathbf{U}_l^{(1,2)}, P_l^{(1,2)}), \quad \mathcal{L}_0(U_{r,l}^{(1,2)}) = -\mathcal{L}_{1,2}(U_\theta^{(0)}) - \mathcal{L}_{1,\theta}(\mathbf{U}_l^{(1,1)}, P_l^{(1,1)}), \quad (3.6)$$

with the operators $\mathcal{L}_{1,1}$, $\mathcal{L}_{1,2}$ and $\mathcal{L}_{1,\theta}$ defined by

$$\mathcal{L}_{1,1}(U) = \left\{ (rD - 2) \left[S(r) \left(Q_{z,1}(r) - \frac{kr}{m} Q_{\theta,1}(r) \right) \right] + kr \frac{S(r) \varrho_0(r)}{\omega_0^D(r)} \left(\frac{kr}{m} Q_{z,1}(r) + Q_{\theta,1}(r) \right) \right. \\ \left. - \frac{\omega_1^D(r)}{\omega_0^D(r)} (rD - 2) [S(r) Q_0(r)] + \frac{k^2 r^2}{m} \frac{S(r) \varrho_0(r)}{\omega_0^D(r)} \left[\frac{\varrho_1(r)}{\varrho_0(r)} - 2 \frac{\omega_1^D(r)}{\omega_0^D(r)} \right] Q_0(r) \right\} \frac{mU}{\omega_0^D(r) r^2}, \quad \text{and} \quad (3.7)$$

$$\mathcal{L}_{1,2}(U) = \frac{km\varrho_0(r)}{r\omega_0^{D^2}(r)}S(r)U\partial_\Theta[k\bar{V}_1(r) - \frac{m}{r}\bar{W}_1(r)] + \frac{m}{\omega_0^D(r)}D\left[\frac{S(r)}{r}U\partial_\Theta[k\bar{W}_1(r) + \frac{m}{r}\bar{V}_1(r)]\right] \quad (3.8)$$

$$\begin{aligned} \mathcal{L}_{1,\theta}(U, P) &= \frac{m\varrho_0(r)}{\omega_0^{D^2}(r)}[\Omega_0(r) - \omega_0\frac{m}{r^2}S(r)]\partial_\Theta U_\theta - m\frac{\Omega_0(r)}{\omega_0^D(r)}\partial_\Theta\partial_\xi U_r \\ &\quad + k\frac{m}{r}\frac{\varrho_0(r)}{\omega_0^{D^2}(r)}S(r)\partial_\Theta[kP - m\Omega_0(r)U_z] \\ &\quad + \frac{mD}{\omega_0^D(r)}\left[S(r)\partial_\Theta\left(\frac{m}{r^2}P + \frac{\omega_0}{r}U_\theta + k\Omega_0(r)U_z\right)\right]. \end{aligned}$$

The first-order Doppler shifted frequency is $\omega_1^D(r) = \omega_1 - m\Omega_1(r) - k\bar{W}_1(r)$. The first-order equivalent Richardson number, derived from (3.7) is given at $r = r_c$ by

$$J_{1,c} = \frac{\varpi}{\varrho_{0,c}}(\varpi Q_{z,1,c} + Q_{\theta,1,c}) - (1 + 2\varpi^2)\omega_{1,c}^D \frac{r_c Q'_{z,0,c}}{m\varrho_{0,c}^2}. \quad (3.9)$$

The radial velocities $U_{r,d}^{(1)}$, $U_{r,ad}^{(1)}$ and $U_{r,\omega d}^{(1)}$ satisfy the equations

$$\mathcal{L}_0(U_{r,d}^{(1,1)}) = -\mathcal{L}_{1,\theta}(\mathbf{U}_d^{(1,2)}, P_d^{(1,2)}), \quad \mathcal{L}_0(U_{r,d}^{(1,2)}) = -\mathcal{L}_{1,d}(\phi^{(0)})U_{0,\Phi} \cos \xi - \mathcal{L}_{1,\theta}(\mathbf{U}_d^{(1,1)}, P_d^{(1,1)}), \quad (3.10)$$

$$\mathcal{L}_0(U_{r,ad}^{(1,1)}) = -\mathcal{L}_{1,\theta}(\mathbf{U}_{ad}^{(1,2)}, P_{ad}^{(1,2)}), \quad \mathcal{L}_0(U_{r,ad}^{(1,2)}) = -\mathcal{L}_{1,d}(\phi_a)a_\Phi U_0 \cos \xi - \mathcal{L}_{1,\theta}(\mathbf{U}_{ad}^{(1,1)}, P_{ad}^{(1,1)}), \quad (3.11)$$

$$\mathcal{L}_0(U_{r,\omega d}^{(1)}) = -\omega_{1,\Phi} T_1 \mathcal{L}_{1,d}(\phi^{(0)})U_0 \sin \xi,$$

$$\text{with } \mathcal{L}_{1,d}(\phi) = \frac{2km}{r_c} \left[\frac{m}{r} \frac{Q_0(r)}{\omega_0^D(r)} - D \right] \left[S^2(r) \left(\frac{m}{r} \frac{Q_0(r)}{\omega_0^D(r)} \phi(r) + D^*[\phi(r)] \right) \right].$$

The Frobenius series related to each radial velocity have the same structure

$$\phi_j^{(1,1)}(\eta) = \sum_{n=0}^{\infty} (b_{j,1,n} \ln^2 |\eta^*| + c_{j,1,n} \ln |\eta^*| + d_{j,1,n}) \eta^n + \frac{\alpha_{j,1}}{r_c} \phi_a + \beta_{j,1} \phi_b, \quad j = l, d, ad, \text{ and } \omega d, \quad (3.12)$$

$$\text{and } \phi_j^{(1,2)}(\eta) = \sum_{n=0}^{\infty} (e_{j,1,n} \ln^2 |\eta^*| + f_{j,1,n} \ln |\eta^*| + g_{j,1,n}) \eta^n + \frac{\gamma_{j,1}}{r_c} \phi_a + \kappa_{j,1} \phi_b, \quad j = l, d, \text{ and } ad. \quad (3.13)$$

The coefficients of the first terms in the series (3.3,3.12,3.13) are given in Appendix A. The integration of the equations (3.6), (3.10) and (3.11) is simplified owing to the Θ -secularity assumption ; any physical quantity in both outer and inner flows is a polynomial of the variable Θ . As a result, the quantity $q(\Theta)$ can be written exactly in a finite Taylor expansion

$$q(\Theta) = q(0) + \partial_\Theta q(0) \Theta + \frac{1}{2} \partial_\Theta^2 q(0) \Theta^2 + \dots$$

From now on, any Θ -differentiation at $\Theta = 0$ will be denoted $q_\Theta(0)$.

4. Low-order inner flow

In this Section, we display the inner expansion, rescale the inner variables and solve the two first orders.

4.1. CL variables and equations

When the amplitude modulated neutral mode is weakly singular, the local equivalent Richardson number at r_c , J_c is small and is assumed to be $O(\epsilon^{1/2})$: $J_c = J_{1,c} \epsilon^{1/2} + O(\epsilon)$. The critical-layer width is then maximum and of order $O(\epsilon^{1/2})$, we will thus take the inner radial scaling $r - r_c = \epsilon^{1/2} R$. The outer-flow expansion following R gives the way with which the inner expansion must proceed

$$\begin{aligned} U &= \epsilon \overline{U}_2(r_a) + \epsilon \left\{ U^{(0)} + \epsilon^{\frac{1}{2}} \ln \epsilon U^{(1)} + \epsilon^{\frac{1}{2}} U^{(2)} + \dots \right\}, \\ V &= \Omega_0(r_a) r + \epsilon^{\frac{1}{2}} \Omega_1(r_a) r + \epsilon^{\frac{1}{2}} \left\{ V^{(0)} + \epsilon^{\frac{1}{2}} \ln \epsilon V^{(1)} + \epsilon^{\frac{1}{2}} V^{(2)} + \dots \right\}, \\ W &= \epsilon^{\frac{1}{2}} \overline{W}_1(r_a) + \epsilon^{\frac{1}{2}} \left\{ \epsilon^{\frac{1}{2}} \ln \epsilon W^{(1)} + \epsilon^{\frac{1}{2}} W^{(2)} + \dots \right\}, \\ \mathcal{P} &= \frac{1}{8} (\varrho_0^2(r_c) - C o_0^2) r^2 + \epsilon \left\{ \mathcal{P}^{(0)} + \epsilon^{\frac{1}{2}} \ln \epsilon \mathcal{P}^{(1)} + \epsilon^{\frac{1}{2}} \mathcal{P}^{(2)} + \dots \right\}. \end{aligned}$$

In order to simplify the CL equations, let us make the following rescaling using the zeroth-order mean flow evaluated at r_c

$$X = \xi + \frac{\pi}{2} (1 - s_i), \quad R = r_c \mathcal{R}, \quad \tau_n = m \varrho_{0,c} \epsilon^{n/2} t, \quad s_i = -\text{sgn}[m \varrho_{0,c} U_0],$$

$$V^{(n)} = \varrho_{0,c} r_c \hat{V}^{(n)}, \quad W^{(n)} = \varpi \varrho_{0,c} r_c \hat{W}^{(n)}, \quad U^{(n)} = s_i m \varrho_{0,c} r_c \hat{U}^{(n)}, \quad \mathcal{P}^{(n)} = s_i \varrho_{0,c}^2 r_c^2 \hat{\mathcal{P}}^{(n)},$$

$$\overline{V}_{n,c} = \mathcal{V}_n \varrho_{0,c} r_c, \quad \overline{W}_{n,c} = \varpi \mathcal{W}_n \varrho_{0,c} r_c, \quad \overline{U}_{n,c} = m \mathcal{U}_n \varrho_{0,c} r_c, \quad \overline{\Gamma}_{n,c} = \mathfrak{P}_n \varrho_{0,c}^2 r_c^2,$$

$$\overline{\Gamma}'_{n,c} = \mathfrak{P}'_n \varrho_{0,c}^2 r_c, \quad \omega_n = m \mathcal{U}_n \varrho_{0,c}, \quad C o_n = \mathcal{C} o_n \varrho_{0,c}, \quad \varrho_{n,c} = \mathcal{S}_n \varrho_{0,c},$$

$$Q_{z,n,c} = \mathcal{Q}_{z,n} \varrho_{0,c}, \quad \overline{W}'_{n,c} = -\mathcal{Q}_{\theta,n} \varrho_{0,c}, \quad r_c Q'_{0,c} = \zeta \varrho_{0,c}, \quad r_c Q'_{z,n,c} = \zeta_{z,n} \varrho_{0,c},$$

$$r_c Q'_{\theta,n,c} = \zeta_{\theta,n} \varrho_{0,c}, \quad r_c^2 Q''_{0,c} = \zeta' \varrho_{0,c}, \quad r_c^2 Q''_{z,n,c} = \zeta'_{z,n} \varrho_{0,c}, \quad r_c^2 Q''_{\theta,n,c} = \zeta'_{\theta,n} \varrho_{0,c},$$

$$\lambda' = \frac{\lambda}{U_0 r_c}, \quad A(\Phi, \tau_2) = \left| \frac{U_0(\Phi, \tau_2)}{m \varrho_{0,c} r_c} \right|.$$

In the following analysis, the hat is dropped with the understanding that we are dealing with the new variables. The rescaled wave amplitude $A(\Phi, \tau_2)$ is solution of a nonlinear space-time evolution equation in the asymptotic quasi-steady regime, a long time after the CL formation when the vorticity wave packet is slowly exchanging momentum and kinetic energy with the basic-state vortex. In this regime, where the zeroth-order mean axial vorticity is taken zero on the CL axis, the CL singularity strength is measured by the axial vorticity radial gradient at r_c , i.e. the dimensionless number ζ . The radius r_c and ζ are finite but $r_c > 1$ while ζ is small, according to observations (Caillol (2015)). If we consider the limit $r_c \rightarrow 0$, we suppose a critical layer in the eye of the tropical cyclone or the tornado. The basic-vortex axial vorticity is nearly constant in the eye, so vorticity waves are strongly damped there. Taking this limit would imply $\zeta \rightarrow 0$; the CL interaction would be weaker since the leading-order CL equations would be postponed to a higher order. If we now consider the limit $r_c \rightarrow \infty$, we suppose a critical layer far away from the eyewall, where the basic radial gradient vorticity is quasi-zero and vorticity waves are also strongly damped. Taking this limit would lead to $\zeta \rightarrow 0$ and a weak WMFI as well, as the vorticity radial gradient fast decreases with r and $r_c Q'_{z,0} \rightarrow 0$.

A general expression of the streamline radius \mathcal{R} is inside the critical layer

$$\mathcal{R} = s_i \rho + H(\rho, X, \Theta, \Phi, \tau_2), \quad (4.1)$$

the function H being expanded following $\epsilon^{1/2}$: $H = \epsilon^{1/2} H_2 + \epsilon H_3 + O(\epsilon^{3/2})$.

We undertake the change of radial variables $R \rightarrow \rho$. The radius ρ is a function of \mathcal{R} , X , Θ , Φ and τ_2 and its partial derivatives are

$$\rho_{\mathcal{R}} = \frac{1}{s_i + H_{\rho}}, \quad \rho_X = -\frac{H_X}{s_i + H_{\rho}}, \quad \rho_{\Theta} = -\frac{H_{\Theta}}{s_i + H_{\rho}}, \dots$$

The resulting system of inner equations is displayed in Appendix B.

4.2. Zeroth- and first-order CL solutions

The zeroth-order inner equations lead to the simple solution as follows:

$$U^{(0)} = -s_i A \sin X, \quad V^{(0)} = -s_i \rho, \quad \mathcal{P}^{(0)} = \frac{1}{2}[\mathcal{S}_1 - \mathcal{C}_0 \mathcal{C}_1 - s_i \rho] \rho + s_i \mathfrak{P}_2.$$

Two compatibility conditions arise from the angular and axial momentum inner equations

$$V_{\Theta}^{(2)} = 0, \quad W_{\Theta}^{(2)} = 0. \quad (4.2)$$

The first-order flow is straightforwardly deduced from the Frobenius series (3.3) and (3.12)

$$U^{(1)} = \frac{1}{2}[\zeta(1 + \varpi^2)\rho - s_i(c_{l,1,0} + c_{ad,1,0}a_{\Phi})A - s_i c_{d,1,0}A_{\Phi}] \sin X \\ - \frac{s_i}{2}[(f_{l,1,0} + f_{ad,1,0}a_{\Phi})A + f_{d,1,0}A_{\Phi}] \cos X,$$

$$\frac{\mathcal{P}^{(1)}}{\rho} + \frac{s_i}{2}\zeta\frac{\mathcal{U}_0}{\rho}\{[(\beta_{l,1,\Theta} + \beta_{ad,1,\Theta}a_{\Phi})A + \beta_{d,1,\Theta}A_{\Phi}] \sin X \\ + [(\kappa_{l,1,\Theta} + \kappa_{ad,1,\Theta}a_{\Phi})A + \kappa_{d,1,\Theta}A_{\Phi}] \cos X\} = W^{(1)} = V^{(1)} = \frac{\zeta}{2}A \cos X.$$

The resonance condition $\mathcal{U}_1^D = 0$ results from the inner momentum equation solvability conditions

$$\mathcal{U}_1 = \mathcal{V}_1 + \varpi^2 \mathcal{W}_1, \quad (4.3)$$

in addition to two other conditions

$$V_{\Theta}^{(4)} = W_{\Theta}^{(4)} = \frac{\zeta}{2}\{[(\beta_{l,1,\Theta} + \beta_{ad,1,\Theta}a_{\Phi})A + \beta_{d,1,\Theta}A_{\Phi}] \cos X \\ - [(\kappa_{l,1,\Theta} + \kappa_{ad,1,\Theta}a_{\Phi})A + \kappa_{d,1,\Theta}A_{\Phi}] \sin X\}.$$

The inner flow inside the separatrices is denoted by the superscript \odot while the jump and the mean of a quantity q at either side of r_c are respectively denoted by $[q]_{\pm}^{\pm} = q^+ - q^-$ and $\{q\}_{\pm}^{\pm} = (q^+ + q^-)/2$. The leading-order flow matchings on the separatrices show that the flows are identical inside and outside the separatrices, so $U^{(n,\odot)} = U^{(n)}$, $V^{(n,\odot)} = V^{(n)}$, ... with $n = 0, 1$. A first consequence is the absence of jump for the mean flow at r_c : $[\mathcal{V}_1]_{\pm}^{\pm} = [\mathcal{W}_1]_{\pm}^{\pm} = [\mathcal{U}_2]_{\pm}^{\pm} = [\mathfrak{P}_2]_{\pm}^{\pm} = 0$. The pressure continuity leads to

$$[(\beta_{l,1,\Theta} + \beta_{ad,1,\Theta}a_{\Phi})A + \beta_{d,1,\Theta}A_{\Phi}]_{\pm}^{\pm} = 0, \quad [(\kappa_{l,1,\Theta} + \kappa_{ad,1,\Theta}a_{\Phi})A + \kappa_{d,1,\Theta}A_{\Phi}]_{\pm}^{\pm} = 0. \quad (4.4)$$

The radial velocity continuity implies

$$[(c_{l,1,0} + c_{ad,1,0}a_{\Phi})A + c_{d,1,0}A_{\Phi}]_{\pm}^{\pm} = 0, \quad \text{and} \quad (4.5)$$

$$[(f_{l,1,0} + f_{ad,1,0}a\Phi)A + f_{d,1,0}A\Phi]_{\pm}^{\pm} = 0. \quad (4.6)$$

5. Low-order CL induced mean flow

In this Section, we characterize the $O(\epsilon^{1/2})$ and $O(\epsilon)$ induced mean flows in the CL neighborhood by analysing the phase averaged system (2.4). We assume a CL confined in a ring between $r = r_B^- < r_a$ and $r = r_B^+ > r_a$. The CL thickness is defined at leading order by $\delta_{cl} = r_B^+ - r_B^- = s_i r_c (\rho_B^+ - \rho_B^-) \epsilon^{1/2} + o(\epsilon)$.

5.1. First-order mean flow

From respectively the equations (2.4d), (2.4c) and (2.4b), we get the Θ -independence of the $O(\epsilon^{1/2})$ induced mean velocities and geopotential at $r \simeq r_a \simeq r_c$

$$\bar{V}_{1,\Theta}(r) = 0, \quad \bar{W}_{1,\Theta}(r) = 0, \quad \bar{T}_{1,\Theta}(r) = 0.$$

While differentiating (2.4b) and (2.4c) with respect to r , we obtain the same result for the mean vorticities

$$Q_{z,1,\Theta}(r) = 0, \quad Q_{\theta,1,\Theta}(r) = 0.$$

The mean vorticity radial gradient is however Θ -dependent at the singularity $r = r_c$. After differentiating (2.4b) and (2.4c) a second time with respect to r and simplifying with the above Θ -independence of the first-order flow, we get

$$m\Omega_0 \bar{V}_{1,\Theta}''(r) = -\frac{\epsilon^{\frac{3}{2}}}{r^2} D^3 [r^2 \overline{U_r U_\theta}] - 2\epsilon^{\frac{3}{2}} D^2 \left[\frac{1}{r} \overline{U_r U_\theta} \right], \quad m\Omega_0 \bar{W}_{1,\Theta}''(r) = -\epsilon^{\frac{3}{2}} D^2 [D^* [\overline{U_r U_z}]]. \quad (5.1)$$

The r.h.s of both equations (5.1) are made of the divergence of the vorticity radial gradient mean radial wave flux that is singular at $r = r_c$. The CL flow smooths this singularity out; so we have to compute the flux expressed with the inner variables. The triple radial gradient is $O(\epsilon^{-3/2})$ inside the CL; as a result, some nonlinear inner terms at the r.h.s. are $O(1)$. Next, rescaling and taking at the l.h.s. of (5.1) the upper CL limit $r \rightarrow r_a^+$ of the outer flow, corresponding at the r.h.s. to the inner boundary ρ_B^+ , we then have

$$\mathcal{U}_0 \zeta_{z,1,\Theta}^+ = -\overline{[U^{(0)} V_{\rho\rho\rho}^{(2)}](\rho_B^+, X)}, \quad \mathcal{U}_0 \zeta_{\theta,1,\Theta}^+ = \overline{\varpi [U^{(0)} W_{\rho\rho\rho}^{(2)}](\rho_B^+, X)}. \quad (5.2)$$

Taking the lower limit yields similar relations, so the spiraling part of the first-order axial vorticity radial gradient admits a jump across the CL since

$$\mathcal{U}_0 [\zeta_{z,1,\Theta}]_{\pm}^{\pm} = -\{ \overline{[U^{(0)} V_{\rho\rho\rho}^{(2)}](\rho_B^+, X)} - \overline{[U^{(0)} V_{\rho\rho\rho}^{(2)}](\rho_B^-, X)} \},$$

with the similar relation for the azimuthal vorticity radial gradient $\zeta_{\theta,1,\Theta}$.

The subsection 7.1 will show that the Θ -secular equations can be written at either CL side in the general way

$$\mathcal{U}_0 \zeta_{z,1,\Theta}^s = \Sigma_{q'}^s, \quad \mathcal{U}_0 \zeta_{\theta,1,\Theta}^s = -\varpi \Sigma_{q'}^s. \quad (5.3)$$

As the zeroth-order flow must remain steady in the quasi-steady régime, in addition to the laminar force F , we must assume the existence of an eddy force with azimuthal and axial components, that prevents the basic-state vortex from being Θ -dependent

$$\mathcal{U}_0 \mathcal{Q}_{z,0,\Theta}'' = -s_i \overline{[U^{(0)} V_{\rho\rho\rho}^{(2)}](\rho_B^+, X)} + F_{ed}^+ = -s_i \overline{[U^{(0)} V_{\rho\rho\rho}^{(2)}](\rho_B^-, X)} + F_{ed}^- = 0, \quad (5.4)$$

$$\mathcal{U}_0 \mathcal{Q}_{\theta,0,\Theta}'' = s_i \varpi \overline{[U^{(0)} W_{\rho\rho\rho}^{(2)}](\rho_B^+, X)} - \varpi F_{ed}^+ = s_i \varpi \overline{[U^{(0)} W_{\rho\rho\rho}^{(2)}](\rho_B^-, X)} - \varpi F_{ed}^- = 0. \quad (5.5)$$

The eddy force ratio azimuthal/axial component is $-\varpi$ and the forcing F_{ed} is undistorted.

5.2. Second-order mean flow

Next, from (2.4b-d), we get the rescaled equations of the $O(\epsilon)$ induced mean flow at r_c

$$\mathfrak{P}_{2,\theta} + \mathcal{U}_0 \mathcal{V}_{2,\theta} = 0, \quad \mathfrak{P}_{1,\phi} + \varpi \mathcal{U}_0 \mathcal{W}_{2,\theta} = 0, \quad \mathcal{U}'_2 + \mathcal{U}_2 + \varpi \mathcal{W}_{1,\phi} + \mathcal{V}_{2,\theta} = 0.$$

Note that the geopotential axial gradient in (2.4c) generates a vertical wind at low orders. This motion is however not relevant to the wave packet dynamics. The mean geopotential is therefore assumed uniform to the first orders at r_c : as a result, $\mathfrak{P}_{1,\phi} = \mathfrak{P}_{2,\theta} = \mathfrak{P}_{2,\phi} = \mathfrak{P}_{3,\theta} = 0$. We thus obtain the Θ -independence of the second-order mean velocities

$$\mathcal{V}_{2,\theta} = 0, \quad \mathcal{W}_{2,\theta} = 0,$$

while the radial-velocity radial gradient at r_c is given by

$$\mathcal{U}'_2 = -\mathcal{U}_2 - \varpi \mathcal{W}_{1,\phi}. \quad (5.6)$$

After r -differentiating the equation (2.4b), and simplifying with (2.4d) and (2.8c), we obtain the Θ -secular equation for the axial vorticity $\mathcal{Q}_{z,2}$ evaluated at $r \simeq r_a$

$$\begin{aligned} m\Omega_0(r)Q_{z,2,\theta}(r) &= \frac{m}{r_c}Q_0(r)\overline{W}_{1,\phi}(r) - m[\Omega_1(r)Q_{z,1}(r)]_\Theta - Q'_0(r)\overline{U}_2(r) \\ &- \frac{\epsilon}{r^2}\{D[r^2\overline{U}_r D^*[U_\theta]] - D[(r^2\partial_z U_z + mr\partial_\Theta U_\theta)U_\theta]\} + \frac{\epsilon}{r^3}D[r^2\overline{U}_r U_\theta] - \frac{m}{r_c}\epsilon^{\frac{3}{2}}\partial_\phi D^*[\overline{U}_z U_\theta]. \end{aligned}$$

The two first terms at the r.h.s. are negligible since $Q_0(r) \simeq 0$, $\overline{V}_{1,\theta}(r) = 0$ and $Q_{z,1,\theta}(r) = 0$. The fourth term at the r.h.s. is $O(1)$ since the double radial gradient is $O(\epsilon^{-1})$ inside the CL whereas the three following terms are negligible. Finally, two terms remain at the r.h.s.: the third term is the divergence of the radial flux of the axial vorticity Q_0 by the radial velocity \overline{U}_2 and the fourth term is the divergence of the leading-order mean radial wave flux of the axial vorticity. Next, introducing the inner variables in the flux divergence, and taking the limit $\rho \rightarrow \rho_B^+$, then taking the upper CL limit $r \rightarrow r_a^+$ for the other terms, and rescaling, we then have

$$\mathcal{U}_0 \mathcal{Q}_{z,2,\theta}^+ = -\zeta \mathcal{U}_2 - s_i \overline{[U^{(0)} V_{\rho\rho}^{(2)}]}(\rho_B^+, X). \quad (5.7)$$

As for the mean azimuthal vorticity, the Θ -gradient of the vorticity $Q_{\theta,2}$ is generated by the divergence of the leading-order mean radial wave flux of the azimuthal vorticity and the vertical gradient of the leading-order mean geopotential radial gradient, so we have, after r -differentiating (2.4c), simplifying with (2.8b), and rescaling as $r \rightarrow r_a^+$

$$\mathcal{U}_0 \mathcal{Q}_{\theta,2,\theta}^+ = \mathcal{V}_{1,\phi} + s_i \varpi \overline{[U^{(0)} W_{\rho\rho}^{(2)}]}(\rho_B^+, X). \quad (5.8)$$

Subsection 7.1 will show that the second-order mean vorticity Θ -secular equation can be written at either CL side in the general way

$$\mathcal{U}_0 \mathcal{Q}_{z,2,\theta}^s = \Sigma_q^s - \zeta \mathcal{U}_2, \quad \mathcal{U}_0 \mathcal{Q}_{\theta,2,\theta}^s = \mathcal{V}_{1,\phi} - \varpi \Sigma_q. \quad (5.9)$$

Subsection 7.1 will also prove that, for a symmetric CL extent such as $\rho_B^- = -\rho_B^+$, we have $\Sigma_q^- = \Sigma_q^+$. The second-order mean vorticity Θ -gradient thus admits no jump across the CL. Taking the mean radial eddy vorticity flux driven forcings into account in the inner equations then comes down to consider altered zeroth-order mean vorticity radial gradients at r_c such as

$$\mathcal{U}_0 \mathcal{Q}_{z,2,\theta} = -\hat{\zeta} \mathcal{U}_2, \quad \mathcal{U}_0 \mathcal{Q}_{\theta,2,\theta} = \mathcal{V}_{1,\phi} - \hat{\zeta}_{\theta,0} \mathcal{U}_2, \quad (5.10)$$

with the modifications of the vorticity radial gradients given by

$$\hat{\zeta} = \zeta - \frac{\Sigma_q}{\mathcal{U}_2}, \quad \hat{\zeta}_{\theta,0} = \varpi \frac{\Sigma_q}{\mathcal{U}_2}. \quad (5.11)$$

As the first-order vorticity radial gradient and the second-order vorticity vary following the azimuthal coordinate under the effect of the wave packet, they therefore evolve with the wave modulation. So that the viscous diffusion may not damp these corrections, the definition of the rescaled force \mathbf{F} near r_c has to be slightly modified and an axial component has to be added

$$F_\theta = s_i \lambda' \left(\mathcal{Q}'_{z,0}(r) - \frac{\Sigma_q}{\mathcal{U}_2} \right) A \epsilon^{\frac{3}{2}}, \quad F_z = s_i \lambda' \frac{\Sigma_q}{\mathcal{U}_2} A \epsilon^{\frac{3}{2}}.$$

5.3. Evolution equations of the first-order mean velocity at r_c

We now determine the τ_2 -evolution equations of \mathcal{V}_1 and \mathcal{W}_1 , knowing that these velocities are inviscidly undistorted and that they do not depend on Θ . The $O(\epsilon^{3/2})$ momentum equations (2.4b) and (2.4c) evaluated at r near r_a are

$$\overline{\mathcal{V}}_{1,T_2} + m\Omega_0 \overline{\mathcal{V}}_{3,\Theta} + \frac{m}{r_c} \overline{\mathcal{W}}_1 \overline{\mathcal{V}}_{1,\Phi} = -\frac{\epsilon^{\frac{1}{2}}}{r^2} \text{D}[r^2 \overline{\mathcal{U}}_r \overline{\mathcal{U}}_\theta] - \mathcal{Q}_{z,1} \overline{\mathcal{U}}_2 - m\Omega_1 \overline{\mathcal{V}}_{2,\Theta} - \frac{m}{r} \overline{\mathcal{T}}_{3,\Theta}, \quad (5.12)$$

$$\overline{\mathcal{W}}_{1,T_2} + m\Omega_0 \overline{\mathcal{W}}_{3,\Theta} + \frac{m}{r_c} \overline{\mathcal{W}}_1 \overline{\mathcal{W}}_{1,\Phi} = -\frac{\epsilon^{\frac{1}{2}}}{r} \text{D}[r \overline{\mathcal{U}}_r \overline{\mathcal{U}}_z] + \mathcal{Q}_{\theta,1} \overline{\mathcal{U}}_2 - m\Omega_1 \overline{\mathcal{W}}_{2,\Theta} - \frac{m}{r_c} \overline{\mathcal{T}}_{2,\Phi}. \quad (5.13)$$

The divergences of the mean radial wave momentum fluxes at the r.h.s of (5.12) and (5.13) are $O(1)$ inside the CL. Introducing the inner variables in these terms, taking the limit $r \rightarrow r_a^s$ otherwise, assuming a uniform pressure at r_c , rescaling, and eliminating $\mathcal{V}_{2,\Theta}$ and $\mathcal{W}_{2,\Theta}$, we obtain finally

$$\mathcal{V}_{1,\tau_2} + \varpi \mathcal{W}_1 \mathcal{V}_{1,\Phi} = \Sigma_v^s - \mathcal{Q}_{z,1}^s \mathcal{U}_2 - \mathcal{U}_0 \mathcal{V}_{3,\Theta}^s, \quad (5.14)$$

$$\mathcal{W}_{1,\tau_2} + \varpi \mathcal{W}_1 \mathcal{W}_{1,\Phi} = \Sigma_v^s + \frac{\mathcal{Q}_{\theta,1}^s}{\varpi} \mathcal{U}_2 - \mathcal{U}_0 \mathcal{W}_{3,\Theta}^s, \quad (5.15)$$

$$\text{where } \Sigma_v^\pm = -\overline{[U^{(0)} V_\rho^{(2)}]}(\rho_B^\pm, X). \quad (5.16)$$

Let us decompose $\mathcal{Q}_{z,1}$ in an undistorted and another distorted terms so that one may separate first and third-order velocity evolutions in (5.14) and (5.15)

$$\mathcal{Q}_{z,1}^s = \{\mathcal{Q}_{z,1}\}_-^+ + \mathcal{Q}_{z,1,d}^s, \quad \text{with } \mathcal{Q}_{z,1,d}^s = \frac{s}{2} [\mathcal{Q}_{z,1}]_-^+.$$

By considering a symmetric CL thickness, $\rho_B^- = -\rho_B^+$, subsection 7.1 will show that $\{\Sigma_v\}_-^+ = 0$, so $\Sigma_v = \Sigma_{v,d}$. The third-order terms $\mathcal{U}_0 \mathcal{V}_{3,\Theta}^s$ and $\mathcal{U}_0 \mathcal{W}_{3,\Theta}^s$ are defined so that they may remove the distorted terms in (5.14) and (5.15), we thus get

$$\mathcal{U}_0 \mathcal{V}_{3,\Theta}^s = \Sigma_v^s - \mathcal{Q}_{z,1,d}^s \mathcal{U}_2, \quad \mathcal{U}_0 \mathcal{W}_{3,\Theta}^s = \Sigma_v^s + \frac{\mathcal{Q}_{\theta,1,d}^s}{\varpi} \mathcal{U}_2. \quad (5.17)$$

As was done in the preceding subsection, the contribution of the mean wave momentum flux is included inside the first-order mean vorticity. The modified vorticities at r_c are

then denoted of the following way

$$\hat{Q}_{z,1} = Q_{z,1} - \frac{\Sigma_v}{U_2}, \quad \hat{Q}_{\theta,1} = Q_{\theta,1} + \varpi \frac{\Sigma_v}{U_2}.$$

The evolution equations of the CL induced velocity $(\mathcal{V}_1, \mathcal{W}_1)$ are therefore

$$\mathcal{V}_{1,\tau_2} + \varpi \mathcal{W}_1 \mathcal{V}_{1,\Phi} = -\{Q_{z,1}\}_-^+ U_2, \quad \mathcal{W}_{1,\tau_2} + \varpi \mathcal{W}_1 \mathcal{W}_{1,\Phi} = \frac{\{Q_{\theta,1}\}_-^+}{\varpi} U_2. \quad (5.18)$$

The first-order mean velocity at r_c , $(\mathcal{V}_1, \mathcal{W}_1)$ is vertically advected by \mathcal{W}_1 and is driven by the undistorted divergence of its radial flux generated by U_2 . The forcing Σ_v is absent since it is antisymmetric, it appears in the definitions of \mathcal{V}_3 and \mathcal{W}_3 . Jointly with the distorted mean vorticities, it generates a Θ -secular growth of the third-order mean velocities. In C17, the latter have a τ_2 -linear growth.

6. The second-order inner flow

This section gives the analytical expressions of the leading-order non-trivial inviscid flow in the critical layer. The azimuthal velocity $V^{(2)}$ defined through the streamfunction-like function $\psi^{(2)}$ is solution of the azimuthal-momentum equation (6.1):

$$V^{(2)} = \frac{1}{2} \rho^2 - s_i \mathcal{S}_1 \rho + \mathcal{V}_2 + \psi_\rho^{(2)},$$

the vertical momentum equation (6.2) follows.

$$\begin{aligned} A \sin X \psi_{\rho\rho}^{(2)} + \rho \psi_{\rho X}^{(2)} - \psi_X^{(2)} &= s_i \psi_{\rho\tau_1}^{(2)} + (U_2 - \mathcal{U}_0 H_{2,\Theta}) (\psi_{\rho\rho}^{(2)} - s_i Q_{z,1}) + s_i \mathcal{U}_0 [V^{(5)} - \mathcal{V}_3]_\Theta \\ &+ s_i \Sigma_v + [\mathcal{P}^{(2)} - s_i \mathfrak{P}_3]_\Theta + [(1 - 2\mathcal{U}_0)\rho - \frac{s_i}{2} (\mathcal{S}_1 - \mathcal{C}_0 \mathcal{C}_1)] H_{2,\Theta} \\ &+ \lambda' (\psi_{i,\rho\rho\rho}^{(2)} - \hat{\zeta}) A + \Pi_{2,X}(X), \end{aligned} \quad (6.1)$$

$$\begin{aligned} A \sin X W_\rho^{(2)} + \rho W_X^{(2)} - \psi_X^{(2)} &= s_i \psi_{\rho\tau_1}^{(2)} + (U_2 - \mathcal{U}_0 H_{2,\Theta}) (W_\rho^{(2)} + s_i \frac{Q_{\theta,1}}{\varpi}) + s_i \mathcal{U}_0 [W^{(5)} - \mathcal{W}_3]_\Theta \\ &+ s_i \Sigma_v + \frac{\mathcal{V}_{1,\Phi}}{\varpi} \rho + \lambda' (W_{i,\rho\rho}^{(2)} + \frac{\hat{\zeta}_{\theta,0}}{\varpi}) A + \Pi_{2,X}(X). \end{aligned} \quad (6.2)$$

The geopotential $\mathcal{P}^{(2)}$ and the radial velocity $U^{(2)}$ are expressed as functions of $\psi^{(2)}$ and $W^{(2)}$ via the radial momentum and mass conservation equations

$$\begin{aligned} \mathcal{P}^{(2)}(\rho, X) &= \frac{1}{2} \rho^3 - \frac{s_i}{4} (3\mathcal{S}_1 + \mathcal{C}_0 \mathcal{C}_1) \rho^2 + [\frac{1}{4} (\mathcal{S}_1^2 - \mathcal{C}_1^2) + \mathcal{V}_2 - H_2] \rho \\ &+ \frac{s_i}{2} (\mathcal{S}_1 - \mathcal{C}_0 \mathcal{C}_1) H_2 + \psi^{(2)} + \Pi_2(X) + s_i \mathfrak{P}_3, \end{aligned} \quad (6.3)$$

$$U_\rho^{(2)}(\rho, X) = U'_2 + A \sin X - \psi_{\rho X}^{(2)} - \varpi^2 W_X^{(2)}. \quad (6.4)$$

The equations (6.1-6.4) are valid inside and outside the separatrices but yield distinct solutions. Note that the forcing Σ_v appearing in both equations (6.1) and (6.2) results from respectively substituting the evolution equations (5.14) and (5.15) for \mathcal{V}_{1,τ_2} and \mathcal{W}_{1,τ_2} , it vanishes inside the separatrices since the related forcing is there equal to the mean $\{\Sigma_v\}_-^+ = 0$.

6.1. Outside the separatrices

The CL flow is decomposed between a Θ -dependent spiraling contribution and a purely oscillating one. For instance, for the fifth-order velocity $V^{(5)}$, we have

$$V^{(5)} = V_{sp}^{(5)}(\rho, X, \Theta) + V_{os}^{(5)}(\rho, X).$$

The matchings of $V_{sp}^{(5)}$ and $W_{sp}^{(5)}$ on the CL edges as $\rho \rightarrow \rho_B^\pm$ give the asymptotic behaviours

$$\begin{aligned} V_{sp}^{(5)} \rightarrow & \frac{1}{2} \zeta_{z,1,sp} \rho^2 + s_i [\mathcal{Q}_{z,2,sp} + (\hat{\zeta} + 2)H_2] \rho + \hat{\zeta} \beta_{l,1} \ln |\rho^*| A \cos X \\ & + \mathcal{V}_{3,sp} + V_{5,sp}(X) + s_i \hat{\zeta} A \frac{\cos X}{\rho} H_2 + O(\rho^{-2}), \end{aligned} \quad (6.5)$$

$$\begin{aligned} W_{sp}^{(5)} \rightarrow & -\frac{1}{2} \frac{\zeta_{\theta,1,sp}}{\varpi} \rho^2 - s_i (\mathcal{Q}_{\theta,2,sp} + \hat{\zeta}_{\theta,0} H_2) \frac{\rho}{\varpi} + \hat{\zeta} \beta_{l,1} \ln |\rho^*| A \cos X \\ & + \mathcal{W}_{3,sp} + W_{5,sp}(X) + s_i \hat{\zeta} A \frac{\cos X}{\rho} H_2 + O(\rho^{-2}), \end{aligned} \quad (6.6)$$

the expressions of $V_{5,sp}$ and $W_{5,sp}$ being displayed in Appendix C.

The radial advections: $\mathcal{U}_2 \psi_{\rho\rho}^{(2)}$ and $\mathcal{U}_2 W_\rho^{(2)}$, the spiraling motions $\mathcal{P}_{sp}^{(2)}$, $V_{sp}^{(5)}$, $W_{sp}^{(5)}$ and the forcing Σ_v bring about a secularity with respect to the phase X in the angular and axial momentum equations (6.1) and (6.2), which makes their integration uneasy. The second-order outer flow gives a spiraling shift $h_2(\eta) = \overline{U}_2(\eta)/[m\Omega_0(\eta)]\Theta$. This deformation can be found out heuristically. Indeed, an air particle located on a streamline η undergoes a radius variation δr after a time interval δt such as $\delta r = \epsilon \delta h_2(\eta) = \epsilon \overline{U}_2(\eta) \delta t$ while it rotates of an angle $\delta \theta = \Omega_0(\eta) \delta t$. An expression for H_2 can be determined by removing the advection terms in (6.1) and (6.2)

$$H_2(\Theta) = \frac{\mathcal{U}_2}{\mathcal{U}_0} \Theta, \quad (6.7)$$

which can be easily matched with h_2 as $\eta \rightarrow 0$: $H_2 = h_2(0)$ in rescaled variables. The deformation H_2 has been found a second time in Appendix F while integrating the streamline equations. Note that inside the separatrices, we have $H_2^\circ = H_2$.

The remaining secularity must be eliminated by determining $V_{sp}^{(5)}$ and $W_{sp}^{(5)}$ properly. Let us now define $V_{sp}^{(5)}$ and $W_{sp}^{(5)}$ in this way

$$V_{sp}^{(5)} = s s_i \zeta_{z,1,sp} \mathcal{K}_{0,\rho^{-1}} A^{\frac{1}{2}} + s_i (\mathcal{Q}_{z,2,sp} + 2H_2) \rho + \mathcal{V}_{3,sp} + V_{5,sp}(X) + \psi_{sp,\rho}^{(5)}, \quad (6.8)$$

$$W_{sp}^{(5)} = -s s_i \frac{\zeta_{\theta,1,sp}}{\varpi} \mathcal{K}_{0,\rho^{-1}} A^{\frac{1}{2}} - s_i [\mathcal{Q}_{\theta,2,sp} + (\hat{\zeta} \varpi + \hat{\zeta}_{\theta,0}) H_2] \frac{\rho}{\varpi} + \mathcal{W}_{3,sp} + W_{5,sp}(X) + \psi_{sp,\rho}^{(5)}. \quad (6.9)$$

The unknown function $\mathcal{K}_0 A^{1/2}$ must tend to $|\rho| \gg 1$ as $\rho \rightarrow \rho_B^\pm$. Substituting the velocities (6.8) and (6.9) in the equations (6.1) and (6.2) simplifies the momentum equations

$$\begin{aligned} A \sin X \psi_{\rho\rho}^{(2)} + \rho \psi_{\rho X}^{(2)} - \psi_X^{(2)} &= s_i \psi_{\rho\tau_1}^{(2)} + s_i \mathcal{U}_0 [\psi_{sp,\rho}^{(5)} + V_{5,sp}] \Theta \\ &- \hat{\zeta} \mathcal{U}_2 \rho + s \Sigma_q' \mathcal{K}_{0,\rho^{-1}} A^{\frac{1}{2}} + s_i \Sigma_v + \lambda' \left(\psi_{i,\rho\rho\rho}^{(2)} - \hat{\zeta} \right) A + \Pi_{2,\Theta} + \Pi_{2,X}, \end{aligned} \quad (6.10)$$

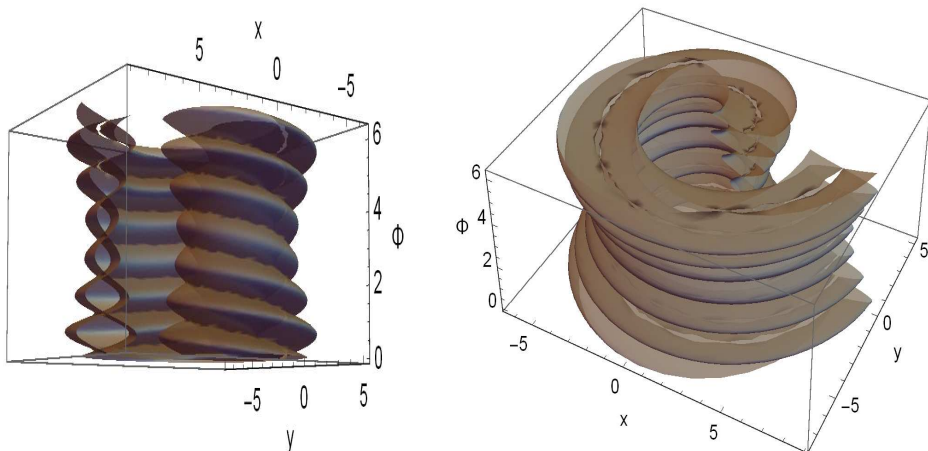


FIGURE 3. Separatrices $Z = A$ as functions of x, y and Φ , $m = 2$, $\epsilon = 0.1$, $\varpi = 2$, $r_c = 2$, $\mathcal{U}_2 = 1$, $\mathcal{U}_0 = 0.5$, $A(\Phi) = [1 + \cos(\Phi)/2]^2$.

$$A \sin X W_\rho^{(2)} + \rho W_X^{(2)} - \psi_X^{(2)} = s_i \psi_{\rho\tau_1}^{(2)} + s_i \mathcal{U}_0 [\psi_{sp,\rho}^{(5)} + W_{5,sp}] \Theta - \hat{\zeta} \mathcal{U}_2 \rho + s \Sigma_q' \mathcal{K}_{0,\rho^{-1}} A^{\frac{1}{2}} + s_i \Sigma_v + \lambda' \left(W_{i,\rho\rho}^{(2)} + \frac{\Sigma_q}{\mathcal{U}_2} \right) A + \Pi_{2,X}. \quad (6.11)$$

A small equivalent Richardson number at r_c enables one to uncouple the axial motion. The vertical motion is thus absent from the equation (6.10), which models the leading-order non-trivial dynamics inside a two-dimensional, cylindrical, steady and unstratified critical layer (Haberman (1972); Caillol & Maslowe (2007); Caillol (2014)). This equation however possesses extra terms, owing to the spiraling motion generated by the mean radial velocity \mathcal{U}_2 , which makes this CL flow more complex. Solving the equation (6.10) gives the second-order azimuthal velocity, then the resolution of Eq. (6.11) yields the axial velocity. To solve (6.10), a second change of radial variables $(\rho, X) \rightarrow (Z, x)$ is performed where

$$Z = \frac{1}{2}\rho^2 + A \cos X. \quad (6.12)$$

Each streamline is described by a unique value of the variable Z but one value of Z yields two streamlines located at either side of the CL axis, each one characterized by $s = \pm$ (cf. figure 2). The variable Z increases from $Z = -A$ in the cat's eye center to $Z = A$ on the separatrices, to reach large values on the CL edges. See in figure 3 the two helical and spiraling sheets corresponding to the outer and inner separatrices for a $m = 2$ CL and for an arbitrary profile $A(\Phi)$. Inside the frame (ρ, X) , the relationship (6.12) characterizes the classic cat's eye CL pattern. Inside the standard frame (r, θ) , the CL pattern is even more deformed with respect to the tangential basic flow; the symmetry with respect to the axis $r = r_a$ is lost. The CL thickness δ_{cl} scales as $\delta_{cl} = 4r_c \sigma (A\epsilon)^{1/2}$ with $1 \ll \sigma \ll \epsilon^{-1/2}$; σ is the ratio of the CL thickness over the cat's eye thickness, whose value remains undetermined by the nonlinear CL theory. The radius ρ expressed with the variables (Z, x) is denoted $Z_\rho(Z, x) = ss_i [2(Z - A \cos x)]^{1/2}$, ρ^X stands for the absolute value of ρ on the separatrix, $\rho^X(x) = \sqrt{2A} [1 - \cos x]^{1/2}$. Putting the superscript * A -normalizes ρ^X and Z : $\rho^{X*} = \rho^X / A^{1/2}$ and $Z^* = Z/A$.

Differentiating (6.10) with respect to ρ and introducing the variables Z and x , we get

$$Z_\rho \psi_{\rho\rho x}^{(2)} = s_i \bar{\mathcal{U}}_0 \psi_{sp,\rho\rho\Theta}^{(5)} - \hat{\zeta} \mathcal{U}_2 + s \Sigma_{q'} \mathcal{K}_0 A^{\frac{1}{2}} + \lambda' Z_\rho \psi_{i,\rho\rho Z}^{(2)} A. \quad (6.13)$$

The average over x at constant Z of the quantity q is defined by: $\langle q(Z) \rangle = 1/(2\pi) \int_0^{2\pi} q(Z, x) dx$. Let us decompose $\psi_{sp,\rho}^{(5)}$ between its x -averaged and oscillating parts

$$\psi_{sp,\rho}^{(5)} = \langle \psi_{sp,\rho}^{(5)} \rangle + \delta \psi_{sp,\rho}^{(5)} H_2. \quad (6.14)$$

Using the antisymmetry property of the forcing generated by the mean radial wave flux of the axial vorticity radial gradient : $\Sigma_{q'}^- = -\Sigma_{q'}^+$ (cf. Section 7), the inviscid secularity condition applied to (6.13) yields $\langle \psi_{sp,\rho}^{(5)} \rangle$

$$\partial_Z \langle \psi_{sp,\rho}^{(5)} \rangle = s_i \left(\hat{\zeta} - \frac{\Sigma_{q'}^+}{\mathcal{U}_2} A^{\frac{1}{2}} \mathcal{K}_0 [Z^*] \right) \left\langle \frac{H_2}{Z_\rho} \right\rangle. \quad (6.15)$$

The equation (6.13), after the $\psi_{sp,\rho}^{(5)}$ substitution, admits the general inviscid solution

$$\psi_{i,\rho\rho}^{(2)}(Z, x) = \mathcal{F}_2(Z^*) + s_i \int_\pi^x \partial_Z \delta \psi_{sp,\rho}^{(5)}(Z, x_1) + s \Xi(Z^*) G_5(Z^*, x_1) A^{-\frac{1}{2}} dx_1 \mathcal{U}_2, \quad (6.16)$$

$$\text{where } \Xi(Z^*) = \hat{\zeta} - \frac{\Sigma_{q'}^+}{\mathcal{U}_2} A^{\frac{1}{2}} \mathcal{K}_0 [Z^*], \text{ and } G_5(Z^*, x) = \text{SM}[Z^*] - [2(Z^* - \cos x)]^{-\frac{1}{2}}.$$

All mathematical functions needed in the paper are defined in the Appendix H.

The viscous secularity condition applied to equation (6.13) namely $\partial_Z \langle \psi_{i,\rho\rho}^{(2)} \rangle = 0$, as well as the inner axial vorticity matching with the outer flow permit to define \mathcal{F}_2 ,

$$\mathcal{F}_2(Z^*) = s s_i \hat{\zeta} \mathcal{K}_0 [Z^*] A^{\frac{1}{2}} + s_i \hat{\mathcal{Q}}_{z,1}, \quad \text{where } \mathcal{K}_0 [Z] = \sqrt{2Z} + K_0 [Z]. \quad (6.17)$$

From Eqs. (6.5-6.6) and (6.8-6.9), the matching on the CL edges requires this asymptotic behaviour for $\psi_{sp,\rho}^{(5)}$

$$\psi_{sp,\rho}^{(5)}(\rho, X) \rightarrow s_i \hat{\zeta} \left(\rho + A \frac{\cos X}{\rho} \right) H_2 - \frac{1}{2} \frac{\Sigma_{q'}}{\mathcal{U}_2} \cos X A H_2 \text{ as } \rho \rightarrow \rho_B^\pm.$$

According to Eq. (6.15), the x -average of $\psi_{sp,\rho}^{(5)}$ asymptotes

$$\langle \psi_{sp,\rho}^{(5)}(Z) \rangle \rightarrow s_i \hat{\zeta} \left(\rho + A \frac{\cos X}{\rho} + O(\rho^{-3}) \right) H_2 - \frac{\Sigma_{q'}}{\mathcal{U}_2} \left(\frac{1}{2} \rho^2 + A \cos X + O(\rho^{-2}) \right) H_2 \text{ as } \rho \rightarrow \rho_B^\pm.$$

As a result, the expression of $\delta \psi_{sp,\rho}^{(5)}$ is firstly determined

$$\delta \psi_{sp,\rho}^{(5)} = \frac{1}{2} \frac{\Sigma_{q'}}{\mathcal{U}_2} A \cos x. \quad (6.18)$$

Secondly, we deduce that the critical layer generates a small distorted and spiraling mean outer flow near r_c that opposes the Θ -gradient of the mean vorticity radial gradient $(\hat{\zeta}_{z,1}, \hat{\zeta}_{\theta,1})$

$$\frac{\overline{V}(r, \Theta)}{\varrho_c r_c} = \frac{\overline{W}(r, \Theta)}{\varpi \varrho_c r_c} = -\frac{1}{2} \frac{\Sigma_{q'}}{\mathcal{U}_2} \left(\frac{r}{r_c} - 1 \right)^2 H_2(\Theta) \epsilon^{\frac{1}{2}};$$

the resulting vorticity radial gradient $(\hat{\zeta}_{z,1}, \hat{\zeta}_{\theta,1})$ is thus Θ -independent.

The vorticity $\psi_{i,\rho\rho}^{(2)}$ is invariant by the transformations $\mathcal{U}_2 \rightarrow -\mathcal{U}_2$ and $x \rightarrow 2\pi - x$. As a result, the CL study can be restricted to positive values of \mathcal{U}_2 . The function \mathcal{F}_2 in

(6.17) is similar to that used in Caillol & Maslowe (2007); Caillol (2012, 2014) because it was again derived from the secularity condition applied to the viscous axial vorticity equation. However, the axial vorticity radial gradient $\hat{\zeta}$ and the induced mean vorticity $\hat{Q}_{z,1}$ are now corrected by the mean radial wave fluxes. In quasi-steady 3D helical or 2D critical layers, each iso axial-vorticity contour was defined so far by a unique value of the variable Z (Maslowe (1986); Caillol & Grimshaw (2007, 2012); Caillol (2014), C17). Here, streamlines do not coincide with isovorticity lines because the CL flow has stronger 3D features. The mean velocity \mathcal{U}_2 considerably alters the inner axial vorticity. The expression obtained in C17 is slightly different because it was derived from the inviscid secularity condition appearing at the next-order axial-vorticity equation. The chosen inner variables did not define weakly spiraling streamlines. As the leading-order mean radial velocity was $O(\epsilon^{3/2})$, the present formulation applied to that study would imply to take $H_2 = 0$ and to define a first spiraling deviation: $H_3(\Theta) = \mathcal{U}_3/\mathcal{U}_0\Theta$. The same function \mathcal{F}_2 in (6.17) would be then deduced but the integral in (6.16) would appear in the expression of the $O(\epsilon)$ axial vorticity. The mean flow at r_c would be however modified in the same way: $\hat{\zeta} = \zeta - \Sigma_q/\mathcal{U}_3$, $\hat{Q}_{z,1} = \mathcal{Q}_{z,1} - \Sigma_v/\mathcal{U}_3$.

The function G_5 is singular on the separatrices, indeed the average $\langle 1/Z_\rho \rangle$ is infinite there. The streamlines need be therefore regularized near the meeting points of the separatrices. To do so, we consider that the corner angle made by both separatrices is equal to 180° at this meeting point. For phases close to $0 [2\pi]$, that is for $|x| \leq \mu$ or $|2\pi - x| \leq \mu$, with $\mu \ll 1$, and for $|Z - A| \ll 1$, we assume that the inner radius ρ has the following behaviour

$$\rho = ss_i \sqrt{2} [Z - A(1 - bx^{1+\gamma})]^{\frac{1}{2}}, \quad \text{with } b = (1 - \cos \mu) \mu^{-(1+\gamma)} \simeq \frac{\mu^{1-\gamma}}{2}.$$

Regularization requires an exponent $\gamma \leq 0$. Integrating $\psi_{i,\rho}^{(2)}$ over ρ yields the second-order azimuthal velocity

$$\begin{aligned} \psi_{i,\rho}^{(2)}(Z, x) &= \hat{\zeta} \left(\int_{\infty}^{Z^*} \frac{K_0[z] dz A}{[2(z - \cos x)]^{\frac{1}{2}}} + [Z(Z - A \cos x)]^{\frac{1}{2}} + A \cos x \ln[A(Z, x)] \right) \quad (6.19) \\ &+ ss_i \int_{\infty}^{Z^*} \int_{\pi}^x G_5(z, x_1) dx_1 \frac{\Xi(z) dz}{Z_\rho(Az, x)} A^{\frac{1}{2}} \mathcal{U}_2 + s_i \hat{Q}_{z,1} Z_\rho + V_2(x), \text{ with} \\ A(Z, x) &= \sqrt{Z} + \sqrt{Z - A \cos x} \quad \text{and} \quad V_2(x) = -[a + 1 - \frac{\hat{\zeta}}{2}(1 + 3\varpi^2) - \varpi \hat{\zeta}_{\theta,0}] \frac{A \cos x}{1 + \varpi^2}. \end{aligned}$$

The solvability condition (4.2) implies $\psi_{\rho\theta}^{(2)} = 0$, which leads to $A_\theta = a_\theta = \mathcal{U}_{2,\theta} = 0$. The leading-order induced mean flow at r_c : $\mathcal{V}_1, \mathcal{W}_1, \mathcal{Q}_{z,1}, \mathcal{Q}_{\theta,1}, \mathfrak{P}_1, \mathcal{V}_2, \mathcal{W}_2, \mathfrak{P}_2$, and \mathcal{U}_2 , the phase jump a and the wave amplitude A are therefore Θ -independent. The mean velocity is thus very weakly spiraling since it starts to be Θ -dependent at the third order whereas the mean vorticity becomes Θ -dependent at the second order and the mean vorticity radial gradient at the first order.

Integrating once again over ρ gives $\psi^{(2)}$

$$\begin{aligned} \psi_i^{(2)}(Z, x) = & \hat{\zeta} \left(\frac{ss_i}{6} (2Z)^{\frac{3}{2}} + \{Z_\rho \ln[A(Z, x)] - ss_i \sqrt{2Z}\} A \cos x \right) \\ & + \hat{\zeta} \left(Z_\rho \int_\infty^{Z^*} \frac{K_0[z] dz}{\sqrt{2(z - \cos x)}} - ss_i \int_\infty^{Z^*} K_0[z] dz A^{\frac{1}{2}} \right) A - \frac{s_i}{2} \Sigma_{q'} \ln Z^* A \sin x \\ & + ss_i \left(Z_\rho \int_\infty^{Z^*} \int_\pi^x G_5(z, x_1) dx_1 \frac{\Xi(z) dz}{Z_\rho(Az, x)} - \int_\infty^{Z^*} \left(\hat{\zeta} - \frac{\Sigma_{q'}^+}{\mathcal{U}_2} A^{\frac{1}{2}} K_0[z] \right) \int_\pi^x G_5(z, x_1) dx_1 dz \right. \\ & \left. + \frac{\Sigma_{q'}^+}{\mathcal{U}_2} A^{\frac{1}{2}} \int_\infty^{Z^*} \sqrt{2z} \int_\pi^x G_5(z, x_1) dx_1 + \frac{\sin x}{2z} dz \right) A^{\frac{1}{2}} \mathcal{U}_2 + s_i \hat{\mathcal{Q}}_{z,1}(Z - A \cos x) + V_2(x) Z_\rho. \end{aligned}$$

The matchings of the equations (6.10) and (6.11) on the CL edges give two distinct expressions of the integration function Π_2

$$\begin{aligned} \Pi_{2,X} = & s_i \{ \hat{\mathcal{Q}}_{z,1} \sin X - \frac{1}{2} \Sigma_{q'} \ln(4A) \cos X \} A - s_i \mathcal{U}_0 V_{5,sp,\Theta}(X) - s_i \psi_{\rho\tau_1}^{(2)} - \Pi_{2,\Theta} \\ = & s_i \{ \hat{\mathcal{Q}}_{z,1} \sin X - \frac{1}{2} \Sigma_{q'} \ln(4A) \cos X \} A - s_i \mathcal{U}_0 W_{5,sp,\Theta}(X) - s_i \psi_{\rho\tau_1}^{(2)}. \quad (6.20) \end{aligned}$$

The pressure matching on the CL edges gives a third expression. Equating the three expressions come down to determine the Θ -gradients of the first-order coefficients β and κ . From the definitions of the Frobenius series terms in Appendix A, the third Π_2 expression is

$$\begin{aligned} \Pi_2(X) = & -s_i \{ \hat{\mathcal{Q}}_{z,1} \cos X + \frac{\Sigma_{q'}}{2} [\ln(4A) - 2] \sin X \} A \\ & + s_i \mathcal{U}_0 \partial_\Theta \left[\left(\alpha_{l,1} - \vartheta \beta_{l,1} + \varpi \hat{\zeta}_{\theta,1} + (1 - \varpi \hat{\zeta}_{\theta,0}) \frac{\hat{\zeta}_{z,1}}{\hat{\zeta}} + \frac{\varpi \mathcal{U}_0^2 (\Xi + 2)}{6 \hat{\zeta} (1 + \varpi^2)} \partial_\Theta^2 [\varpi \zeta_{z,1}'' + \zeta_{\theta,1}''] \right) (0) \right] A \\ & \quad + (\alpha_{d,1} - \vartheta \beta_{d,1}) A_\Phi + (\alpha_{ad,1} - \vartheta \beta_{ad,1}) a_\Phi A \Big] \frac{\sin X}{1 + \varpi^2} \\ & + s_i \mathcal{U}_0 \partial_\Theta \left[\left(\gamma_{l,1} - \vartheta \kappa_{l,1} - \frac{\mathcal{U}_0}{\hat{\zeta}} \left(\frac{\hat{\zeta}}{2} \varpi^2 + \varpi \hat{\zeta}_{\theta,0} - 1 \right) \zeta'_{z,1,\Theta}(0) + \frac{\mathcal{U}_0}{2} \varpi \zeta'_{\theta,1,\Theta}(0) \right. \right. \\ & \left. \left. - \frac{\varpi \mathcal{U}_0^2 (\Xi + 2)}{24 \hat{\zeta} (1 + \varpi^2)} \partial_\Theta^3 \left(\mathcal{U}_0 [\varpi \zeta_{z,1}'''' + \zeta_{\theta,1}'''] + \varpi [\mathcal{U}_0 \hat{\zeta} (1 + \varpi^2) + 4(\mathcal{U}_0 - 1)] \zeta_{z,1}'' \right) (0) \right) \right] A \\ & \quad + (\gamma_{d,1} - \vartheta \kappa_{d,1}) A_\Phi + (\gamma_{ad,1} - \vartheta \kappa_{ad,1}) a_\Phi A \Big] \frac{\cos X}{1 + \varpi^2}, \quad (6.21) \end{aligned}$$

with $\vartheta = \hat{\zeta}(2 + 3\varpi^2) + \varpi \hat{\zeta}_{\theta,0} - 1$ and $\Xi = \hat{\zeta}(1 - \varpi^2) - 2\varpi \hat{\zeta}_{\theta,0}$.

The double radial gradients of the first-order mean vorticity: $\zeta'_{z,1}$ and $\zeta'_{\theta,1}$ cannot be calculated here because they are deduced from the next-order radial wave fluxes. The higher gradients $\zeta''_{z,1}$, $\zeta''_{\theta,1}$, $\zeta'''_{z,1}$ and $\zeta'''_{\theta,1}$ are calculated through higher-order wave fluxes. As the Θ -dependence increases algebraically with the order, we then assume that $\zeta'_{z,1}$ and $\zeta'_{\theta,1}$ have a quadratic dependence on Θ . We also assume that $\zeta''_{z,1}$, $\zeta''_{\theta,1}$, $\zeta'''_{z,1}$ and $\zeta'''_{\theta,1}$ have a Θ -dependence at least up to the fourth power. Removing a $O(\epsilon^{3/2}/\eta)$ singular outer radial velocity gives one condition on the fourth-order Θ -partial derivatives of $\zeta''_{z,1}$ and $\zeta''_{\theta,1}$

$$\partial_\Theta^4 \zeta''_{\theta,1}(0) = -\varpi \partial_\Theta^4 \zeta''_{z,1}(0). \quad (6.22)$$

Supposing the first-order coefficients α , β , γ and κ linear in Θ , we deduce that Π_2 is Θ -independent. Introducing the expressions of $V_{5,sp}$ and $W_{5,sp}$, (C1) and (C2) of

Appendix C in the equality (6.20), two relationships then appear, respectively involving the coefficients β and κ

$$\hat{\zeta}(1 + \varpi^2)(\hat{\zeta}\varpi + \hat{\zeta}_{\theta,0})[\beta_{l,1} + \beta_{d,1}\frac{A_{\Phi}}{A} + \beta_{ad,1}a_{\Phi}]_{\Theta} = \frac{\mathfrak{U}_0^2}{6}\Xi\partial_{\Theta}^3[\varpi\zeta''_{z,1} + \zeta''_{\theta,1}](0), \quad (6.23)$$

$$\begin{aligned} &(\hat{\zeta}\varpi + \hat{\zeta}_{\theta,0})[\kappa_{l,1} + \kappa_{d,1}\frac{A_{\Phi}}{A} + \kappa_{ad,1}a_{\Phi}]_{\Theta} = \frac{\mathfrak{U}_0}{2}\partial_{\Theta}^2\left[\zeta'_{\theta,1} - (\hat{\zeta}\varpi + 2\hat{\zeta}_{\theta,0})\frac{\zeta'_{z,1}}{\hat{\zeta}}\right](0) \\ &- \frac{\mathfrak{U}_0^2\Xi}{24\hat{\zeta}(1 + \varpi^2)}\partial_{\Theta}^4\left[[\mathfrak{U}_0\hat{\zeta}(1 + \varpi^2) + 4(\mathfrak{U}_0 - 1)]\varpi\zeta''_{z,1} + \mathfrak{U}_0(\varpi\zeta'''_{z,1} + \zeta'''_{\theta,1})\right](0). \end{aligned} \quad (6.24)$$

Then, comparing (6.20) and (6.21), we find that the r.h.s of (6.24) vanishes and get

$$\mathfrak{U}_0\hat{\zeta}[\beta_{l,1} + \beta_{d,1}\frac{A_{\Phi}}{A} + \beta_{ad,1}a_{\Phi}]_{\Theta} = 0, \quad (6.25)$$

if we take $\psi_{\rho\tau_1}^{(2)} = -\Sigma_{q'}A\cos x$. The Θ -gradients of $\zeta'_{z,1}$, $\zeta'_{\theta,1}$, $\zeta''_{z,1}$ and $\varpi\zeta'''_{z,1} + \zeta'''_{\theta,1}$ are thus linked in this way

$$\begin{aligned} &\hat{\zeta}(1 + \varpi^2)\partial_{\Theta}^2\left[\zeta'_{\theta,1} - (\hat{\zeta}\varpi + 2\hat{\zeta}_{\theta,0})\frac{\zeta'_{z,1}}{\hat{\zeta}}\right](0) \\ &= \frac{\mathfrak{U}_0}{12}\Xi\partial_{\Theta}^4\left[[\mathfrak{U}_0\hat{\zeta}(1 + \varpi^2) + 4(\mathfrak{U}_0 - 1)]\varpi\zeta''_{z,1} + \mathfrak{U}_0(\varpi\zeta'''_{z,1} + \zeta'''_{\theta,1})\right](0). \end{aligned} \quad (6.26)$$

The second no-jump condition of (4.4) is trivially satisfied, but insuring the first no-jump condition imposes the existence of a τ_1 -secular distorted evolution of the phase jump a

$$a_{\tau_1}^s = (1 + \varpi^2)\Sigma_{q'}^s. \quad (6.27)$$

Next, combining (6.23) and (6.25) yields the same relationship (6.22) for the third-order Θ -derivatives of $\zeta''_{z,1}$ and $\zeta''_{\theta,1}$

$$\partial_{\Theta}^3\zeta''_{\theta,1}(0) = -\varpi\partial_{\Theta}^3\zeta''_{z,1}(0). \quad (6.28)$$

According to the expressions of the coefficients $c_{j,1,0}$ and $f_{j,1,0}$, $j = l, d$ and ad in Appendix A, the no-jump condition of (4.5) imposes

$$[J_{1,c}]_{-}^{+} = 0, \quad (6.29)$$

while the condition (4.6) is straightforwardly satisfied. In order to derive the most general evolution equations, any dependence relationships must be avoided between A , A_{Φ} and $a_{\Phi}A$, which imposes

$$\beta_{j,1\Theta} = 0, \text{ and } \kappa_{j,1,\Theta} = 0, \quad j = l, d \text{ and } ad. \quad (6.30)$$

The particular solution is obtained through the viscous secularity condition $\partial_Z(W_{i,\rho}^{(2)} - \psi_{i,\rho\rho}^{(2)} + \zeta Z_{\rho}) = 0$ and the CL edge matching, the found axial velocity is then roughly proportional to the azimuthal velocity, once again highlighting the helical motion inside the nonlinear critical layer

$$W_i^{(2)}(Z, x) = \psi_{i,\rho}^{(2)}(Z, x) - \zeta Z - ss_i\frac{J_{1,c}}{\varpi^2}\mathcal{K}_0[Z^*]A^{\frac{1}{2}} + W_2. \quad (6.31)$$

The expression (6.4) of the radial velocity $U^{(2)}$ can be then calculated

$$\begin{aligned}
 U^{(2)}(Z, x) = & \hat{\zeta}(1 + \varpi^2) \left(Z_\rho \int_\infty^{Z^*} \frac{K_0[z] dz A^{\frac{3}{2}}}{|Z_\rho(Az, x)|^3} + \left\{ \ln[A(Z, x)] + \frac{1}{2} \right\} Z_\rho - s s_i \sqrt{2Z} \right) A \sin x \\
 & - s s_i (1 + \varpi^2) \left(Z_\rho \int_\infty^{Z^*} \Xi(z) \frac{G_5(z, x)}{Z_\rho(Az, x)} dz - Z_\rho \int_\infty^{Z^*} \int_\pi^x G_5(z, x_1) dx_1 \frac{\Xi(z) dz}{Z_\rho(Az, x)^3} A \sin x \right. \\
 & - \int_\infty^{Z^*} \left(\hat{\zeta} - \frac{\Sigma_{q'}^+}{\mathcal{U}_2} A^{\frac{1}{2}} K_0[z] \right) G_5(z, x) dz + \frac{\Sigma_{q'}^+}{\mathcal{U}_2} A^{\frac{1}{2}} \int_\infty^{Z^*} \sqrt{2z} G_5(z, x) + \frac{\cos x}{2z} dz \Big) A^{\frac{1}{2}} \mathcal{U}_2 \\
 & + \frac{s_i}{2} (1 + \varpi^2) \Sigma_{q'} \left((\ln Z^* - 2) \cos x - \frac{\sin^2 x}{Z^*} \right) A + [(1 - \zeta \varpi^2) A \sin x - (1 + \varpi^2) V_2'(x) + \mathcal{U}_2'] Z_\rho \\
 & - s s_i J_{1,c} \left(K_1[Z^*, x] + \ln[A(Z, x)] \right) A \sin x + \Upsilon_2(x) + s_i \mathcal{U}_3.
 \end{aligned} \tag{6.32}$$

The matching of $U^{(2)}$ with the outer flow gives the integration function

$$\begin{aligned}
 \Upsilon_2(x) = & -s_i \{ [\beta_{l,1} + d_{l,1,0} + (\beta_{\omega d,1} + d_{\omega d,1,0}) \mathcal{U}_{1,\Phi} \tau_1] A + (\beta_{d,1} + d_{d,1,0}) A_\Phi \\
 & + (\beta_{ad,1} + d_{ad,1,0}) a_\Phi A \} \sin x - s_i \{ (\kappa_{l,1} + g_{l,1,0}) A + (\kappa_{d,1} + g_{d,1,0}) A_\Phi \\
 & + (\kappa_{ad,1} + g_{ad,1,0}) a_\Phi A \} \cos x - \kappa_{h,1} A \cos(2x), \tag{6.33}
 \end{aligned}$$

the different coefficients $d_{j,1,0}$ and $g_{j,1,0}$, $j = l, d, ad$ and ωd being given in Appendix A.

Owing to the extra terms in (6.16) generated by the velocity \mathcal{U}_2 and the mean radial wave fluxes, the symmetry with respect to the CL axis is broken due to the appearance of a Fourier sine series in $\psi_{\rho\rho}^{(2)}(\rho, x)$, $V^{(2)}$ and $W^{(2)}$, which allows for non-zero leading-order inviscid mean radial wave fluxes since the zeroth-order radial velocity is simply taken $U^{(0)} \equiv A \sin x$. The wave/vortex interaction is thus enhanced in the quasi-steady régime when the wave envelope is taken with a short height scale $O(\epsilon^{-1/2})$ whereas the scale $O(\epsilon^{-1})$ postpones the appearance of the inviscid mean wave fluxes to the next order.

6.2. Within the separatrices

We here solve the second-order inner flow equations (6.1), (6.2) inside the cat's eye and match the solution with the preceding-subsection inner flow on the separatrices. Firstly, we match the leading-order vorticity, then pressure and velocity. We will finally obtain an unique inviscid CL solution at the first non-trivial order.

The second-order velocity inside the cat's eye is defined through the function $\psi^{(2,\odot)}$

$$V^{(2,\odot)} = \frac{1}{2} \rho^2 - s_i \mathcal{S}_1 \rho + \{ \mathcal{V}_2 \}_\pm^\pm + \psi_\rho^{(2,\odot)}.$$

An explicit and exact solution for the axial vorticity $\psi_{\rho\rho}^{(2,\odot)}$ cannot be found. We then seek an approximate solution through a Galerkin method. According to the symmetry properties of $\psi_{\rho\rho}^{(2)}$, the vorticity $\psi_{\rho\rho}^{(2,\odot)}$ is expanded as a Fourier sine series:

$$\psi_{\rho\rho}^{(2,\odot)}(\rho, X) = \mathcal{F}_2^\odot(Z, \Phi) + \Xi(1) \sum_{n=1}^{\infty} b_n(\bar{\rho}) \sin(nX) \frac{\mathcal{U}_2}{A^{\frac{1}{2}}}. \tag{6.34}$$

The order n term b_n is itself a weighted sum of odd Chebyshev polynomials of the variable $\bar{\rho} = \rho/\rho^X$. Applying the Prandtl-Batchelor theorem inside the cat's eye (cf. Appendix E) leads to the following restrictive condition

$$\mathcal{F}_2^\odot(Z, \Phi) = Q^{(2,\odot)}(\Phi).$$

The fifth-order azimuthal and axial spiraling velocities are defined of the following way

$$V_{sp}^{(5,\odot)} = s_i \left(2H_2 + \{\mathcal{Q}_{z,2,sp}\}_-^+ \right) \rho + \{\mathcal{V}_{3,sp}\}_-^+ + \{V_{5,sp}(x)\}_-^+ + \psi_{sp,\rho}^{(5,\odot)}, \quad (6.35)$$

$$W_{sp}^{(5,\odot)} = -s_i \left((\hat{\zeta}\varpi + \hat{\zeta}_{\theta,0})H_2 + \{\mathcal{Q}_{\theta,2,sp}\}_-^+ \right) \frac{\rho}{\varpi} + \{\mathcal{W}_{3,sp}\}_-^+ + \{W_{5,sp}(x)\}_-^+ + \psi_{sp,\rho}^{(5,\odot)}. \quad (6.36)$$

Differentiating the equation (6.1) with respect to ρ and substituting the expression (6.35) for $V_{sp}^{(5,\odot)}$, we obtain the axial-vorticity equation inside the separatrices in the frame (Z, x)

$$Z_\rho \psi_{\rho\rho x}^{(2,\odot)} = s_i \mathcal{U}_0 \psi_{sp,\rho\rho\Theta}^{(5,\odot)} - \hat{\zeta} \mathcal{U}_2 + \lambda' Z_\rho \psi_{i,\rho\rho Z}^{(2,\odot)} A. \quad (6.37)$$

The velocity $\psi_{sp,\rho}^{(5,\odot)}$ is defined by introducing the function G_5^\odot such as

$$\psi_{sp,\rho}^{(5,\odot)}(Z, x, \Theta) = s_i \hat{\zeta} Z_\rho H_2 + s \Xi(1) \int_1^{Z^*} G_5^\odot(z, x) dz A^{\frac{1}{2}} H_2 + V_{5,sp}^\odot(x, \Theta), \quad (6.38)$$

which results in the solution $\psi_{i,\rho\rho}^{(2,\odot)}$ of (6.37)

$$\psi_{i,\rho\rho}^{(2,\odot)}(Z, x) = Q^{(2,\odot)} + s s_i \Xi(1) \int_\pi^x G_5^\odot(Z^*, x_1) dx_1 \frac{\mathcal{U}_2}{A^{\frac{1}{2}}}. \quad (6.39)$$

We identify G_5^\odot by differentiating with respect to x the expression (6.34) of $\psi_\rho^{(2,\odot)}$:

$$G_5^\odot(Z^*, x) = s s_i \sum_{n=1}^{\infty} \left[b_n [\bar{\rho}(Z^*, x)] \sin(nx) \right]_x, \quad \text{with } \bar{\rho}(Z^*, x) = s s_i \left(\frac{Z^* - \cos x}{1 - \cos x} \right)^{\frac{1}{2}}.$$

The inviscid secularity condition applied to (6.37) is then straightforwardly satisfied on a streamline $Z \leq A$. The axial-vorticity matching involving the expressions (6.16) and (6.34) leads to the determination of the terms $b_n(1)$:

$$b_n(1) = \frac{2}{n} \langle G_5(1, x) \cos(nx) \rangle, \quad \forall n \geq 1. \quad (6.40)$$

The same matching also yields the first-order mean-vorticity jump and the uniform cat's eye vorticity $Q^{(2,\odot)}$

$$[\hat{\mathcal{Q}}_{z,1}]_-^+ = -2\mathcal{C} \hat{\zeta} A^{\frac{1}{2}}, \quad [\mathcal{Q}_{z,1}]_-^+ = 2 \frac{\Sigma_v^+}{\mathcal{U}_2} - 2\mathcal{C} \hat{\zeta} A^{\frac{1}{2}}, \quad Q^{(2,\odot)} = s_i \{\mathcal{Q}_{z,1}\}_-^+, \quad (6.41)$$

where $\mathcal{C} = \mathcal{K}_0[1] = \sqrt{2} + K_0[1] \simeq 1.3788$. The jump of $\mathcal{Q}_{z,1}$ is altered by the mean wave flux induced corrections. The C17 jump is thus erroneous since the mean radial fluxes were omitted. We shall see in Section 7 that this jump is still proportional to $\zeta A^{1/2}$ like in previous studies (Caillol & Maslowe (2007); Caillol (2014)). The jump (6.41) again shows the dynamical coupling between the induced mean flow and the wave packet, coupling that has been omitted until now in wave packet studies in the presence of a critical layer (Benney & Maslowe 1975). The uniform vorticity $Q^{(2,\odot)}$ is still the average between the mean vorticities at either CL side. Moreover, the wave packet assumption keeps unchanged the steady nonlinear CL logarithmic phase shift (Caillol (2014)); it is proportional to λ' as follows

$$\frac{\phi(\lambda')}{\lambda'} = 4s_i \mathcal{C} A^{-\frac{1}{2}}, \quad \lambda' \rightarrow 0.$$

After Eqs. (6.1) and (6.2), the inviscid axial velocity can be written in a general way

within the separatrices

$$\begin{aligned}
 W_i^{(2,\odot)}(Z, x) &= \psi_{i,\rho}^{(2,\odot)}(Z, x) - \zeta Z + \mathcal{J}_2(Z^*) + \{\mathcal{W}_2\}_-^+, \quad \text{where} \\
 \psi_{i,\rho}^{(2,\odot)}(\rho, X) &= \Xi(1) \sum_{n=1}^{\infty} \left[\int_1^{\bar{\rho}} b_n(r) dr \sin(nX) \right] \rho^{X^*} \mathcal{U}_2 + Q^{(2,\odot)} \rho + V_2^\odot(X).
 \end{aligned} \tag{6.42}$$

The function \mathcal{J}_2 must be s -independent owing to the continuity at $\rho = 0$ (see more details in Caillol (2014)). Using Eq. (6.29), the azimuthal and radial vorticity matchings on the separatrices yield the same results

$$\mathcal{J}_2'(1) = 0, \quad J_{1,c} = 0. \tag{6.43}$$

The leading-order induced mean vorticities are then proportional in such a way that the first-order local equivalent Richardson number is zero

$$\mathcal{Q}_{\theta,1} = -\varpi \mathcal{Q}_{z,1}. \tag{6.44}$$

This relationship is identical to the previous studies: the steady vortical mode without any mean radial velocity (Caillol 2014) and the $O(\epsilon^{3/2})$ mean radial-velocity wave packet (C17). The equivalent Richardson number is therefore of order $O(\epsilon)$ at r_c . Moreover, the relationship (6.44) implies the same driven term at the r.h.s of the equations (5.18) of evolution of \mathcal{V}_1 and \mathcal{W}_1 . The trivial solution $\mathcal{W}_1 = \mathcal{V}_1 + Cst$ arises, which orientates the CL induced mean flow toward a helical motion perpendicular to the isophase lines, since on a line $\xi = Cst$, axial and azimuthal velocities are linked by $v \equiv -\varpi w$ at $r \simeq r_c$. The evolution equations are also identical to those in C17, the slow time τ_2 is here faster.

Next, we match the pressure $\mathcal{P}^{(2)}$ that is given inside the cat's eyes by

$$\begin{aligned}
 \mathcal{P}_i^{(2,\odot)} &= \frac{1}{2} \rho^3 - \frac{s_i}{4} (3\mathcal{S}_1 + \mathcal{C}_0 \mathcal{C}_1) \rho^2 + \left[\frac{1}{4} (\mathcal{S}_1^2 - \mathcal{C}_1^2) + \{\mathcal{V}_2\}_-^+ - H_2 \right] \rho \\
 &\quad + \frac{s_i}{2} (\mathcal{S}_1 - \mathcal{C}_0 \mathcal{C}_1) H_2 + \psi^{(2,\odot)} + \Pi_2^\odot(X) + s_i \{\mathfrak{P}_3\}_-^+. \tag{6.45}
 \end{aligned}$$

The pressure continuity through the separatrices enables one to determine $V_2^\odot(x)$:

$$\begin{aligned}
 V_2^\odot(x) &= \hat{\zeta} \left\{ [1 - \cos x]^{\frac{1}{2}} + \cos x \ln[A(A, x)] - \int_1^\infty \frac{K_0[z] dz}{|Z_\rho(Az, x)|} A^{\frac{1}{2}} \right\} A \\
 &\quad - \int_1^\infty \int_\pi^x G_5(z, x_1) dx_1 \frac{\Xi(z) dz \mathcal{U}_2}{[2(z - \cos x)]^{\frac{1}{2}}} + [\hat{\mathcal{Q}}_{z,1}]_+^+ \frac{\rho^X}{2} + \{\mathcal{V}_2(x)\}_-^+ \\
 &+ \int_1^\infty \left(\hat{\zeta} - \frac{\Sigma_q^+}{\mathcal{U}_2} A^{\frac{1}{2}} K_0[z] \right) \int_\pi^x G_5(z, x_1) dx_1 \frac{dz \mathcal{U}_2}{\rho^{X^*}(x)} - \Sigma_q^+ \int_1^\infty \sqrt{2z} \int_\pi^x G_5(z, x_1) dx_1 + \frac{\sin x}{2z} \frac{dz A^{\frac{1}{2}}}{\rho^{X^*}(x)} \\
 &\quad + \frac{\Xi(1)}{2} \sum_{n=1}^{\infty} \left[\int_{-1}^1 b_n(r) r dr \sin(nx) \right] \rho^{X^*} \mathcal{U}_2; \tag{6.46}
 \end{aligned}$$

it also yields the following jumps through the Π_2 expression (6.21) jointly with the relationships (6.26), (6.28) and (6.30)

$$[\mathfrak{P}_3]_\pm^+ = 2 \hat{\zeta} \left(\frac{2^{\frac{3}{2}}}{3} - \int_1^\infty K_0[z] dz - \mathcal{C} \right) A^{\frac{3}{2}}, \tag{6.47}$$

$$\mathcal{U}_0 \left[[\alpha_{l,1} + \alpha_{d,1} \frac{A_\Phi}{A} + \alpha_{ad,1} a_\Phi] \Theta \right]_\pm^+ = (1 + \varpi^2) [\ln(4A) - 2] \Sigma_q^+, \tag{6.48}$$

$$\text{and } \hat{\zeta} \left[\gamma_{l,1} + \gamma_{a,1} \frac{A_\Phi}{A} + \gamma_{ad,1} a_\Phi \right]_\Theta^+ = -\mathcal{U}_0 \partial_\Theta^2 [\zeta'_{z,1}]_\Theta^+ \\ + \frac{\mathcal{U}_0^2 \varpi}{12(1+\varpi^2)} \left\{ \varpi [\mathcal{U}_0 \hat{\zeta} (1+\varpi^2) + 4(\mathcal{U}_0 - 1)] \left[\partial_\Theta^4 \zeta''_{z,1}(0) \right]_\Theta^+ + \mathcal{U}_0 \left[\partial_\Theta^4 [\varpi \zeta'''_{z,1} + \zeta'''_{\theta,1}(0)] \right]_\Theta^+ \right\}. \quad (6.49)$$

Note that the ratios of the second and third double integrals in (6.46) over ρ^X are not singular at $x = 0 [2\pi]$. The pressure continuity also permits to determine the function

$$\Pi_2^{(\odot)}(x) = \{ \Pi_2(x) \}_\pm^+ + \frac{s_i}{2} [V_2(x) + \mathcal{V}_2]_\pm^+ \rho^X.$$

Next, the rotational and axial velocity matchings on the separatrices yield the absences of jump for the phase and the second-order mean velocity, then the value of $\mathcal{J}_2(1)$

$$[a]_\pm^+ = 0, \quad [\mathcal{V}_2]_\pm^+ = 0, \quad [\mathcal{W}_2]_\pm^+ = 0, \quad \mathcal{J}_2(1) = 0, \quad (6.50)$$

as well as a second expression for $V_2^{(\odot)}(x)$

$$V_2^{(\odot)}(x) = \hat{\zeta} \left\{ [1 - \cos x]^{\frac{1}{2}} + \cos x \ln[\Lambda(A, x)] - \int_1^\infty \frac{K_0[z] dz}{|Z_\rho(Az, x)|} A^{\frac{1}{2}} \right\} A \\ - \int_1^\infty \int_\pi^x G_5(z, x_1) dx_1 \frac{\Xi(z) dz \mathcal{U}_2}{[2(z - \cos x)]^{\frac{1}{2}}} + [\hat{\mathcal{Q}}_{z,1}]_\pm^+ \frac{\rho^X}{2} + \{V_2(x)\}_\pm^+. \quad (6.51)$$

However, these matchings cannot be completed successfully since the distortion of a secularly grows according to (6.27).

Equating (6.46) with (6.51), a second relationship constraining the series terms b_n arises, whose projection on the n^{th} harmonics $\sin(nx)$ is

$$\Xi(1) \int_{-1}^1 [b_{n+1}(r) + b_{n-1}(r) - 2b_n(r)] r dr = 4 \left\langle \int_1^\infty \left(\hat{\zeta} - \frac{\Sigma_q^+}{\mathcal{U}_2} A^{\frac{1}{2}} K_0[z] \right) \int_\pi^x G_5(z, x_1) dx_1 dz \sin(nx) \right\rangle \\ - 4 \frac{\Sigma_q^+}{\mathcal{U}_2} A^{\frac{1}{2}} \left\langle \int_1^\infty \sqrt{2z} \int_\pi^x G_5(z, x_1) dx_1 + \frac{\sin x}{2z} dz \sin(nx) \right\rangle \quad n \geq 1. \quad (6.52)$$

The equation (6.4) evaluated within the cat's eye gives the radial velocity

$$U^{(2,\odot)}(Z, x) = \Xi(1)(1 + \varpi^2) \sum_{n=1}^\infty \left[\frac{\bar{\rho}}{2} \int_1^{\bar{\rho}} b_n(r) dr [\cos(n-1)x - \cos(n+1)x] \right. \\ \left. - \left(\bar{\rho} \int_1^{\bar{\rho}} b_n(r) dr - \int_0^{\bar{\rho}} b_n(r) r dr \right) [2n \cos(nx) - (n+1) \cos(n+1)x - (n-1) \cos(n-1)x] \right] A^{\frac{1}{2}} \mathcal{U}_2 \\ + \varpi^2 \int_{\cos x}^{Z^*} \frac{\mathcal{J}_2'(z) dz}{Z_\rho(Az, x)} A \sin x + [(1 - \zeta \varpi^2) A \sin x - (1 + \varpi^2) V_2^{(\odot)'}(x) + \mathcal{U}'_2] Z_\rho + \Upsilon_2^{(\odot)}(x) + s_i \{ \mathcal{U}_3 \}_\pm^+. \quad (6.53)$$

After a tedious calculation involving the equations (6.32), (6.51) and (6.53), the radial-velocity continuity on the separatrices yields an equation determining \mathcal{J}_2'

$$2\varpi^2 \int_1^{\cos x} \frac{\mathcal{J}_2'(z) dz}{|Z_\rho(Az, x)|} A \sin x = \frac{1}{2} (1 + \varpi^2) \Sigma_q^+ A [1 + 4 \cos x - \cos(2x)] - [\mathcal{U}_3]_\pm^+ \\ - s_i [\Upsilon_2(x)]_\pm^+ - (1 + \varpi^2) [\hat{\mathcal{Q}}_{z,1}]_\pm^+ A \sin x, \quad (6.54)$$

and the integration function Υ_2^\odot

$$\Upsilon_2^\odot(x) = \{\Upsilon_2(x)\}_-^+ - \frac{S_i}{2}(1 + \varpi^2)[V_2'(x)]_-^+ \rho^X.$$

Averaging the equation (6.54) over x leads to the the third-order mean radial velocity distortion while the projection of the same equation on $\cos(nx)$, $n = 1, 2$ gives, according to the expressions of Υ_2 in (6.33) and the terms $g_{j,1,0}$, $j = l, d, ad$, in Appendix A, the jumps of $\kappa_{h,1}$ and the sum of the $O(\epsilon^{3/2})$ outer flow coefficients κ . The latter is a function of the mean radial wave flux Σ_q^+ and the jumps of $\zeta'_{z,1,\theta}(0)$, $\partial_\theta^3 \zeta''_{z,1}(0)$ and $\partial_\theta^3 [\varpi \zeta'''_{z,1} + \zeta'''_{\theta,1}](0)$.

$$[\mathcal{U}_3]_-^+ = \frac{1}{2}(1 + \varpi^2)\Sigma_q^+ A, \quad [\kappa_{h,1}]_-^+ = \frac{S_i}{2}(1 + \varpi^2)\Sigma_q^+, \quad (6.55)$$

by using the relationships (6.28), (6.30) and (6.48), the jump of the sum of the coefficients κ gets simplified in this way

$$\begin{aligned} & \hat{\zeta}([\kappa_{l,1}]_-^+ + [\kappa_{d,1}]_-^+ \frac{A_\Phi}{A} + [\kappa_{ad,\Phi}]_-^+ a_\Phi) = \\ & - \{2\hat{\zeta}(1 + \varpi^2) + [\hat{\zeta}(1 + 2\varpi^2) + \varpi \hat{\zeta}_{\theta,0}][\ln(4A) - 2]\}\Sigma_q^+ - \mathcal{U}_0[\zeta'_{z,1,\theta}(0)]_-^+ \\ & + \frac{\varpi \mathcal{U}_0^2}{12(1 + \varpi^2)} \left\{ \varpi \{ \mathcal{U}_0 \hat{\zeta}(1 + \varpi^2) + 4(\mathcal{U}_0 - 1) \} [\partial_\theta^3 \zeta''_{z,1}(0)]_-^+ + \mathcal{U}_0 [\partial_\theta^3 [\varpi \zeta'''_{z,1} + \zeta'''_{\theta,1}](0)]_-^+ \right\}. \end{aligned} \quad (6.56)$$

θ -derivating (6.54) projected on $\cos x$ then gives a relationship between various θ -derivatives of the mean flow distortion

$$\begin{aligned} (1 + \varpi^2)\partial_\theta^2 [\zeta'_{z,1}(0)]_-^+ &= \varpi \frac{\mathcal{U}_0^2}{12} [\partial_\theta^4 [\varpi \zeta'''_{z,1} + \zeta'''_{\theta,1}](0)]_-^+ \\ &+ \varpi^2 \frac{\mathcal{U}_0}{12} [\mathcal{U}_0 \hat{\zeta}(1 + \varpi^2) + 4(\mathcal{U}_0 - 1)] \partial_\theta^4 [\zeta''_{z,1}(0)]_-^+, \end{aligned} \quad (6.57)$$

which yields, using (6.26), the link between the jumps of $\partial_\theta^2 \zeta'_{z,1}$ and $\partial_\theta^2 \zeta'_{\theta,1}$

$$\partial_\theta^2 [\zeta'_{z,1}]_-^+ = \varpi \partial_\theta^2 [\zeta'_{\theta,1}]_-^+. \quad (6.58)$$

Finally, the projection of (6.54) on $\sin x$ gives the following integro-differential equation

$$\begin{aligned} 2\varpi^2 \int_1^{\cos x} \frac{\mathcal{J}_2'(z) dz}{[2(z - \cos x)]^{\frac{1}{2}}} &= \{[\beta_{l,1} + d_{l,1,0} + (\beta_{\omega d,1} + d_{\omega d,1,0})\mathcal{U}_{1,\Phi}\tau_1]_-^+ + [\beta_{d,1} + d_{d,1,0}]_-^+ \frac{A_\Phi}{A} \\ &+ [(\beta_{ad,1} + d_{ad,1,0})_-^+ a_\Phi - (1 + \varpi^2)[\hat{\mathcal{Q}}_{z,1}]_-^+ \} A^{\frac{1}{2}}. \end{aligned} \quad (6.59)$$

The previous matching conditions (6.43) and (6.50) imply the trivial solution $\mathcal{J}_2(Z) = 0$; as a result, the r.h.s of (6.59) vanishes. The expressions of $d_{j,1,0}$, $j = l, d, ad$ and ωd , in Appendix A, jointly with the relationships (6.30), (6.41), (6.44) and (6.49) leads to a first continuous coefficient: $[\beta_{\omega d,1}]_-^+ = 0$, whereas the sum of the other coefficients β admits a jump linked to the distortions of $\hat{\mathcal{Q}}_{z,1}$, $\hat{\zeta}_{z,1}$, $\partial_\theta^2 \zeta'_{z,1}$, $\partial_\theta^4 \zeta''_{z,1}(0)$, $\partial_\theta^4 \zeta'''_{z,1}(0)$, $\partial_\theta^4 \zeta'''_{\theta,1}(0)$, $\partial_\theta^2 [\varpi \zeta'''_{z,1} + \zeta'''_{\theta,1}](0)$ and $\partial_\theta^4 [\varpi \zeta_{z,1}^{IV} + \zeta_{\theta,1}^{IV}](0)$. The jump of the sum of the coefficients β is

namely

$$\begin{aligned}
& \hat{\zeta}([\beta_{l,1}]_+^+ + [\beta_{d,1}]_+^+ \frac{A_\Phi}{A} + [\beta_{ad,1}]_+^+ a_\Phi) = [\hat{\zeta}_{z,1}]_+^+ - 2\mathcal{C}\hat{\zeta}[\hat{\zeta}(2 + 3\varpi^2) + \varpi\hat{\zeta}_{\theta,0}] A^{\frac{1}{2}} \\
& - \mathcal{U}_0 \left[\mathcal{U}_0 \hat{\zeta} [13 + 2a + 2\varpi(\varpi^2 - 3)\hat{\zeta}_{\theta,0} + \varpi^2(5 + 2a) + 2\hat{\zeta}(2 + \varpi^2 + \varpi^4)] - 2\hat{\zeta}(1 + \varpi^2) \right. \\
& + 2\mathcal{U}_0 [\varpi(3 - 2\varpi\hat{\zeta}_{\theta,0})\hat{\zeta}_{\theta,0} + \zeta'(1 + \varpi^2)] \left. \right] \frac{\partial_\Theta^2 [\zeta'_{z,1}]_+^+}{2\hat{\zeta}(1 + \varpi^2)} - \frac{\varpi\mathcal{U}_0^2}{3(1 + \varpi^2)} \left[\partial_\Theta^2 [\varpi\zeta''_{z,1} + \zeta''_{\theta,1}](0) \right]_+^+ \\
& + \frac{\varpi^2\mathcal{U}_0^2}{120\hat{\zeta}(1 + \varpi^2)^2} \left(\hat{\zeta}\mathcal{M}_b + 10\mathcal{U}_0[\hat{\zeta}(1 + 2\varpi^2) + \varpi\hat{\zeta}_{\theta,0}][\mathcal{U}_0\hat{\zeta}(1 + \varpi^2) + 4(\mathcal{U}_0 - 1)] \right) \left[\partial_\Theta^4 \zeta''_{z,1}(0) \right]_+^+ \\
& \quad + \frac{\mathcal{U}_0^4\varpi}{12\hat{\zeta}(1 + \varpi^2)^2} [\hat{\zeta}(1 + 2\varpi^2) + \varpi\hat{\zeta}_{\theta,0}] \left[\partial_\Theta^4 [\varpi\zeta'''_{z,1} + \zeta'''_{\theta,1}](0) \right]_+^+ \\
& - \frac{\varpi\mathcal{U}_0^3}{120(1 + \varpi^2)^2} \left[\partial_\Theta^4 [\mathcal{M}_c\varpi\zeta'''_{z,1} + \mathcal{M}_d\zeta'''_{\theta,1}](0) \right]_+^+ + \frac{\varpi\mathcal{U}_0^4}{60(1 + \varpi^2)} \left[\partial_\Theta^4 [\varpi\zeta_{z,1}^{IV} + \zeta_{\theta,1}^{IV}](0) \right]_+^+.
\end{aligned} \tag{6.60}$$

The coefficients \mathcal{M}_b , \mathcal{M}_c and \mathcal{M}_d are given in Appendix A. Next, Θ -differentiating (6.54) projected on $\sin x$ gives the jump relationship related to (6.28). The triple radial gradients of the first-order mean vorticity $\zeta''_{z,1}$ and $\zeta''_{\theta,1}$ are computed from higher-order radial fluxes involving the $O(\epsilon^2)$ inner rotational and azimuthal velocities and the $O(\epsilon^{5/2})$ inner radial velocity.

The velocity $V_{5,sp}^\ominus$ in Equation (6.38) is determined in such a way that the velocities $V_{sp}^{(5,\ominus)}$ and $W_{sp}^{(5,\ominus)}$ may not admit a jump on the CL axis at $\rho = 0$, that is $V_{5,sp}^\ominus(x) = -s\Xi(1) \int_1^{\cos x} G_5^\ominus(z, x) dz A^{1/2} H_2$. The expression of $V_{5,sp}^\ominus$ can be then deduced from the relationship (6.52)

$$\frac{V_{5,sp}^\ominus(x)}{A^{\frac{1}{2}} H_2} = \frac{\Sigma_{q'}^-}{\mathcal{U}_2} A^{\frac{1}{2}} \int_1^\infty \sqrt{2z} G_5(z, x) + \frac{\cos x}{2z} dz - s \int_1^\infty \left(\hat{\zeta} - \frac{\Sigma_q^+}{\mathcal{U}_2} A^{\frac{1}{2}} K_0[z] \right) G_5(z, x) dz. \tag{6.61}$$

The matchings of the fifth-order azimuthal and axial spiraling velocities on the separatrices, that is the conditions $V_\Theta^{(5)} = V_\Theta^{(5,\ominus)}$ and $W_\Theta^{(5)} = W_\Theta^{(5,\ominus)}$ as $Z = A$, according to the equations (6.8-6.9), (6.14), (6.35-6.36) and (6.38) are only possible if $[V_{5,sp}(x)]_+^+ = -\Sigma_q^+/\mathcal{U}_2 A \ln(4A) H_2 \cos x$, which is compatible with the relationships (6.48) and (6.49), and if the mean velocities $\mathcal{V}_{3,sp}$, $\mathcal{W}_{3,sp}$ are undistorted. However, the third-order mean velocity distortion (5.17) implies

$$[\mathcal{V}_{3,sp}]_+^+ = [\mathcal{W}_{3,sp}]_+^+ = 2\mathcal{C}\hat{\zeta} A^{\frac{1}{2}} H_2, \tag{6.62}$$

which means that $V_{sp}^{(5)}$ and $W_{sp}^{(5)}$ are not matchable on the separatrices owing to the presence of the third-order distorted induced mean flow. The matching can be carried out by adding a boundary layer along the separatrices.

The choice of the radial variable ρ in (4.1) jointly with a secular azimuthal angle is here very convenient because permits to describe the spiraling streamlines and to get rid of the time secularity used in C17 where the induced mean flow secularly evolved over τ_2 as soon as the first order for the mean vorticity ($\mathcal{Q}_{z,1}$, $\mathcal{Q}_{\theta,1}$) and $\mathcal{Q}^{(2,\ominus)}$. The subsequent CL blow up highlighted a wave breaking modeling weakness. The time secularity is not nevertheless discarded. Indeed, the phase jump a evolves linearly over τ_1 but in a very slowly way since the growth is proportional to $\Sigma_{q'}$. These variables structure all the

other fields not modeled here like reflectivity, convection... in spiral bands as well. The diffusion boundary layers located at either side of the nonlinear critical layer are strongly coupled to the latter and similarly exhibit a helical motion as was proved in C17. The same variables describe the spiraling motion in these layers.

Matching conditions have linked the Frobenius series term jumps with the mean flow distortions. Those relationships will be relevant while deriving the evolution equations because most of the coefficients of those equations are proportional to the mean flow distortions.

7. Numerical computation of the CL flow

This section uses the analytical results obtained in the previous sections to evaluate the relevant mean radial wave fluxes and to solve the Galerkin problem inside the separatrices in order to quantitatively describe the leading-order flow inside the critical layer.

7.1. Computation of the mean radial wave flux induced forcings

7.1.1. Forcing Σ_q driven by the mean wave vorticity flux

According to Eqs. (5.7-5.8) and Section 6, the Θ -gradient of the second-order mean vorticity is given for a CL symmetry with respect to the axis r_a ($\rho_B^+ = -\rho_B^-$), by

$$\mathcal{U}_0 \mathcal{Q}_{z,2,\Theta}^s = \overline{\sin X \psi_{\rho\rho\rho}^{(2)}(\rho_B^s, X)} A - \zeta \mathcal{U}_2 = \Sigma_q^s - \zeta \mathcal{U}_2, \quad (7.1)$$

$$\mathcal{U}_0 \mathcal{Q}_{\theta,2,\Theta}^s = \mathcal{V}_{1,\Phi} - \varpi \overline{\sin X \psi_{\rho\rho\rho}^{(2)}(\rho_B^s, X)} A = \mathcal{V}_{1,\Phi} - \varpi \Sigma_q^s. \quad (7.2)$$

We define $\rho_B = |\rho_B^+|$ and the corresponding variable Z : $Z_B = 1/2\rho_B^2 + A \cos X$. The forcing is obtained after ρ -differentiating the axial vorticity $\psi_{\rho\rho}^{(2)}$ in (6.16); its expression (G1) is given in Appendix G, showing a first relationship between the forcings Σ_q^s and Σ_q^s :

$$(1 + \mathcal{A}_3)\Sigma_q^s + s(\mathcal{A}_4 - \mathcal{B}_2)\Sigma_q^s A^{\frac{1}{2}} = \zeta \mathcal{A}_3 \mathcal{U}_2, \quad (7.3)$$

where the various coefficients \mathcal{A}_i and \mathcal{B}_i are X -averages at constant ρ_B and are functions of ρ_B^* only. Their expression is displayed in the same Appendix G.

7.1.2. Forcing $\Sigma_{q'}$ driven by the mean wave flux of the vorticity radial gradient

After Eq. (5.2) and Section 6, the Θ -gradient of the first-order mean vorticity radial gradient is given at either side of r_a , for a symmetric CL, by

$$\mathcal{U}_0 \zeta_{z,1,\Theta}^s = s_i \overline{\sin X \psi_{\rho\rho\rho\rho}^{(2)}(\rho_B^s, X)} A = \Sigma_{q'}^s, \quad (7.4)$$

$$\mathcal{U}_0 \zeta_{\theta,1,\Theta}^s = -s_i \varpi \overline{\sin X \psi_{\rho\rho\rho\rho}^{(2)}(\rho_B^s, X)} A = -\varpi \Sigma_{q'}^s. \quad (7.5)$$

The calculation yields after twice ρ -differentiating $\psi_{\rho\rho}^{(2)}$ in (6.16) the expression (G2) in Appendix G. A second relationship between the forcings Σ_q^s and $\Sigma_{q'}^s$ is thus deduced:

$$s[\rho_B^* + \mathcal{A}_4 - \mathcal{B}_2 + \rho_B^{*3}(\mathcal{A}_6 + \mathcal{B}_3)]\Sigma_q^s A^{\frac{1}{2}} + (\mathcal{A}_3 + \rho_B^{*3}\mathcal{A}_5)\Sigma_q^s = \zeta(\mathcal{A}_3 + \rho_B^{*3}\mathcal{A}_5)\mathcal{U}_2, \quad (7.6)$$

involving similar coefficients \mathcal{A}_i and \mathcal{B}_i expressed in Appendix G.

The forcings Σ_q and $\Sigma_{q'}$ are solutions of the linear system (7.3-7.6) whose variables are only A , \mathcal{U}_2 and ρ_B^* . For a symmetric CL extent, the rescaled radius ρ_B^* is linked to the CL thickness: $\delta_{cl} \simeq 2r_c \rho_B^* (\epsilon A)^{1/2}$. This radius is roughly twice the ratio σ of the

CL thickness over the cat's eye thickness and is thus bounded such as $\rho_B^* > 2$. The ratio can be taken constant, that is we assume a CL extent that varies according to the wave modulation, which is more realistic than a constant-extent CL. Both forcings are hence only functions of the slow modulation scales Φ and τ_2 , namely

$$\frac{\Sigma_{q'}^s}{\mathcal{U}_2} = s\zeta \mathbb{B} A^{-\frac{1}{2}}, \quad \frac{\Sigma_q}{\mathcal{U}_2} = \zeta \frac{\mathcal{A}_3}{1 + \mathcal{A}_3} - \zeta \frac{\mathcal{A}_4 - \mathcal{B}_2}{1 + \mathcal{A}_3} \mathbb{B}, \quad (7.7)$$

where \mathbb{B} is a ratio of various coefficients \mathcal{A}_i and \mathcal{B}_i and whose long expression is given in Appendix G. For a symmetric CL, the forcing $\Sigma_{q'}$ is antisymmetric vis-à-vis the CL axis r_a and proportional to $\zeta \mathcal{U}_2 A^{-1/2}$ whereas Σ_q is symmetric and proportional to $\zeta \mathcal{U}_2$.

The expressions of the first-order spiraling mean vorticity radial gradient and second-order spiraling mean vorticity are now derived

$$\zeta_{z,1,sp}^s = s\zeta \mathbb{B} \frac{H_2}{A^{\frac{1}{2}}}, \quad \zeta_{\theta,1,sp}^s = -s\zeta \varpi \mathbb{B} \frac{H_2}{A^{\frac{1}{2}}}, \quad (7.8)$$

$$\mathcal{Q}_{z,2,sp} = -\zeta \left(1 + (\mathcal{A}_4 - \mathcal{B}_2) \mathbb{B} \right) \frac{H_2}{1 + \mathcal{A}_3}, \quad (7.9a)$$

$$\mathcal{Q}_{\theta,2,sp} = \zeta \varpi \left((1 + \mathcal{A}_3) \frac{\mathcal{V}_{1,\Phi}}{\zeta \varpi \mathcal{U}_2} - \mathcal{A}_3 + (\mathcal{A}_4 - \mathcal{B}_2) \mathbb{B} \right) \frac{H_2}{1 + \mathcal{A}_3}. \quad (7.9b)$$

The leading-order mean radial velocity was determined in the second-order inner analysis in C17 ($\mathcal{U}_3 = \mathcal{V}_{1,\Phi}/(\zeta \varpi)$) but in the present approach, it will be necessary to go to the next order to find \mathcal{U}_2 out as a function of the first-order induced mean flow at r_c . We can heuristically determine a close value to \mathcal{U}_2 by introducing $\hat{\zeta}$ in the mean azimuthal vorticity Θ -secular equation

$$\mathcal{U}_0 \mathcal{Q}_{\theta,2,\Theta} = \mathcal{V}_{1,\Phi} - \varpi \Sigma_q = \mathcal{V}_{1,\Phi} - \zeta \varpi \mathcal{U}_2 + \hat{\zeta} \varpi \mathcal{U}_2.$$

Equating $\mathcal{V}_{1,\Phi}$ with $\zeta \varpi \mathcal{U}_2$ then permits to write the Θ gradient of the azimuthal vorticity as a slight correction of the vertical rotational-velocity shear $\mathcal{V}_{1,\Phi}$: $\mathcal{U}_0 \mathcal{Q}_{\theta,2,\Theta} = \hat{\zeta}/\zeta \mathcal{V}_{1,\Phi}$. Finally, we obtain the same result as in C17, the radial velocity is generated by the small vertical wind shear, then we get the relationship $\mathcal{Q}_{\theta,2,sp} = -\varpi \mathcal{Q}_{z,2,sp}$.

The advantage of taking the azimuthal variable as the secular variable is evident as soon as the second order since \mathcal{V}_2 and $\mathcal{Q}_{z,2}$ quadratically vary over τ_2 while $\mathcal{Q}_{\theta,2}$ cubically evolves over τ_2 in C17. The dependence on τ_2 fast algebraically increases with the expansion order making the expansions divergent if the vertical shear is not assumed very small.

7.1.3. Forcing Σ_v driven by the mean wave momentum flux

According to subsection (5.3) and Section 6, the forcing on the first-order velocity ($\mathcal{V}_1, \mathcal{W}_1$) is given at either side of r_a , for a symmetric CL, by

$$\Sigma_v^s = s_i \overline{\sin X \psi_{\rho\rho}^{(2)}(\rho_B^s, X) A}. \quad (7.10)$$

Substituting the expression (6.16) for the axial vorticity $\psi_{\rho\rho}^{(2)}$, we straightforwardly get the forcing (G3) in Appendix G. A relationship linking the forcing Σ_v^s to the two previous ones: Σ_q^s and $\Sigma_{q'}^s$ is then found

$$\Sigma_v^s + s \Sigma_q^s \mathcal{A}_1 A^{\frac{1}{2}} + \Sigma_{q'}^s (\mathcal{A}_2 + \mathcal{B}_1) A = s\zeta \mathcal{A}_1 A^{\frac{1}{2}} \mathcal{U}_2.$$

We deduce the expression of Σ_v^s as a function of only ζ , A and \mathcal{U}_2 as well as of the coefficients \mathcal{A}_i and \mathcal{B}_i (cf. Appendix G).

$$\frac{\Sigma_v^s}{\mathcal{U}_2} = s \frac{\zeta \mathcal{A}_1}{1 + \mathcal{A}_3} [1 + (\mathcal{A}_4 - \mathcal{B}_2)\mathbb{B}] A^{\frac{1}{2}} - s \zeta (\mathcal{A}_2 + \mathcal{B}_1)\mathbb{B} A^{\frac{1}{2}}. \quad (7.11)$$

The forcing is antisymmetric with respect to r_a and is proportional to $\zeta A^{1/2} \mathcal{U}_2$. As for the first-order mean axial vorticity, its jumps follows after (6.41)

$$\frac{[\mathcal{Q}_{z,1}]_{\pm}^+}{2\zeta A^{\frac{1}{2}}} = -\frac{\mathcal{C} - \mathcal{A}_1}{1 + \mathcal{A}_3} [1 + (\mathcal{A}_4 - \mathcal{B}_2)\mathbb{B}] - (\mathcal{A}_2 + \mathcal{B}_1)\mathbb{B}, \quad (7.12)$$

this is a correction of the steady-state jump: $-2\mathcal{C}\zeta A^{1/2}$ (Caillol 2014).

The eddy forcing F_{ed} applied at r_c in order to keep the double radial gradient of the basic-state axial vorticity constant there, scales like $\zeta \mathcal{U}_2/A$. Let us write it in this way

$$F_{ed} = \zeta f_{ed}(\rho_B^*) \mathcal{U}_2 A^{-1}.$$

Exerting a constant forcing F_{ed} at r_c therefore links \mathcal{U}_2 and A proportionally

$$\mathcal{U}_2 = \frac{F_{ed}}{\zeta f_{ed}(\rho_B^*)} A. \quad (7.13)$$

The coefficients \mathcal{A}_i and \mathcal{B}_i being decreasing functions of the CL thickness, computation shows that they are small for a value of $\rho_B^* > 2$. As a result, in practice, the rescaled forcings $\Sigma_{q'}/(\zeta \mathcal{U}_2) A^{1/2}$, $\Sigma_q/(\zeta \mathcal{U}_2)$ and $\Sigma_v/(\zeta \mathcal{U}_2) A^{-1/2}$ are small and they are actually very small for a value of $\rho_B^* \geq 4$. Figure 4 a) shows these forcings in a logarithmic scale as a function of ρ_B^* . Their magnitude steeply decreases with ρ_B^* . The wave flux induced vorticity radial gradient $-\Sigma_q/\mathcal{U}_2$ is thus a slight correction term with respect to the basic-state vorticity radial gradient at r_c , ζ in the expression of $\mathcal{Q}_{z,2,sp}$. The wave flux induced vorticity $-\Sigma_v/\mathcal{U}_2$ is also a slight correction with respect to the mean vorticity $\mathcal{Q}_{z,1}$. For examples, as $\rho_B^* = 3$, Σ_q/\mathcal{U}_2 induces a 2% correction to ζ while Σ_v/\mathcal{U}_2 and Σ_q/\mathcal{U}_2 induce a 0.6% correction to the axial vorticity distortion $[\mathcal{Q}_{z,1}]_{\pm}^+$. As $\rho_B^* = 4$, the first correction only reaches 0.6% and the second shrinks to 0.03%. The forcing Σ_q/\mathcal{U}_2 is negative, so $\hat{\zeta} \gtrsim \zeta$; the basic-state vortex stability at r_c has then slightly diminished but the θ -gradient of the second-order mean vorticity has decreased. The forcing Σ_v^+/\mathcal{U}_2 is positive, so $[\hat{\mathcal{Q}}_{z,1}]_{\pm}^+ \lesssim [\mathcal{Q}_{z,1}]_{\pm}^+$; the first-order mean vorticity distortion is hence reduced. In literature, the eddy contribution to vortex intensification is generally weaker than the axisymmetric contribution. Numerical simulations of a full-physics model of a tropical cyclone-like vortex examine the intensification generated by moist-convection driven vorticity waves (Wang 2002a; Qiu *et al.* 2010). The mean rotational wind acceleration is observed near r_c , the mean wave fluxes bring about smaller contributions of one order of magnitude. The critical layer was unfortunately not resolved in these numerical schemes; we wonder what the eddy contributions would be if the CL was properly modeled. Time and azimuthally-averaged absolute angular momentum budget was computed from mesoscale resolving Doppler observations of Hurricane Guillermo (1997), the tendency also results in stronger axisymmetric contributions (Reasor *et al.* 2009).

7.2. Resolution of the spectral method

The Fourier sine series in $\psi_{\rho\rho}^{(2,\odot)}$ of (6.34) is truncated at $n = N$. Every b_n , $n = 1, \dots, N$ is a weighted sum of the odd Chebyshev polynomials T_1 and T_3 , whose weights are computed by using both matching conditions (6.40) and (6.52). Note that these weights are independent on ζ , A and \mathcal{U}_2 . They mainly depend on the mathematical

properties of the function G_5 . They also slightly depend on the CL boundary ρ_B^* and on the corner parameters γ and μ . As new matching conditions involving the series terms b_n are encountered at higher orders, new polynomials T_5 , T_7 etc. must be added. The computation shows that the series convergence is slow; the fundamental mode $n = 1$ is weakly dominating (cf. figure 4 b)). As $N = 20$, adding the next harmonics $n = 21$ changes the integrated series L^2 norm $[\int_0^1 \sum_{n=1}^N b_n^2(r) dr]^{1/2}$ by 5% for any $\rho_B^* \geq 3$; as $N = 30$, adding another harmonics changes this integrated norm by 3%. From now on, we will take the truncature $N = 20$. If $\rho_B^* \geq 4$, the effect of the CL thickness is negligible. For example, with $\gamma = 0$, $\mu = 0.2$, $N = 20$, the departure between the series computed with distinct thicknesses: $\rho_B^* = 3$ and $\rho_B^* = \infty$ in the sense of the L^2 norm is only 2%.

Figure 5 displays the contour lines of the axial-vorticity $\psi_{\rho\rho}^{(2)}$. In figure 5 a) the radial velocity \mathcal{U}_2 is zero and in b) $\mathcal{U}_2 = A$. The isovorticity contours coincide with the streamlines in a) and are symmetric with respect to the axis $x = \pi$. Inside the separatrices, the axial vorticity is constant. The symmetry is broken in b) for the contours outside and near the separatrix. Indeed, the new terms brought about by the mean radial velocity only alter the flow near the separatrix. Far from the separatrix, the vorticity is given by the radially monotonic function $\mathcal{F}_2(Z)$ and the inner vorticity profile then follows the basic-vorticity profile. We study a linearly stable basic-state vortex; as a result, $\zeta < 0$ and the inner axial vorticity decreases with the radius. However, near the separatrix and inside the cat's eye, the axial vorticity is no longer monotonic. Inside the separatrices, the axial vorticity is quadripolar with one negative pole at $x < \pi$ for $s = +$ and another one at $x > \pi$ for $s = -$ as $\mathcal{U}_2 > 0$; as a result, the fundamental mode $n = 1$ is prevailing ($\sin x$). Both upper poles are not of opposite strengths, the negative pole is stronger. The CL emergence in the presence of a $O(\epsilon)$ mean radial velocity has thus generated secondary vorticity extrema outside the eyewall. In spiral rainbands, these extrema are usually associated in pairs of local positive and negative PV anomalies (Chen & Yau 2001). The contours intersect the separatrix at an angle $x \gtrsim \pi$ for $\mathcal{U}_2 > 0$. The contours $\psi_{\rho\rho}^{(2)+} - s_i \hat{Q}_{z,1}^+ = -0.177, -0.152$ penetrate the cat's eye at $x > \pi$, go out at $x \lesssim 2\pi$ on forming a bend to fulfil the 2π periodicity at $x = 2\pi$. The particular contour $\psi_{\rho\rho}^{(2)} - s_i \hat{Q}_{z,1}^+ = -s_i/2[\hat{Q}_{z,1}]_-^+ \simeq -0.138$ starts at $x = 0$, on the meeting point of the separatrices and crosses the separatrix at $x = \pi$, it coincides with the vertical axis $x = \pi$ inside the cat's eye. This contour coincides with the separatrix as $\mathcal{U}_2 = 0$ in figure 5 a). Two new branches depart at either side of this axis in a nearly symmetric way and join both of the saddle points forming a closed lobe at $x < \pi$. The contour $\psi_{\rho\rho}^{(2)} - s_i \hat{Q}_{z,1}^+ = -0.198$ has a first branch that does not cut the separatrix. A second and closed branch is located at either side of the separatrix for $x > \pi$. As the mean radial velocity \mathcal{U}_2 is stronger, isovorticity lines are even more deformed as we can see in figure 6 a) where $\mathcal{U}_2 = 10$; more contours penetrate the cat's eye. The contour $\psi_{\rho\rho}^{(2)+} - s_i \hat{Q}_{z,1}^+ = 0$ starts on the separatrix near the corner and forms a positive-vorticity lobe that cuts the separatrix a second time at $x < \pi$. The contours $\psi_{\rho\rho}^{(2)+} - s_i \hat{Q}_{z,1}^+ = -0.244, -0.198, -0.177$ intersect the separatrix at $x > \pi$, go out and bend at $x \lesssim 2\pi$. The contour $\psi_{\rho\rho}^{(2)} - s_i \hat{Q}_{z,1}^+ = -0.339$ has a branch that does not cut the separatrix and another one that is located at either side of the separatrix at $x > \pi$. The contour $\psi_{\rho\rho}^{(2)} - s_i \hat{Q}_{z,1}^+ = -0.315$ has an only branch that penetrates the cat's eye at $x \gtrsim \pi$ after making a large bend, goes out at $x \lesssim 2\pi$ making a so large second bend that quasi connects with the first. For a greater clarity, the part of the contour inside the cat's eye is not drawn. The level -0.315 is thus nearly the strongest negative-vorticity level for which a 2π -range contour can penetrate the cat's eye. Since A , ρ_B^* and ζ have not

changed in figures 5 and 6, the same contour $\psi_{\rho\rho}^{(2)} - s_i \hat{Q}_{z,1}^+ = -0.138$ divides the cat's eye at $x = \pi$ into two parts in the same way. The vorticity extrema are higher in each pole, of magnitudes greater than one, so they may be much stronger than the neighboring basic-state vorticity.

Owing to the inner-flow distortions, the cat's eye is not strictly symmetric with respect to the level $\rho = 0$. As a result, though we have used a coordinate Z describing the streamlines in a refined way, this variable Z only gives a first approximation of the dividing-streamline location. A better variable, the stressed coordinate \tilde{Z} is needed in order to correctly describe the deformed trajectory of the streamlines inside the critical layer. Thus, it is necessary to ensure that the tangential and axial velocities are linked in the frame moving with the linear-wave vertical speed, at the core of the cat's eye and at the crossing point of the separatrices, by the relationship (D2), topological property which has previously been overlooked, see for instance (Benney & Bergeron 1969; Maslowe 1986). The variable Z does not allow to satisfy (D2) as soon as the first inner-flow order. As a result, Z is rescaled in an asymptotic expansion following \tilde{Z} ; the method is explained in Appendix D. The new fields, denoted by a tilde, are thus expanded in the following way, for instance for the radial velocity

$$\tilde{U}(\tilde{Z}, x) = \epsilon [\tilde{U}^{(0)} + \epsilon^{\frac{1}{2}} \ln \epsilon \tilde{U}^{(1)} + \epsilon^{\frac{1}{2}} \tilde{U}^{(2)} + \dots].$$

Using these analytical expressions of the 3D velocity field, we were able to analytically compute the CL streamlines (cf. Appendix F). For instance, the characteristic pattern associated to a nonlinear vorticity wave packet is shown in figures 6-9, in a horizontal plane at a constant height Φ and in a vertical plane at a constant angle θ . For the three lowest azimuthal wavenumbers, the charts exhibit dipolar, tripolar and quadrupolar vortices whose satellites wind and spiral along the vortex axis and are asymmetric with respect to both the critical radius, and the axis $\theta = 0 [2\pi/m], \pi/m [2\pi/m]$ (the azimuthal angle being calculated from a reference axis passing by a meeting point of the separatrices). These low azimuthal wavenumber patterns dominate asymmetric disturbances in a rapidly rotating vortex (Reasor *et al.* 2000). The contours in these figures are not the trajectories of air particles but their envelopes, the surfaces on which particles slide but cannot cross, given by the radial coordinate $\mathcal{R}_{st}(x, \Phi)$ in the parameterized representation $(\mathcal{R}_{st}(x, \Phi), z_{st}(x, \Phi))$ of a 3D Z_{st} -streamline. These contours are drawn in the local referential moving with the vertical linear-wave speed $c_z = \hat{\omega}/k = \tilde{\omega}/k + \overline{W}_c/\varpi\omega_\Phi T_1 \equiv \tilde{U}/\varpi + \mathcal{W}\mathcal{U}_\Phi\tau_1$.

The parameters ϵA , $\hat{\zeta}$, ϖ^2 and \mathcal{U}_2/A are crucial as for the asymptotic-expansion convergence. If these are large in absolute value, expansions may diverge. Increasing the phase tilt $|\varpi|$ strongly reduces the values of ζ and/or the wave amplitude ϵA ; for example in figure 9 a) $\varpi = 1/3$, $\epsilon A = 0.07$ and $\zeta = 0.5$, in b) $\varpi = 20/3$, ϵ and ζ are then reduced to $\epsilon A = 0.04$ and $\zeta = -0.0125$, in figure 6 b), $\varpi = 20$ so ζ is shrunk to $\zeta = -0.0005$ for $\epsilon A = 0.1$. We observe that the satellites become larger as $|\varpi|$ increases. This weakly nonlinear approach does not permit to model singular vorticity waves with large phase tilts (see Caillol (2014, 2015) for more details about the limitations on the parameter ϖ). Small phase tilts are usually related to small-size intense vortices with small vertical wavenumbers k and moderate $r_c \geq 1$. For instance, the wavenumber $k = 1$ in a tornado characterized by $R_{mw} = 100$ m is linked to a vertical wavelength $L_z \simeq 628$ m. The wavenumber $k = 10$ in a hurricane with $R_{mw} = 20$ km is related to a wavelength $L_z \simeq 12.6$ km. The critical radius is chosen $r_c \geq 1$ since associated to the outer eyewall edge where the rotational-wind profile is decreasing monotonically. The plots of the rotational and axial velocity (not shown) reveal that the cat's eye is not a

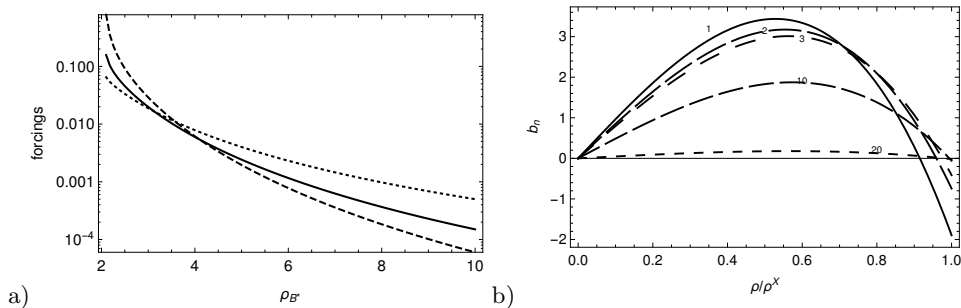


FIGURE 4. a) Forcings: $\Sigma_q/(\zeta\mathcal{U}_2)$ (solid line), $\Sigma_q^+/(|\zeta|\mathcal{U}_2)A^{1/2}$ (dashed line) and $\Sigma_v^+/(|\zeta|\mathcal{U}_2)A^{-1/2}$ (dotted line) as a function of ρ_B^* . b) $b_n(\bar{\rho})$ as a function of $\bar{\rho}$ as $\rho_B^* = 5$, $\gamma = 0$, $\mu = 0.2$ and $N = 20$, b) Forcings: $\Sigma_q/(\zeta\mathcal{U}_2)$ (solid line), $\Sigma_q^+/(|\zeta|\mathcal{U}_2)A^{1/2}$ (dashed line) and $\Sigma_v^+/(|\zeta|\mathcal{U}_2)A^{-1/2}$ (dotted line) as a function of ρ_B^* .

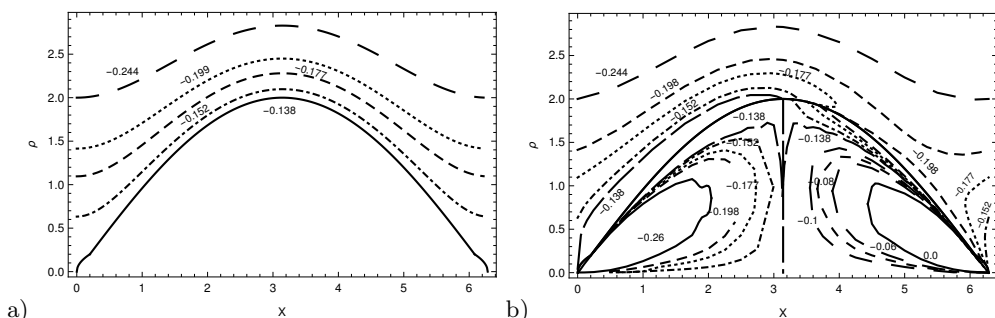


FIGURE 5. Isovorticity lines: $\psi_{\rho\rho}^{(2)+} - s_i \hat{Q}_{z,1}^+ = Cst$, $A = 1$, $\zeta = -0.1$, $s_i = 1$, $\gamma = 0$, $\mu = 0.2$, $\rho_B^* = 5$, a) $U_2 = 0$, b) $U_2 = 1$, $\Sigma_q^+/\mathcal{U}_2 A^{1/2} = 1.957 \cdot 10^{-4}$, $\Sigma_q/\mathcal{U}_2 = -2.420 \cdot 10^{-4}$. The vorticity level is indicated on each curve.

velocity maximum location. The azimuthal velocity gradually decreases with the radius inside the critical layer.

Figures 7 and 8 exhibit a vortex perturbed by a $m = 2$ vortical wave whose chosen envelope is $A = (1 + 0.5 \cos \Phi)^2$. Figure 7 shows the related tripole at various heights: a) $\Phi = 0$ where $A = 9/4$ is maximum and $\mathcal{U}_2 = 0$, b) $\Phi = \pi/2$ where $A = 1$ and $\mathcal{U}_2 = 2$ is maximum. Figure 8 a) shows the horizontal plane $\Phi = \pi$ where $A = 1/4$ is minimum and $\mathcal{U}_2 = 0$; the vortex is quasi-axisymmetric, both satellites are thin. For the heights where $\mathcal{U}_2 = 0$, the CL pattern is symmetric vis-à-vis the axis $\theta = \pi/2$ and π but not with respect to the critical radius. These symmetries are broken in 7 b). Though A in figure 7 a) is more than twice as large as in b), the cat's eye thickness is roughly equal; the radial velocity \mathcal{U}_2 then affects the CL thickness too. Figure 8 b) shows a vertical cross-section at $\theta = 0$ that spans three vertical wave periods, from $\Phi = 0$ up to $\Phi = 6\pi/\varpi\epsilon^{1/2} > 2\pi$. Note that as the ratio: envelope period/vertical wave period = $\varpi\epsilon^{-1/2} = \sqrt{5}$ is here irrational, the vertical pattern is then not periodical and all cat's eyes have a distinct shape. For $0 < \Phi < \pi [2\pi]$, the spiral extends cyclonically and, for $\pi < \Phi < 2\pi [2\pi]$ anticyclonically.

We can notice after the figures 6-9 that, though the critical layer is vertically unbounded and spiraling, the particles are trapped within the separatrices. As a result, a generalization of the Batchelor integral condition applied to a steady and closed 2D flow (Batchelor 1956) can be carried out here within the quasi-steady 3D cat's eyes in order to find a unique inviscid inner flow there.

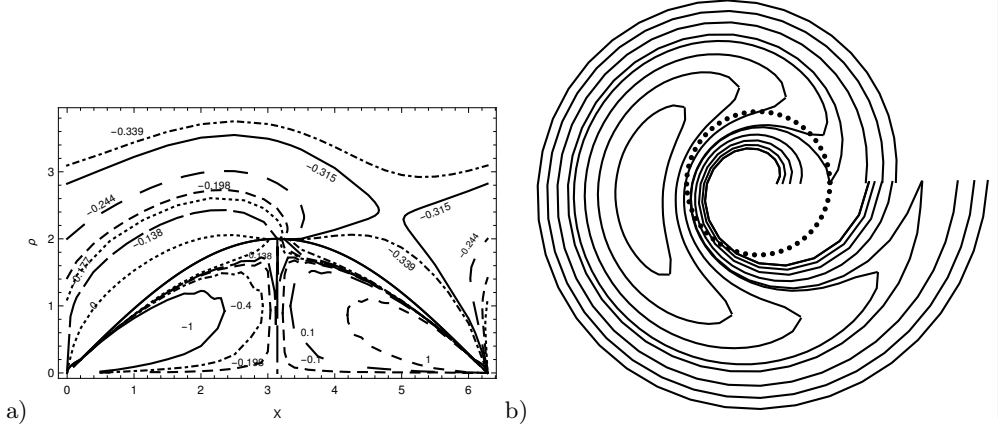


FIGURE 6. $A = 1$, $s_i = 1$, $\gamma = 0$, $\mu = 0.2$, $\rho_B^* = 5$, a) Isovorticity lines: $\psi_{\rho\rho}^{(2)+} - s_i \hat{Q}_{z,1}^+ = Cst$, $\zeta = -0.1$, $U_2 = 10$, $\Sigma_q^+/\mathcal{U}_2 A^{1/2} = 1.957 \cdot 10^{-4}$, $\Sigma_q/\mathcal{U}_2 = -2.420 \cdot 10^{-4}$. The vorticity level is indicated on each curve. b) Mode: $m = 1$, $\varpi = 20$, $\epsilon = 0.1$, $a = -1$, $\mathcal{U}_0 = 0.49$, $\beta_{l,1}^+ + d_{l,1,0}^+ + (\beta_{d,1}^+ + d_{d,1,0}^+)A_\Phi/A + (\beta_{ad,1}^+ + d_{ad,1,0}^+)a_\Phi = 1.5A^{1/2}$, $\kappa_{l,1}^+ + g_{l,1,0}^+ + (\kappa_{d,1}^+ + g_{d,1,0}^+)A_\Phi/A + (\kappa_{ad,1}^+ + g_{ad,1,0}^+)a_\Phi = 10^{-4}\Theta$, mean flow: $\zeta = -0.0005$, $\mathcal{Q}_{z,1}^+ = 0.001$, $\mathcal{S}_1 = 1$, $\mathcal{U}_2 = 1$, $\mathcal{U}'_2 = -2.04$, $\Sigma_q/\mathcal{U}_2 = -1.0299 \cdot 10^{-6}$, $\Sigma_q^+/\mathcal{U}_2 A^{1/2} = 9.783 \cdot 10^{-7}$ and $\Sigma_v^+/\mathcal{U}_2 A^{-1/2} = 2.0 \cdot 10^{-6}$. The critical radius $r_c = 2$ is shown in dotted line.

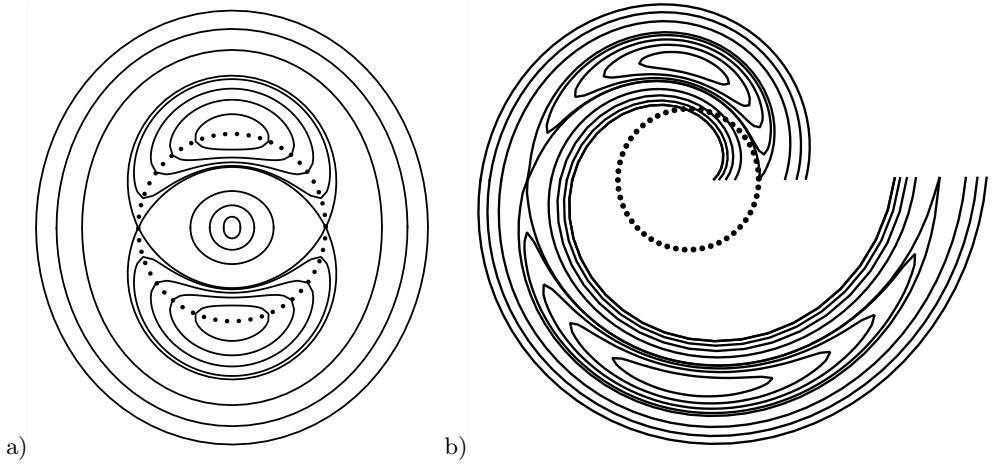


FIGURE 7. Mode: $m = 2$, $\varpi = 0.5$, $\epsilon = 0.05$, $\mathcal{U}_0 = 0.49$, $a = -1$, $A = (1 + \cos\Phi/2)^2$, $s_i = 1$, $\beta_{l,1}^+ + d_{l,1,0}^+ + (\beta_{d,1}^+ + d_{d,1,0}^+)A_\Phi/A + (\beta_{ad,1}^+ + d_{ad,1,0}^+)a_\Phi = -2A^{1/2}$, $\kappa_{l,1}^+ + g_{l,1,0}^+ + (\kappa_{d,1}^+ + g_{d,1,0}^+)A_\Phi/A + (\kappa_{ad,1}^+ + g_{ad,1,0}^+)a_\Phi = 10^{-4}\Theta$, mean flow: $\zeta = -0.1$, $\mathcal{Q}_{z,1}^+ = A^{1/2}$, $\mathcal{S}_1 = 0.4A^{1/2} + 0.2$, $\mathcal{U}_2 = -0.1 \sin\Phi/(\zeta\varpi)$, $\mathcal{U}'_2 = -\mathcal{U}_2/\mathcal{U}_0$, $\rho_B^* = 5$, $\Sigma_q/\mathcal{U}_2 = -2.4198 \cdot 10^{-4}$, $\Sigma_q^+/\mathcal{U}_2 A^{1/2} = 1.9566 \cdot 10^{-4}$ and $\Sigma_v^+/\mathcal{U}_2 A^{-1/2} = 4.0085 \cdot 10^{-4}$ a) $\Phi = 0$ b) $\Phi = \pi/2$. The critical radius $r_c = 1$ is shown in dotted line.

The vorticity wave packet/vortex CL interaction could partly explain the formation of spiral rainbands. Indeed, the latter are strongly associated to vorticity wave dynamics. Propagating PV waves characterized by spiral structures in PV fields in the mid-lower troposphere are either neutral or nearly neutral discrete modes, or the continuous modes described by the CL theory. The radial wind shear gradually axisymmetrizes

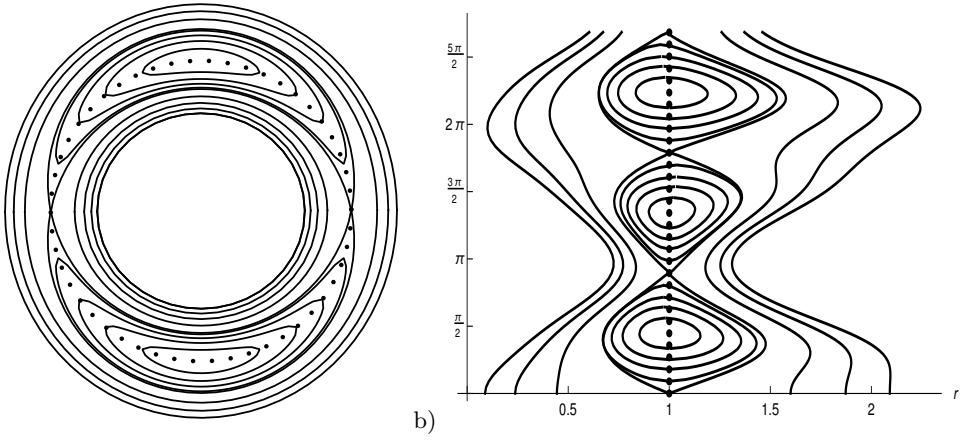


FIGURE 8. Mode: $m = 2$, $k = 1$, $a = -1$, $\bar{U}_0 = 0.49$, $\epsilon = 0.05$, $A = (1 + \cos \Phi/2)^2$, $s_i = 1$, $\beta_{l,1}^+ + d_{l,1,0}^+ + (\beta_{d,1}^+ + d_{d,1,0}^+)A_\Phi/A + (\beta_{ad,1}^+ + d_{ad,1,0}^+)a_\Phi = -2A^{1/2}$, $\kappa_{l,1}^+ + g_{l,1,0}^+ + (\kappa_{d,1}^+ + g_{d,1,0}^+)A_\Phi/A + (\kappa_{ad,1}^+ + g_{ad,1,0}^+)a_\Phi = 10^{-4}\Theta$, mean flow: $\zeta = -0.1$, $\mathcal{Q}_{z,1}^+ = A^{1/2}$, $\mathcal{S}_1 = 0.4A^{1/2} + 0.2$, $\mathcal{U}_2 = -0.1 \sin \Phi / (\zeta \varpi)$, $\mathcal{U}_2^* = -\mathcal{U}_2 / \bar{U}_0$, $\rho_B^* = 5$, $\Sigma_q / \mathcal{U}_2 = -2.4198 \cdot 10^{-4}$, $\Sigma_q^+ / \mathcal{U}_2 A^{1/2} = 1.9566 \cdot 10^{-4}$ and $\Sigma_v^+ / \mathcal{U}_2 A^{-1/2} = 4.0085 \cdot 10^{-4}$ a) $\Phi = \pi$, b) $\theta = 0$ between the heights $\Phi = 0$ and $\Phi = 6\pi / \varpi \epsilon^{1/2} \simeq 2.68 \pi$. The critical radius $r_c = 1$ is shown in dotted line.

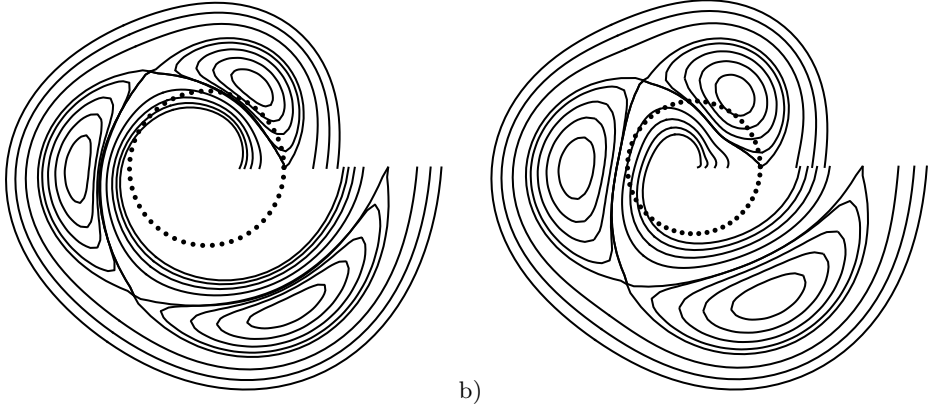


FIGURE 9. Mode: $m = 3$, $A = 1$, $s_i = 1$, $a = -1.5$, $\bar{U}_0 = 0.49$, $\beta_{l,1}^+ + d_{l,1,0}^+ + (\beta_{d,1}^+ + d_{d,1,0}^+)A_\Phi/A + (\beta_{ad,1}^+ + d_{ad,1,0}^+)a_\Phi = -1.5A^{1/2}$, $\kappa_{l,1}^+ + g_{l,1,0}^+ + (\kappa_{d,1}^+ + g_{d,1,0}^+)A_\Phi/A + (\kappa_{ad,1}^+ + g_{ad,1,0}^+)a_\Phi = 10^{-4}\Theta$, mean flow: $\mathcal{Q}_{z,1}^+ = 0.2$, $\mathcal{U}_2 = -2.04$, $\rho_B^* = 5$, $\mu = 0.2$, $\gamma = 0$, a) $k = 1$, $r_c = 1$, $\zeta = -0.5$, $\epsilon = 0.07$, $\mathcal{U}_2 = 0.5$, $\mathcal{S}_1 = 1$, $\Sigma_q / \mathcal{U}_2 = -1.2099 \cdot 10^{-3}$, $\Sigma_q^+ / \mathcal{U}_2 A^{1/2} = 9.7830 \cdot 10^{-4}$ and $\Sigma_v^+ / \mathcal{U}_2 A^{-1/2} = 2.0043 \cdot 10^{-3}$ b) $k = 10$, $r_c = 2$, $\zeta = -0.0125$, $\epsilon = 0.04$, $\mathcal{U}_2 = 1$, $\mathcal{S}_1 = -1$, $\Sigma_q / \mathcal{U}_2 = -3.025 \cdot 10^{-5}$, $\Sigma_q^+ / \mathcal{U}_2 A^{1/2} = 2.446 \cdot 10^{-5}$ and $\Sigma_v^+ / \mathcal{U}_2 A^{-1/2} = 5.0011 \cdot 10^{-5}$. The critical radius r_c is shown in dotted line.

outward propagating PV waves that turn into circular filaments (Guinn & Schubert 1993; Montgomery & Enagonio 1998; Moller & Montgomery 2000; Wang 2002a,b; Wang *et al.* 2018). Montgomery & Kallenbach (1997) suggested that PV waves are responsible for the inner spiral rainband initiation. In the inner core, continuous modes decay to the benefit of the vortex through the WMFI. Discrete unstable modes may be excited by

the subsequent basic-state vorticity profile modification, favor the formation of unstable inner spiral rainbands, mix vorticity between the eyewall and the eye and then lead to the vortex weakening (Moller & Montgomery 1999; Ruan *et al.* 2014). Reasor *et al.* (2000) found evidence in weakening Hurricane Olivia (1994) inner core of a $m = 2$ spiral PV wave packet. Spiral rainbands detected by an enhanced reflectivity were observed in the wave vicinity. The majority of inner vorticity bands observed in intensifying Hurricane Guillermo (1997) were associated with enhanced reflectivity and all coincided with an enhanced upward motion (Reasor *et al.* 2009). Inner spiraling rainbands in Katrina (2005) were also vorticity wave manifestations (Judt & Chen 2010). Chen & Yau (2001) detected inner spiral rainbands near spiral PV bands in their numerical intensifying TC-like vortex model. A modal analysis inside the spiral rainbands showed that the leading wave activity $m = 1, 2$ modes were continuous PV modes (Chen *et al.* 2003). No discrete unstable PV mode was found in spite of the unstable vorticity profile. Inertia-gravity waves had a smaller wave activity contribution, and their main components were unstable. Their propagation velocity is much faster than the observed moving speed of spiral cloud bands (Wang *et al.* 1998). An earlier modal analysis of a f -plane shallow water vortex model showed that banded features were composed almost entirely of vorticity modes (Guinn & Schubert 1993). Montgomery & Kallenbach (1997) suggested as well that outer spiral rainbands could form around the stagnation radius, while the basic flow is intensifying. In the numerical TC-like vortex simulations, Wang (2002b) observed the presence of outer spiral rainbands at this radius. Radar-observation of intensifying Hurricane Elena (1985) showed four inner convective bands whose azimuthal and radial propagation speeds were consistent with vorticity-wave dispersion relationship. They spiralled outward to a stagnation radius where they began to thin and lose their convective signature (Corbosiero *et al.* 2006).

Spiral vorticity anomaly bands are here produced by the continuous vortex erosion inside the critical layer. During the slowly evolving WMFI, the CL gradually expels vorticity into the diffusion boundary layers. The erosion is generated by the presence of hyperbolic points in the related Lagrangian flow located near the saddle points, where the separatrices meet, in the quasi-steady regime. CL vorticity then flows away along the unstable manifolds on forming filaments (Velasco Fuentes 2005). Owing to the nonlinear CL coupling, the diffusion layers are also helical and elongated by the mean radial velocity. They generate, far from the vortex center, through a slow viscous diffusion process, long, thin and spiraling high-vorticity filaments. In the earlier, unsteady and stronger vortex/wave interaction, the expelled vorticity rate is clearly higher but the mean radial velocity is smaller, so filaments are not likely to be initially perfect spiraling helices.

8. Conclusions

The theory of the nonlinear critical layer has been extended to a quasi-steady state to model the long-time asymptotic interaction between a compact and resonant 3D vorticity wave packet, and a linearly stable, columnar, dry and rapidly rotating vortex.

The critical layer generates a mean flow of higher amplitude than the wave packet that has created it and whose evolution is strongly coupled with the wave dynamics. Indeed, the matching conditions of the CL flow on the separatrices and non-zero mean radial wave fluxes at the critical radius show that the induced mean flow is modulated in the same way as the wave.

Removing the secular terms generated by this mean flow in the motion equations inside the critical layer is carried out by considering that the azimuthal angle is a secular variable. The resulting complex CL motion, evolving with the wave modulation but

also advected by its own induced mean flow, forms a spiraling and phase-oscillating helix winding around the vortex axis. Handling a secular azimuthal angle is then more relevant than the secular time scale previously used in the wave packet study C17 that causes a CL flow blow-up, since spiral bands have been observed near a critical radius in the presence of vorticity waves (Chen & Yau 2001; Wang 2002*b*).

The chosen envelope régime induces a mean radial velocity of same amplitude as the wave. This velocity breaks two CL pattern radial symmetries. Small inviscid mean radial wave fluxes result as soon as the leading order, and subsequently a larger WMFI occurs; in C17, the mean radial fluxes appear at the next order and in the steady case, they are viscous (Caillol 2014). In these previous cases, assuming a leading-order uniform axial vorticity inside the cat's eye at each vortex height was possible through the Prandtl-Batchelor theorem but it is no longer possible here. The CL flow has stronger 3D features; the streamlines and iso-axial vorticity lines do not coincide any longer at leading order. They are therefore much more distorted within the wave packet CL than within a steady CL or a large-extent wave packet CL, highlighting the vorticity wave packet breaking. The first non-trivial order vorticity can be nevertheless matched on the separatrices.

The leading-order induced mean vorticities are still proportional in such a way that the first-order equivalent Richardson number is zero at r_c , the vorticity wave packet/vortex interaction in the quasi-steady stage is still very weak as the amplitude-modulated neutral vortical mode is very weakly singular like in the past CL steady or quasi-steady studies in a vortex (Caillol (2014),C17).

The nonlinear critical layer theory could partly explain the formation of inner spiral rainbands. Indeed, in spite of the absence of a moist convection modeling, spiral vorticity bands are here produced by the vorticity wave packet CL breaking at either CL sides, through the vortex erosion inside the critical layer.

A future work will consist of solving the inner-flow fourth and fifth orders and deriving the leading-order phase-averaged outer-flow evolution equations so that the coupled system including the wave packet with the leading-order induced mean flow may be studied numerically. Dispersion should not appear in those evolution equations with such an envelope scaling. A smaller envelope wavelength is required; that seems to be a general result while handling waves resonating with a background shear flow (Voronovich *et al.* (1998*a*); Caillol & Grimshaw (2008, 2012)). New nonlinear terms coming from the mean radial wave fluxes will be likely to be present but should have a small amplitude. The crucial effect of the small wind vertical shear on the wave dynamics will be examined; the smaller shear in C17 leads the wave packet to break. An important issue will be to know if the spiraling motion favors or opposes the breaking? if so, can it saturate it?

Acknowledgements

The author is grateful to four anonymous reviewers for many helpful comments that greatly improved the quality and presentation of the paper. This research was supported by the Chilean funding organisation, National Fund for Scientific and Technological Development, as the project Fondecyt Regular 1150600.

A. The outer flow

This section gives the first terms of the Frobenius series, outer-flow solutions valid around the critical radius r_c .

A1. Order ϵ

The first coefficients of ϕ_a and ϕ_b are

$$b_0 = -\frac{\hat{\zeta}}{r_c}(1 + \varpi^2), \quad a_{0,2}r_c = -\frac{\hat{\zeta}}{2}(1 + \varpi^2) - \frac{1}{2} - \frac{1}{1 + \varpi^2},$$

$$b_{0,2}r_c^2 = \frac{\hat{\zeta}^2}{4}[\varpi^4 - 4(1 + \varpi^2)^2] - \frac{\zeta'}{4}(2 + \varpi^2) - \hat{\zeta}\left(\frac{1}{1 + \varpi^2} + \frac{3}{4}\varpi^2\right) - \frac{1}{2}\frac{1 - \varpi^2}{1 + \varpi^2} + \frac{m^2}{2}(1 + \varpi^2)$$

$$+ \varpi\frac{\hat{\zeta}_{\theta,0}}{4}\left(1 + \varpi\hat{\zeta}_{\theta,0} + 2\hat{\zeta}\varpi^2 + 2\frac{2 + \hat{\zeta}\varpi^2}{1 + \varpi^2}\right).$$

 A2. Order $\epsilon^{\frac{3}{2}}$

The first coefficients of the Frobenius series related to the inviscid flow are

$$c_{l,1,0} = \mathcal{U}_0\partial_{\Theta}\left[\left(\mu + 1\right)\kappa_{l,1} + \frac{\mathcal{U}_0}{2}\varpi\partial_{\Theta}\left[\left(\hat{\zeta}\varpi + 2\hat{\zeta}_{\theta,0}\right)\frac{\hat{\zeta}'_{z,1}}{\hat{\zeta}} - \zeta'_{\theta,1}\right](0)\right] + J_{1,c}$$

$$+ \frac{\varpi\mathcal{U}_0^3\Xi}{24\hat{\zeta}(1 + \varpi^2)}\partial_{\Theta}^4\left[\mathcal{U}_0\left[\varpi\zeta'''_{z,1} + \zeta'''_{\theta,1}\right] + \varpi\left[\mathcal{U}_0\hat{\zeta}(1 + \varpi^2) + 4(\mathcal{U}_0 - 1)\right]\zeta''_{z,1}\right](0),$$

$$f_{l,1,0} = \mathcal{U}_0\partial_{\Theta}\left[\varpi\frac{\hat{\zeta}_{\theta,0}}{\hat{\zeta}}\hat{\zeta}_{z,1} - \varpi\hat{\zeta}_{\theta,1} - (\mu + 1)\beta_{l,1}\right] + \frac{\varpi\mathcal{U}_0^3\Xi}{6\hat{\zeta}(1 + \varpi^2)}\partial_{\Theta}^3\left[\varpi\zeta''_{z,1} + \zeta''_{\theta,1}\right](0),$$

$$c_{j,1,0} = \mathcal{U}_0(\mu + 1)\kappa_{j,1,\Theta}, \quad f_{j,1,0} = -\mathcal{U}_0(\mu + 1)\beta_{j,1,\Theta}, \quad j = d, ad, \quad c_{\omega d,1,0} = 0,$$

$$d_{l,1,0} = \mathcal{S}_1 - \frac{\hat{\zeta}_{z,1}}{\hat{\zeta}} - \frac{1 + 3\varpi^2}{1 + \varpi^2}\hat{Q}_{z,1} - \frac{2 + a}{1 + \varpi^2}\frac{J_{1,c}}{\hat{\zeta}} + \frac{2\varpi^3}{1 + \varpi^2}\hat{Q}_{\theta,1} + \varpi\frac{\hat{\zeta}_{\theta,0}}{\hat{\zeta}}\left(\mathcal{S}_1 - \mathcal{Q}_{z,1} + \frac{2J_{1,c}}{1 + \varpi^2}\right)$$

$$+ \frac{\partial_{\Theta}}{\hat{\zeta}(1 + \varpi^2)}\left[\left(3(3 + 2a - 2\varpi\hat{\zeta}_{\theta,0}) + 4\hat{\zeta}(3 + \varpi^2)\right)\frac{\mathcal{U}_0^2}{6}\varpi\zeta'_{\theta,1,\Theta} - (\mu + 1)\mathcal{U}_0\gamma_{l,1} - \hat{\zeta}\mathcal{M}_a\kappa_{l,1}\right.$$

$$\left. + \left(3\hat{\zeta}\{\mathcal{U}_0[8 + 2\varpi(\varpi^2 - 2)\hat{\zeta}_{\theta,0} + \varpi^2(1 + 2a)] - 2(1 + \varpi^2) - 2\mathcal{N}\} + 2\mathcal{U}_0\hat{\zeta}^2\varpi^2(1 + 3\varpi^2)\right)\frac{\mathcal{U}_0}{6\hat{\zeta}}\zeta'_{z,1,\Theta}\right]$$

$$+ \frac{\varpi\mathcal{U}_0^2}{3\hat{\zeta}(1 + \varpi^2)}\left(\partial_{\Theta}^2[\varpi\zeta''_{z,1} + \zeta''_{\theta,1}](0) + \partial_{\Theta}^3[\varpi\zeta''_{z,1} + \zeta''_{\theta,1}](0)\Theta\right) - \frac{\varpi^2\mathcal{U}_0^2\mathcal{M}_b}{120\hat{\zeta}(1 + \varpi^2)^2}\partial_{\Theta}^4\zeta''_{z,1}(0),$$

$$+ \frac{\varpi\mathcal{U}_0^3}{120\hat{\zeta}(1 + \varpi^2)^2}\partial_{\Theta}^4[\mathcal{M}_c\varpi\zeta'''_{z,1} + \mathcal{M}_d\zeta'''_{\theta,1}](0) - \frac{\varpi\mathcal{U}_0^4}{60\hat{\zeta}(1 + \varpi^2)}\partial_{\Theta}^4[\varpi\zeta_{z,1}^{IV} + \zeta_{\theta,1}^{IV}](0),$$

$$g_{l,1,0} = \frac{\partial_{\Theta}}{\hat{\zeta}(1 + \varpi^2)}\left[(\mu + 1)\mathcal{U}_0\alpha_{l,1} + \hat{\zeta}\mathcal{M}_a\beta_{l,1} - \left(\frac{5}{2}\varpi\hat{\zeta}_{\theta,0} - 2 - a + \frac{3}{2}\hat{\zeta}(\varpi^2 - 1)\right)\mathcal{U}_0\varpi\hat{\zeta}_{\theta,1}\right.$$

$$\left. + \left(a(1 + 2\varpi^2) + \frac{\hat{\zeta}}{2}(3 + 9\varpi^2 + 4\varpi^4) + \varpi\frac{\hat{\zeta}_{\theta,0}}{\hat{\zeta}}[2\varpi\hat{\zeta}_{\theta,0} - 2 + \hat{\zeta}(\varpi^2 - \frac{1}{2})] - (1 + \varpi^2)\frac{\zeta'}{\hat{\zeta}}\right)\mathcal{U}_0\hat{\zeta}_{z,1}\right]$$

$$+ \frac{\mathcal{U}_0}{\hat{\zeta}}\zeta'_{z,1,\Theta} - \frac{\varpi^2\mathcal{U}_0^2}{6\hat{\zeta}(1 + \varpi^2)^2}\{2[\mathcal{U}_0(8 + a) - 4] + 2\varpi^2[\mathcal{U}_0(2 + a) - 2] + \mathcal{U}_0\varpi(\varpi^2 - 7)\hat{\zeta}_{\theta,0}$$

$$+ \frac{\mathcal{U}_0}{2}\hat{\zeta}(11 + 7\varpi^2 + 4\varpi^4) - 2\mathcal{N}\}\partial_{\Theta}^3\zeta''_{z,1}(0)$$

$$-\frac{\varpi \mathcal{U}_0^2}{6\hat{\zeta}(1+\varpi^2)^2} \{2[\mathcal{U}_0(7+a)-3] + 2\varpi^2[\mathcal{U}_0(1+a)-1] + \mathcal{U}_0\varpi(\varpi^2-7)\hat{\zeta}_{\theta,0} \\ + \frac{\mathcal{U}_0}{2}\hat{\zeta}(10+5\varpi^2+3\varpi^4) - 2\mathcal{N}\} \partial_{\Theta}^3 \zeta''_{\theta,1}(0)$$

$$-\frac{\mathcal{U}_0^2 \varpi}{12\hat{\zeta}(1+\varpi^2)} \left(\mathcal{U}_0 \{ \partial_{\Theta}^3 [\varpi \zeta'''_{z,1} + \zeta'''_{\theta,1}] (0) + \partial_{\Theta}^4 [\varpi \zeta'''_{z,1} + \zeta'''_{\theta,1}] (0) \Theta \} \right. \\ \left. + \varpi [\mathcal{U}_0 \hat{\zeta}(1+\varpi^2) + 4(\mathcal{U}_0-1)] \partial_{\Theta}^4 \zeta''_{z,1}(0) \Theta \right),$$

$$g_{d,1,0} = 2km \frac{S_c}{r_c} + (\mu+1) \frac{\mathcal{U}_0 \alpha_{d,1,\Theta}}{\hat{\zeta}(1+\varpi^2)} + \mathcal{M}_a \frac{\beta_{d,1,\Theta}}{1+\varpi^2},$$

$$g_{ad,1,0} = (\mu+1) \frac{\mathcal{U}_0 \alpha_{ad,1,\Theta}}{\hat{\zeta}(1+\varpi^2)} + \mathcal{M}_a \frac{\beta_{ad,1,\Theta}}{1+\varpi^2},$$

$$d_{j,1,0} = -(\mu+1) \frac{\mathcal{U}_0 \gamma_{j,1,\Theta}}{\hat{\zeta}(1+\varpi^2)} - \mathcal{M}_a \frac{\kappa_{j,1,\Theta}}{1+\varpi^2}, \quad j = d, ad, \quad d_{\omega d,1,0} = 2km \frac{S_c}{r_c},$$

where we recall $\mu = \hat{\zeta}(1+2\varpi^2) + \varpi \hat{\zeta}_{\theta,0} - 1$, $\mathcal{N} = \mathcal{U}_0 / \hat{\zeta} [2\varpi \hat{\zeta}_{\theta,0}(1 - \varpi \hat{\zeta}_{\theta,0}) + \zeta'(1+\varpi^2)]$ and

$$\mathcal{M}_a = \mathcal{U}_0 [5 + 7\varpi^2 + \hat{\zeta}_{\theta,0} \varpi(1 - 3\varpi^2) + \hat{\zeta}(1 + 3\varpi^2)] - 2\varpi^2 \mathcal{N},$$

$$\mathcal{M}_b = \mathcal{U}_0 \left(2[\mathcal{U}_0(109+5a)-70] - 5\mathcal{U}_0\varpi(1+\varpi^2)(9+\varpi^2)\hat{\zeta}_{\theta,0} + 2\varpi^2[2\mathcal{U}_0(57+5a)-65] \right. \\ \left. + 10\varpi^4[\mathcal{U}_0(9+a)-7] \right) \hat{\zeta} + 5\mathcal{U}_0^2 \hat{\zeta}^2(1+\varpi^2)(7+5\varpi^2+2\varpi^4) + 40(1-\mathcal{U}_0)\mathcal{N} \\ + 5 \left(2\{2\mathcal{U}_0^2(17+2a) - \mathcal{U}_0(47+3a) + 16 + 2\mathcal{U}_0\varpi[7-9\mathcal{U}_0-\varpi^2(1+\mathcal{U}_0)]\hat{\zeta}_{\theta,0} + 2\mathcal{U}_0^2\varpi^2(1+\varpi^2)\hat{\zeta}_{\theta,0}^2\} \right. \\ \left. + \varpi^2[8-3\mathcal{U}_0(5+a) + 2\mathcal{U}_0^2(5+2a)] \right) - \mathcal{U}_0^2 \zeta'(1+\varpi^2)^2),$$

$$\mathcal{M}_c = -5\{\mathcal{U}_0(19+2a) - 10 + \varpi^2[\mathcal{U}_0(7+2a) - 6] - 8\varpi\mathcal{U}_0\hat{\zeta}_{\theta,0}\} - 2\mathcal{U}_0\hat{\zeta}(16+11\varpi^2+5\varpi^4) + 10\mathcal{N},$$

$$\mathcal{M}_d = -5\{\mathcal{U}_0(17+2a) - 8 + \varpi^2[\mathcal{U}_0(5+2a) - 4] - 8\varpi\mathcal{U}_0\hat{\zeta}_{\theta,0}\} - 2\mathcal{U}_0\hat{\zeta}(15+9\varpi^2+4\varpi^4) + 10\mathcal{N}.$$

B. Inner flow equations

The system (2.1) after the change of variables of Section 4 is turned into the following inner momentum equations

$$-\frac{\epsilon^{-\frac{1}{2}}}{1+s_i H_\rho} \left[\frac{\mathcal{P}}{m^2} + \frac{1}{2} s_i U^2 \right]_\rho + s_i \left(\tilde{\mathcal{U}} - \frac{V}{1+\epsilon^{\frac{1}{2}}\mathcal{R}} - \varpi \tilde{\omega} W \right) \left(U_X - \frac{s_i H_X U_\rho}{1+s_i H_\rho} \right) \\ + \left(\mathcal{C}_o + \frac{V}{1+\epsilon^{\frac{1}{2}}\mathcal{R}} \right) \frac{V}{m^2} - s_i \left(U_\Theta - \frac{s_i H_\Theta U_\rho}{1+s_i H_\rho} \right) \frac{V}{1+\epsilon^{\frac{1}{2}}\mathcal{R}} \\ - \epsilon^{\frac{1}{2}} s_i \varpi W \left(U_\Phi - \frac{s_i H_\Phi U_\rho}{1+s_i H_\rho} \right) - \epsilon s_i \left(U_{\tau_2} - \frac{s_i H_{\tau_2} U_\rho}{1+s_i H_\rho} \right) = \frac{\lambda' \epsilon^{\frac{1}{2}} A}{1+s_i H_\rho} \left\{ \left[\frac{U_\rho}{1+s_i H_\rho} \right]_\rho + \frac{s_i \epsilon^{\frac{1}{2}} U_\rho}{1+\epsilon^{\frac{1}{2}}\mathcal{R}} \right\}, \quad (\text{B1})$$

$$\begin{aligned}
& -\frac{s_i \epsilon^{-\frac{1}{2}} V_\rho}{1+s_i H_\rho} U + s_i \left(\tilde{U} - \frac{V}{1+\epsilon^{\frac{1}{2}} \mathcal{R}} - \varpi \tilde{\omega} W \right) \left(V_X - \frac{s_i H_X V_\rho}{1+s_i H_\rho} \right) - s_i \epsilon^{\frac{1}{2}} \varpi W \left(V_\Phi - \frac{s_i H_\Phi V_\rho}{1+s_i H_\rho} \right) \\
& - \frac{1}{1+\epsilon^{\frac{1}{2}} \mathcal{R}} \left(\mathcal{P}_\Theta + \mathcal{P}_X - \frac{s_i (H_\Theta + H_X) \mathcal{P}_\rho}{1+s_i H_\rho} \right) - s_i \left(s_i U + V_\Theta - \frac{s_i H_\Theta V_\rho}{1+s_i H_\rho} \right) \frac{V}{1+\epsilon^{\frac{1}{2}} \mathcal{R}} - \mathcal{C}_o U \\
& - s_i \epsilon \left(V_{\tau_2} - \frac{s_i H_{\tau_2} V_\rho}{1+s_i H_\rho} \right) = \frac{\lambda' \epsilon^{\frac{1}{2}} A}{1+s_i H_\rho} \left\{ \left[\frac{V_\rho}{1+s_i H_\rho} \right]_\rho + \frac{s_i \epsilon^{\frac{1}{2}} V_\rho}{1+\epsilon^{\frac{1}{2}} \mathcal{R}} \right\} - \lambda' \epsilon^{\frac{3}{2}} \mathcal{Q}'_0(r), \quad (\text{B2})
\end{aligned}$$

$$\begin{aligned}
& -\frac{s_i \epsilon^{-\frac{1}{2}} W_\rho}{1+s_i H_\rho} U + s_i \left(\tilde{U} - \frac{V}{1+\epsilon^{\frac{1}{2}} \mathcal{R}} - \varpi \tilde{\omega} W \right) \left(W_X - \frac{s_i H_X W_\rho}{1+s_i H_\rho} \right) \\
& - \frac{\tilde{\omega}}{\varpi} \left(\mathcal{P}_X - \frac{s_i H_X \mathcal{P}_\rho}{1+s_i H_\rho} \right) - \frac{s_i}{\varpi} \epsilon^{\frac{1}{2}} \left(\mathcal{P}_\Phi - \frac{s_i H_\Phi \mathcal{P}_\rho}{1+s_i H_\rho} \right) - s_i \left(W_\Theta - \frac{s_i H_\Theta W_\rho}{1+s_i H_\rho} \right) \frac{V}{1+\epsilon^{\frac{1}{2}} \mathcal{R}} \\
& - s_i \epsilon^{\frac{1}{2}} \varpi W \left(W_\Phi - \frac{s_i H_\Phi W_\rho}{1+s_i H_\rho} \right) - s_i \epsilon \left(W_{\tau_2} - \frac{s_i H_{\tau_2} W_\rho}{1+s_i H_\rho} \right) = \frac{\lambda' \epsilon^{\frac{1}{2}} A}{1+s_i H_\rho} \left\{ \left[\frac{W_\rho}{1+s_i H_\rho} \right]_\rho + \frac{s_i \epsilon^{\frac{1}{2}} W_\rho}{1+\epsilon^{\frac{1}{2}} \mathcal{R}} \right\}, \quad (\text{B3})
\end{aligned}$$

where $\tilde{\omega} = \tilde{k} r_c / m$.

The divergenceless condition stands for

$$\begin{aligned}
& \frac{\epsilon^{-\frac{1}{2}} U_\rho}{1+s_i H_\rho} + \left(s_i U + V_\Theta + V_X - \frac{s_i (H_\Theta + H_X) V_\rho}{1+s_i H_\rho} \right) \frac{1}{1+\epsilon^{\frac{1}{2}} \mathcal{R}} \\
& + \varpi \epsilon^{\frac{1}{2}} \left(W_\Phi - \frac{s_i H_\Phi W_\rho}{1+s_i H_\rho} \right) + \varpi \tilde{\omega} \left(W_X - \frac{s_i H_X W_\rho}{1+s_i H_\rho} \right) = 0. \quad (\text{B4})
\end{aligned}$$

For simplicity sake, only the leading-order terms in the viscous diffusions are mentioned.

C. Particular CL velocities

The long functions of integration obtained by CL edge matching are listed in this Section.

$$\begin{aligned}
V_{5,sp}(X) &= \partial_\Theta \left[\left(\mu \beta_{l,1} - \alpha_{l,1} + \varpi \hat{\zeta}_{\theta,1} + (1 - \varpi \hat{\zeta}_{\theta,0}) \frac{\hat{\zeta}_{z,1}}{\hat{\zeta}} - \frac{\mathcal{U}_0^2 \varpi (\Xi + 2)}{6 \hat{\zeta} (1 + \varpi^2)} \partial_\Theta^2 [\varpi \zeta''_{z,1} + \zeta''_{\theta,1}] (0) \right) A \right. \\
& \quad \left. + (\mu \beta_{d,1} - \alpha_{d,1}) A_\Phi + (\mu \beta_{ad,1} - \alpha_{ad,1}) a_\Phi A \right] \frac{\Theta \cos X}{1 + \varpi^2} \\
& - \partial_\Theta \left[\left(\mu \kappa_{l,1} - \gamma_{l,1} - \frac{\mathcal{U}_0}{2} \varpi \zeta'_{\theta,1,\Theta} (0) + \frac{\mathcal{U}_0}{\hat{\zeta}} \left(\frac{\hat{\zeta}}{2} \varpi^2 + \varpi \hat{\zeta}_{\theta,0} - 1 \right) \zeta'_{z,1,\Theta} (0) \right. \right. \\
& \quad \left. \left. + \frac{\mathcal{U}_0^2 \varpi (\Xi + 2)}{24 \hat{\zeta} (1 + \varpi^2)} \partial_\Theta^3 \left(\mathcal{U}_0 [\varpi \zeta'''_{z,1} + \zeta'''_{\theta,1}] + [\mathcal{U}_0 \hat{\zeta} (1 + \varpi^2) + 4(\mathcal{U}_0 - 1)] \varpi \zeta''_{z,1} \right) (0) \right) A \right. \\
& \quad \left. + (\mu \kappa_{d,1} - \gamma_{d,1}) A_\Phi + (\mu \kappa_{ad,1} - \gamma_{ad,1}) a_\Phi A \right] \frac{\Theta \sin X}{1 + \varpi^2}, \quad (\text{C1})
\end{aligned}$$

$$\begin{aligned}
W_{5,sp}(X) = & \partial_{\Theta} \left[\left(\chi\beta_{l,1} - \alpha_{l,1} + \left(1 + \frac{\hat{\zeta}_{\theta,0}}{\varpi}\right) \frac{\hat{\zeta}_{z,1}}{\hat{\zeta}} - \frac{\hat{\zeta}_{\theta,1}}{\varpi} + \frac{\mathcal{U}_0^2(\Xi - 2\varpi^2)}{6\hat{\zeta}\varpi(1 + \varpi^2)} \partial_{\Theta}^2 [\varpi\zeta''_{z,1} + \zeta''_{\theta,1}](0) \right) A \right. \\
& \left. + (\chi\beta_{d,1} - \alpha_{d,1})A_{\Phi} + (\chi\beta_{ad,1} - \alpha_{ad,1})a_{\Phi}A \right] \frac{\Theta \cos X}{1 + \varpi^2} \\
& - \partial_{\Theta} \left[\left(\chi\kappa_{l,1} - \gamma_{l,1} - \frac{\mathcal{U}_0}{\hat{\zeta}} \left(\frac{\hat{\zeta}_{\theta,0}}{\varpi} + \frac{\hat{\zeta}}{2} + 1 \right) \zeta'_{z,1,\Theta}(0) + \frac{\mathcal{U}_0}{2\varpi} \zeta'_{\theta,1,\Theta}(0) \right. \right. \\
& \left. \left. - \frac{\mathcal{U}_0^2(\Xi - 2\varpi^2)}{24\hat{\zeta}\varpi(1 + \varpi^2)} \partial_{\Theta}^3 \left(\mathcal{U}_0[\varpi\zeta'''_{z,1} + \zeta'''_{\theta,1}] + \varpi[\mathcal{U}_0\hat{\zeta}(1 + \varpi^2) + 4(\mathcal{U}_0 - 1)]\zeta''_{z,1} \right)(0) \right) A \right. \\
& \left. + (\chi\kappa_{d,1} - \gamma_{d,1})A_{\Phi} + (\chi\kappa_{ad,1} - \gamma_{ad,1})a_{\Phi}A \right] \frac{\Theta \sin X}{1 + \varpi^2}, \quad (\text{C2})
\end{aligned}$$

where $\mu = \hat{\zeta}(1 + 2\varpi^2) + \varpi\hat{\zeta}_{\theta,0} - 1$, and $\chi = \hat{\zeta}\varpi^2 - \varpi^{-1}\hat{\zeta}_{\theta,0} - 1$.

D. New parametrization of the streamlines

The meeting points MP of the separatrices and the centre points CP (the core of the cat's eye) are located on specific isophases: spiraling helices. The velocity at these points must then satisfy certain relationships. The velocity field is expressed through the strained coordinate \tilde{Z} so that the latter may be satisfied, for the velocity defined with the independent variable Z does not generally satisfy them. The variable Z is thus expanded as follows

$$Z = \tilde{Z} + \epsilon^{\frac{1}{2}} \ln \epsilon \varphi^{(1)}(\tilde{Z}, x) + \epsilon^{\frac{1}{2}} \varphi^{(2)}(\tilde{Z}, x) + \epsilon \ln^2 \epsilon \varphi^{(3)}(\tilde{Z}, x) + \dots \quad (\text{D1})$$

The deformation functions $\varphi^{(i)}$ describe how high the streamlines are deformed inside the CL. A new radius $\tilde{\rho}$ can be then defined by analogy such as $\tilde{Z} = 1/2\tilde{\rho}^2 + A \cos x$. In the distorted frame $(\tilde{\rho}, x)$, the MPs are defined by $\tilde{\rho} = 0$ and $x = 0 [2\pi]$ ($\tilde{Z} = A$). From the expression of the height z , we deduce the first relationship after time-derivating

$$z = \frac{\xi - m\theta + \omega t}{k}, \quad w = \frac{\tilde{\omega} + m/r_c \overline{W}_c \omega_{\Phi} T_1}{k} - \frac{m}{k} \dot{\theta}.$$

The angular time-derivative $\dot{\theta}$ is linked to the azimuthal velocity at MP in this way $v(MP) = r(MP) \dot{\theta}$. So, the axial and azimuthal velocities are constrained at MP by the following relationship

$$w(MP) = -\frac{m}{k} \left(\frac{v(MP)}{r(MP)} - \frac{\hat{\omega}}{m} \right).$$

In the referential moving with the vertical speed $\hat{\omega}/k$, the relative vertical velocity is proportional to the rotational velocity. At CP defined by $\tilde{\rho} = 0$ and $x = \pi [2\pi]$ ($\tilde{Z} = -A$), both velocities satisfy the same relationship that is written with the inner rescaled variables

$$\varpi^2 \tilde{W} - \hat{\mathcal{U}} + \frac{\tilde{V}}{1 + \epsilon^{\frac{1}{2}}(s_i \rho + H)} = 0, \quad \text{with} \quad \hat{\mathcal{U}} = \tilde{\mathcal{U}} + \varpi \mathcal{W} \mathcal{U}_{\Phi} \tau_1. \quad (\text{D2})$$

The deformation functions calculated from (D2) are defined by

$$\begin{aligned}
\varphi^{(1)}(\tilde{Z}, x) &= \varphi^{(1,\odot)}(\tilde{Z}, x) = \frac{s_i}{2} \hat{\zeta}(1 + \varpi^2) A \tilde{\rho} \cos x, \\
\varphi^{(2)}(\tilde{Z}, x) &= s_i \tilde{\rho} \left(V^{(2)}(MP) + \varpi^2 W^{(2)}(MP) - \hat{\mathcal{U}}_2 \right), \\
\varphi^{(2,\odot)}(\tilde{Z}, x) &= s_i \tilde{\rho} \left(V^{(2,\odot)}(\tilde{Z}, x_0) + \varpi^2 W^{(2,\odot)}(\tilde{Z}, x_0) - \hat{\mathcal{U}}_2 \right),
\end{aligned}$$

where the phase $x_0 = \arccos[\tilde{Z}^*]$ is the intersection of the \tilde{Z} -streamline with the new CL axis $\tilde{\rho} = 0$. The continuity of Z at either side of the separatrix implies $\varphi^{(2,\odot)}(A) = \varphi^{(2)}(A)$; this gives the condition

$$V^{(2,\odot)}(MP) + \varpi^2 W^{(2,\odot)}(MP) = V^{(2)}(MP) + \varpi^2 W^{(2)}(MP).$$

This condition is easily satisfied thanks to the matching conditions (6.50) and (6.51).

E. Prandtl-Batchelor extended theorem

Batchelor (1956) found a closure equation enabling him to determine the steady motion in a unique way within a two-dimensional and closed domain: he proved that the vorticity was a constant. That procedure has to be here adapted to the three-dimensionality of the flow. The momentum equations are in the frame moving with the angular rotation $\Omega_c = \Omega_{c,0} + \epsilon^{1/2}\Omega_{c,1}$

$$\partial_t \mathbf{u} + \epsilon^{\frac{3}{2}} \partial_{T_2} \Omega_{1,c} \times \mathbf{r} + \mathbf{Q} \times \mathbf{u} + \nabla H = \frac{1}{Re} \Delta \mathbf{u} + \mathbf{F}, \quad (\text{E1})$$

with the absolute vorticity $\mathbf{Q} = \nabla \times \mathbf{u} + (\varrho_{0,c} + \epsilon^{1/2}\varrho_{1,c}) \mathbf{e}_z$ and $H = P + 1/2|\mathbf{u}|^2 - (\varrho_{0,c} + \epsilon^{1/2}\varrho_{1,c})^2 r^2/8$. The air particles have coupled helical and spiral motions in the CL neighborhood but inside the cat's eye, their trajectory is trapped since they cannot cross the surface $\tilde{Z} = Cst$ (cf. figures 6-9 and Appendix D). The sheet $\tilde{Z} = Cst$ is an envelope of the air particle trajectories, has a funnel-like shape centered around the axis of the vortex (see figure 3). Decomposing the motion into inviscid and viscous components, a curvilinear integral is therefore performed over a line \mathbf{l} , intersection of the sheet $\tilde{Z} = Cst$ and, either the plane $z = cst$ in which case θ varies over a bounded range smaller than $2\pi/m$, or the plane $\theta = cst$ in which case z varies over a range smaller than $2\pi/k$. We then obtain two integral conditions on the cat's eye viscous flow.

$$\oint [\mathbf{Q}_i \times \mathbf{u}_v] \cdot d\mathbf{l} + \oint [\mathbf{Q}_v \times \mathbf{u}_i] \cdot d\mathbf{l} + \epsilon^{\frac{3}{2}} \oint [\nabla \times \mathbf{Q}_i + \Delta_r \bar{V}_0 \mathbf{e}_\theta] \cdot d\mathbf{l} = - \oint \partial_t \mathbf{u}_v \cdot d\mathbf{l}. \quad (\text{E2})$$

Both first integrands do not vanish like in Batchelor (1956) because \mathbf{l} is not tangent to a streamline.

E1. Condition (E2) in a horizontal plane

The axial-vorticity solution (6.34) is assumed inside the cat's eye and one integrates at constant z over θ on a \tilde{Z} -contour bounded by $x = x_0$ and $2\pi - x_0$, (E2) then becomes

$$\int_{x_0/m}^{2\pi/m - x_0/m} \psi_{i,\rho\rho\rho}^{(2,\odot)+}(\tilde{Z}, m\theta) - \psi_{i,\rho\rho\rho}^{(2,\odot)-}(\tilde{Z}, m\theta) d\theta = 0,$$

After the symmetry properties of the Sine Fourier series in (6.34), the above integral is greatly simplified and we obtain

$$\mathcal{F}_2^{\odot'}(Z) = 0. \quad (\text{E3})$$

E2. Condition (E2) in a vertical plane

The axial-velocity solution (6.42) is assumed and one integrates this time at constant θ over z on a \tilde{Z} -contour, (E2) thus becomes

$$\int_{x_0/k}^{2\pi/k - x_0/k} W_{i,\rho\rho}^{(2,\odot)+}(\tilde{Z}, kz) - W_{i,\rho\rho}^{(2,\odot)-}(\tilde{Z}, kz) dz = 0,$$

we get the same condition (E3).

F. Streamlines

This section gives the radius of the parameterized CL streamline representation. In the frame moving with the linear wave vertical speed $\hat{\omega}/k$, the streamlines obey the following differential equations

$$\frac{dr}{u} = r \frac{d\theta}{v} = \frac{dz}{w - \frac{\hat{\omega}}{k}}. \quad (\text{F1})$$

The streamline geometry is here more complex than in the steady mode/vortex interaction case. The streamline radius r_{st} becomes a function of ξ and Θ since the streamlines are generated by the coupling of the wave induced oscillatory motion and the mean flow induced spiraling motion. The first equality in (F1) yields

$$v \left[\left(k \frac{dz}{d\theta} + m \right) \partial_\xi + m \partial_\Theta \right] r_{st} = u r_{st}. \quad (\text{F2})$$

Introducing $dz/d\theta$ from the second equality in (F1), the streamline radius r_{st} is given by the integration of the equation

$$[k r_{st} (w - \hat{\omega}/k) + m v] \partial_\xi r_{st} + m v \partial_\Theta r_{st} = u r_{st}, \quad (\text{F3})$$

while the streamline height z_{st} is given by

$$[k r_{st} (w - \hat{\omega}/k) + m v] \partial_\xi z_{st} + m v \partial_\Theta z_{st} = (w - \hat{\omega}/k) r_{st}. \quad (\text{F4})$$

The rescaled inner radius \mathcal{R}_{st} is expanded in this way

$$\mathcal{R}_{st} = \mathcal{R}_{st,0} + \epsilon^{\frac{1}{2}} \ln \epsilon \mathcal{R}_{st,1} + \epsilon^{\frac{1}{2}} \mathcal{R}_{st,2} + \dots$$

The zeroth-order equation of (F3) is $\mathcal{R}_{st,0} \mathcal{R}_{st,0,x} - s_i \hat{\mathcal{U}}_0 \partial_\Theta \mathcal{R}_{st,2} = A \sin x - \mathcal{U}_2$,

$$\text{whose solution is } \mathcal{R}_{st,0} = \mathcal{R}_{st,0}^\odot = s s_i \sqrt{2(Z_{st} - A \cos x)}, \quad (\text{F5})$$

in which the integration constant Z_{st} uniquely defines each streamline. The \mathcal{U}_2 induced spiraling motion appears in the Θ variation of $\mathcal{R}_{st,2}$ which is integrated straightforwardly. We obtain again the expression (6.7): $\mathcal{R}_{st,2,sp} = s_i H_2(\Theta)$.

The first-order solution of (F3) is $\mathcal{R}_{st,1} = \mathcal{R}_{st,1}^\odot = \frac{s_i}{2} \hat{\zeta} (1 + \varpi^2) A \cos x$.

The second-order equation of (F3) is

$$\begin{aligned} [\mathcal{R}_{st,0} \mathcal{R}_{st,os,2}]_x - s_i \hat{\mathcal{U}}_0 \partial_\Theta \mathcal{R}_{st,5} &= s_i [V^{(2)} + \varpi^2 W^{(2)} - \hat{\mathcal{U}}_2] \mathcal{R}_{st,0,x} \\ &+ s_i (A \mathcal{R}_{0,st} \sin x - U^{(2)}) + (\mathcal{V}_1 - s_i \mathcal{R}_{st,0}) \frac{\mathcal{U}_2}{\hat{\mathcal{U}}_0}. \end{aligned} \quad (\text{F6})$$

The terms in (F6) yielding a non-zero x -average at constant Z_{st} are eliminated. They generate the spiraling motion of $\mathcal{R}_{st,5}$. The solution $\mathcal{R}_{st,2,os}$ is hence

$$\begin{aligned} \mathcal{R}_{st,2,os} &= s_i \left\{ \frac{1}{3} \mathcal{R}_{st,0}^2(Z_{st}, x) - \hat{\mathcal{U}}_2 + \mathcal{R}_{st,0}^{-1}(Z_{st}, x) \left[A \int_0^x \frac{V^{(2)}(Z_{st}, u)}{\mathcal{R}_{st,0}(Z_{st}, u)} \sin u \, du \right. \right. \\ &+ \varpi^2 A \int_0^x \frac{W^{(2)}(Z_{st}, u)}{\mathcal{R}_{st,0}(Z_{st}, u)} \sin u \, du - \int_0^x U^{(2)}(Z_{st}, u) - \mathcal{U}'_2 \mathcal{R}_{st,0}(Z_{st}, u) - s_i \mathcal{U}_3 \, du \\ &\left. \left. + (\mathcal{U}'_2 + \frac{\mathcal{U}_2}{\hat{\mathcal{U}}_0}) \int_0^x \langle \mathcal{R}_{st,0}(Z_{st}) \rangle - \mathcal{R}_{st,0}(Z_{st}, u) \, du + C(Z_{st}) \right] \right\}. \end{aligned}$$

The spiraling fifth-order motion is given by

$$\mathcal{U}_0 \partial_\Theta \mathcal{R}_{st,5} = \mathcal{U}_0 \partial_\Theta \mathcal{R}_{st,5}^\circ = s_i (\mathcal{U}_3 - \frac{\mathcal{V}_1}{\mathcal{U}_0} \mathcal{U}_2) + (\mathcal{U}'_2 + \frac{\mathcal{U}_2}{\mathcal{U}_0}) \langle \mathcal{R}_{st,0} \rangle. \quad (\text{F7})$$

The integration constant $C(Z_{st})$ is chosen so that the singularity at the meeting point of the separatrices ($Z_{st} = A$, $x = 0 [2\pi]$) may vanish. After passing to the stressed variable \tilde{Z}_{st} , we get simpler expressions

$$\tilde{\mathcal{R}}_{st,0} = \mathcal{R}_{st,0}(\tilde{Z}_{st}, x), \quad \tilde{\mathcal{R}}_{st,1} = \tilde{\mathcal{R}}_{st,1}^\circ = 0,$$

$$\begin{aligned} \tilde{\mathcal{R}}_{st,2,os}^s(x) = & s_i \left\{ \frac{1}{6} (1 + 2\zeta \varpi^2) \tilde{\mathcal{R}}_{st,0}^2 + s_i [(\kappa_{l,1} + g_{l,1,0})A + (\kappa_{d,1} + g_{d,1,0})A_\Phi \right. \\ & + (\kappa_{ad,1} + g_{ad,1,0})a_\Phi A] \frac{\sin x}{\tilde{\mathcal{R}}_{st,0}} + \frac{s_i}{2} [\beta_{l,1} + d_{l,1,0} + (\beta_{d,1} + d_{d,1,0}) \frac{A_\Phi}{A} \\ & + (\beta_{ad,1} + d_{ad,1,0})a_\Phi] \tilde{\mathcal{R}}_{st,0} + \kappa_{h,1} \frac{A \sin(2x)}{2 \tilde{\mathcal{R}}_{st,0}} + \frac{s_i}{2} [s\hat{\zeta}(1 + \varpi^2)(2\tilde{Z}_{st})^{1/2} - \mathcal{S}_1] \tilde{\mathcal{R}}_{st,0} \\ & - \zeta \varpi^2 (\tilde{Z}_{st} - A) + (1 + \varpi^2) \left[\hat{\zeta} \{ \cos x \ln[A(\tilde{Z}_{st}, x)] - \ln(A^{\frac{1}{2}}) \} A + V_2(x) - V_2(0) \right. \\ & + \frac{s_i}{2} \hat{\mathcal{Q}}_{z,1}^s \tilde{\mathcal{R}}_{st,0} + s s_i \hat{\zeta} \left(\int_0^\infty K_0 [\frac{1}{2} u^2 + 1] du - \int_{\tilde{\mathcal{R}}_{st,0}^*}^\infty K_0 [\frac{1}{2} u^2 + \cos x] du \right) A + N_1(\tilde{Z}_{st}^*, x) \mathcal{U}_2 \\ & + \frac{1}{2} [2 - \ln(Z^*)] \Sigma_q^+ A \frac{\sin x}{|\tilde{\mathcal{R}}_{st,0}|} + \left(\frac{\Sigma_q^+}{\mathcal{U}_2} A^{\frac{1}{2}} N_2(\tilde{Z}_{st}^*, x) - N_3(\tilde{Z}_{st}^*, x) \right) \frac{A^{\frac{1}{2}} \mathcal{U}_2}{|\tilde{\mathcal{R}}_{st,0}|} \left. \right] \\ & \left. + \int_\pi^x \langle |\tilde{\mathcal{R}}_{st,0}(\tilde{Z}_{st})| \rangle - |\tilde{\mathcal{R}}_{st,0}(\tilde{Z}_{st}, x_1)| dx_1 \frac{(\mathcal{U}'_2 + \frac{\mathcal{U}_2}{\mathcal{U}_0})}{|\tilde{\mathcal{R}}_{st,0}|} \right\}, \quad (\text{F8}) \end{aligned}$$

$$\text{where } N_1(Z, x) = \int_\infty^Z \Xi(z) \frac{\int_\pi^x G_5(z, x_1) dx_1}{[2(z - \cos x)]^{\frac{1}{2}}} dz,$$

$$N_2(Z, x) = \int_\infty^Z \sqrt{2z} \int_\pi^x G_5(z, x_1) dx_1 + \frac{\sin x}{2z} dz, \quad N_3(Z, x) = \int_\infty^Z \left(\hat{\zeta} - \frac{\Sigma_q^+}{\mathcal{U}_2} K_0[z] A^{\frac{1}{2}} \right) \int_\pi^x G_5(z, x_1) dx_1 dz,$$

and inside the separatrices

$$\begin{aligned} \tilde{\mathcal{R}}_{st,2,os}^\circ(x) = & s_i \left\{ \frac{1}{6} (1 + 2\zeta \varpi^2) \tilde{\mathcal{R}}_{st,0}^2 + s_i \{ (\kappa_{l,1} + g_{l,1,0})A + (\kappa_{d,1} + g_{d,1,0})A_\Phi \right. \\ & + (\kappa_{ad,1} + g_{ad,1,0})a_\Phi A \}^+ \frac{\sin x}{\tilde{\mathcal{R}}_{st,0}} + \frac{s_i}{2} \{ \beta_{l,1} + d_{l,1,0} + (\beta_{d,1} + d_{d,1,0}) \frac{A_\Phi}{A} \\ & + (\beta_{ad,1} + d_{ad,1,0})a_\Phi - \mathcal{S}_1 \}^+ \tilde{\mathcal{R}}_{st,0} + \{ \kappa_{h,1} \}^+ \frac{A \sin(2x)}{2 \tilde{\mathcal{R}}_{st,0}} \\ & + (1 + \varpi^2) \left[2\Xi(1) \sum_{n=1}^\infty \left(\overline{\tilde{\mathcal{R}}_{st,0}} \int_1^{\overline{\tilde{\mathcal{R}}_{st,0}}} b_n(r) dr - \int_0^{\overline{\tilde{\mathcal{R}}_{st,0}}} b_n(r) r dr \right) \sin(nx) \frac{(1 - \cos x)}{\tilde{\mathcal{R}}_{st,0}} A^{\frac{1}{2}} \mathcal{U}_2 \right. \\ & + \Xi(1) \sum_{n=1}^\infty \int_0^1 b_n(r) dr \sin(nx_0) \sqrt{2(1 - \tilde{Z}_{st}^*)} \mathcal{U}_2 + \frac{Q^{(2,\circ)}}{2} \tilde{\mathcal{R}}_{st,0} + V_2^\circ(x) - V_2^\circ(x_0) \left. \right] \\ & \left. + \int_\pi^x \langle |\tilde{\mathcal{R}}_{st,0}(\tilde{Z}_{st})| \rangle - |\tilde{\mathcal{R}}_{st,0}(\tilde{Z}_{st}, x_1)| dx_1 \frac{(\mathcal{U}'_2 + \frac{\mathcal{U}_2}{\mathcal{U}_0})}{|\tilde{\mathcal{R}}_{st,0}|} \right\}. \quad (\text{F9}) \end{aligned}$$

The radius $\tilde{\mathcal{R}}_{st,2}^\odot = 0$ does vanish on the axis $\tilde{\mathcal{R}}_{st,0} = 0$ as $\tilde{Z}_{st} = A \cos x_0$. The matching of $\tilde{\mathcal{R}}_{st}$ on the separatrices, $\tilde{\mathcal{R}}_{st,2}^\odot(A, x) = \tilde{\mathcal{R}}_{st,2}(A, x)$, is realized thanks to the appropriate values of the deformation functions $\varphi^{(2)}$ and $\varphi^{(2,\odot)}$ (cf. Appendix D). Comparing \mathcal{R} and $\tilde{\mathcal{R}}_{st}$, we deduce that the departure of Z from \tilde{Z}_{st} is $Z = \tilde{Z}_{st} + \mathcal{O}(\epsilon^{1/2})$.

G. The forcings and the related coefficients \mathcal{A}_i and \mathcal{B}_i

The expressions of the various forcings $\Sigma_q^s, \Sigma_{q'}^s$ and Σ_v^s are displayed here

$$\Sigma_q^s = \overline{\int_{\pi}^X \partial_Z G_5(Z_B^*, x_1) dx_1 \Xi(Z_B^*) \sin X \rho_B^* \mathcal{U}_2} - s \Sigma_{q'}^s A^{\frac{1}{2}} \overline{\int_{\pi}^X G_5(Z_B^*, x_1) dx_1 \frac{\sin X}{\text{SE}[Z_B^*]} \rho_B^*} + \frac{s}{2} \Sigma_{q'}^s A^{\frac{1}{2}} \overline{\frac{\sin^2 X}{Z_B^{*2}} \rho_B^*}, \quad (\text{G1})$$

$$\begin{aligned} \Sigma_{q'}^s &= s \overline{\int_{\pi}^X \partial_Z G_5(Z_B^*, x_1) dx_1 \Xi(Z_B^*) \sin X \frac{\mathcal{U}_2}{A^{\frac{1}{2}}}} - \Sigma_{q'}^s \overline{\int_{\pi}^X G_5(Z_B^*, x_1) dx_1 \frac{\sin X}{\text{SE}[Z_B^*]}} \\ &+ s \overline{\int_{\pi}^X \partial_Z^2 G_5(Z_B^*, x_1) dx_1 \Xi(Z_B^*) \sin X \rho_B^{*2} \frac{\mathcal{U}_2}{A^{\frac{1}{2}}}} - 2 \Sigma_{q'}^s \overline{\int_{\pi}^X \partial_Z G_5(Z_B^*, x_1) dx_1 \frac{\sin X}{\text{SE}[Z_B^*]} \rho_B^{*2}} \\ &+ \Sigma_{q'}^s \overline{\int_{\pi}^X G_5(Z_B^*, x_1) dx_1 \frac{\text{SM}[Z_B^*]}{\text{SE}^2[Z_B^*]} \sin X \rho_B^{*2}} + \Sigma_{q'}^s \left(\frac{1}{2} \overline{\frac{\sin^2 X}{Z_B^{*2}}} - \overline{\frac{\sin^2 X}{Z_B^{*3}} \rho_B^{*2}} \right), \quad (\text{G2}) \end{aligned}$$

$$\text{and } \Sigma_v^s = s \overline{\int_{\pi}^X G_5(Z_B^*, x_1) dx_1 \Xi(Z_B^*) \sin X A^{\frac{1}{2}}} - \frac{1}{2} \Sigma_{q'}^s \overline{\frac{\sin^2 X}{Z_B^*}} A. \quad (\text{G3})$$

These expressions involve the following coefficients

$$\begin{aligned} \mathcal{A}_1 &= \overline{\int_{\pi}^X G_5(Z_B^*, x_1) dx_1 \sin X}, & \mathcal{A}_2 &= \overline{\int_{\pi}^X G_5(Z_B^*, x_1) dx_1 \mathcal{K}_0[Z_B^*] \sin X}, \\ \mathcal{A}_3 &= \overline{\int_{\pi}^X \partial_Z G_5(Z_B^*, x_1) dx_1 \sin X \rho_B^*}, & \mathcal{A}_4 &= \overline{\int_{\pi}^X \partial_Z G_5(Z_B^*, x_1) dx_1 \mathcal{K}_0[Z_B^*] \sin X \rho_B^*} \\ &+ \overline{\int_{\pi}^X G_5(Z_B^*, x_1) dx_1 \frac{\sin X}{\text{SE}[Z_B^*]} \rho_B^*}, & \mathcal{A}_5 &= \overline{\int_{\pi}^X \partial_Z^2 G_5(Z_B^*, x_1) dx_1 \sin X}, \\ \mathcal{A}_6 &= \overline{\int_{\pi}^X \partial_Z^2 G_5(Z_B^*, x_1) dx_1 \mathcal{K}_0[Z_B^*] \sin X} - \overline{\int_{\pi}^X G_5(Z_B^*, x_1) dx_1 \frac{\text{SM}[Z_B^*]}{\text{SE}^2[Z_B^*]} \sin X} \\ &+ 2 \overline{\int_{\pi}^X \partial_Z G_5(Z_B^*, x_1) dx_1 \frac{\sin X}{\text{SE}[Z_B^*]}}, & \mathcal{B}_1 &= \frac{1}{2} \overline{\frac{\sin^2 X}{Z_B^*}} = \frac{1}{4} \rho_B^{*2} - \frac{1}{4} \sqrt{\rho_B^{*4} - 4}, \\ \mathcal{B}_2 &= \frac{1}{2} \overline{\frac{\sin^2 X}{Z_B^{*2}} \rho_B^*} = \frac{1}{2} \left(\frac{\rho_B^{*2}}{\sqrt{\rho_B^{*4} - 4}} - 1 \right) \rho_B^*, & \mathcal{B}_3 &= \overline{\frac{\sin^2 X}{Z_B^{*3}}} = \frac{4}{(\rho_B^{*4} - 4)^{\frac{3}{2}}}, \\ \mathbb{B} &= \frac{\mathcal{A}_3 + \rho_B^{*3} \mathcal{A}_5}{(1 + \mathcal{A}_3)[\rho_B^* + \mathcal{A}_4 - \mathcal{B}_2 + \rho_B^{*3}(\mathcal{A}_6 + \mathcal{B}_3)] - (\mathcal{A}_4 - \mathcal{B}_2)(\mathcal{A}_3 + \rho_B^{*3} \mathcal{A}_5)}. \end{aligned}$$

H. Special functions

The functions that we have used in the study are defined here:

- $E[Z]$ is the complete elliptic integral,
- $SE[Z] = \frac{2^{\frac{3}{2}}}{\pi} [Z + 1]^{\frac{1}{2}} E\left[\frac{2}{Z + 1}\right] = \frac{2^{-\frac{1}{2}}}{\pi} \int_0^{2\pi} [Z - \cos x]^{\frac{1}{2}} dx,$
- $SM[Z] = \frac{2^{-\frac{3}{2}}}{\pi} \int_0^{2\pi} [Z - \cos x]^{-\frac{1}{2}} dx,$
- $K_0[Z] = \int_{\infty}^Z \frac{1}{SE[z]} - \frac{1}{\sqrt{2z}} dz,$
- $K_1[Z, x] = 2^{-\frac{1}{2}} \int_{\infty}^Z \frac{1}{\sqrt{z - \cos x}} \left(\frac{1}{SE[z]} - \frac{1}{\sqrt{2z}} \right) dz.$

REFERENCES

- BATCHELOR, G. K. 1956 On steady laminar flow with closed streamlines at large Reynolds number. *J. Fluid Mech.* **1**, 177–190.
- BENNEY, D. J. & BERGERON, R. F. 1969 A new class of nonlinear waves in parallel flows. *Stud. Appl. Math.* **48**, 181–204.
- BENNEY, D. J. & MASLOWE, S. A. 1975 The evolution in space and time of nonlinear waves in parallel shear flows. *Stud. Appl. Math.* **54** (3), 181–205.
- CAILLOL, P. 2012 Multiple vortices induced by a tridimensional critical layer within a rapidly rotating vortex. *IMA J. Applied Maths.* **77** (3), 282–292.
- CAILLOL, P. 2014 A steady nonlinear and singular vortex Rossby wave within a rapidly rotating vortex, Part I: Theory. *Geophys. Astrophys. Fluid Dyn.* **108** (4), 387–436.
- CAILLOL, P. 2015 A steady nonlinear and singular vortex Rossby wave within a rapidly rotating vortex, Part II: Application to geophysical vortices. *Geophys. Astrophys. Fluid Dyn.* **109** (2), 111–144.
- CAILLOL, P. 2017 A singular vortex Rossby wave packet within a rapidly rotating vortex. *Phys. Fluids* **29** (046601), 1–30.
- CAILLOL, P. & GRIMSHAW, R. H. J. 2004 Steady multi-polar planar vortices with nonlinear critical layers. *Geophys. Astrophys. Fluid Dyn.* **98**, 473–506.
- CAILLOL, P. & GRIMSHAW, R. H. J. 2007 Rossby solitary waves in the presence of a critical layer. *Studies in Appl. Maths.* **118**, 313–364.
- CAILLOL, P. & GRIMSHAW, R. H. J. 2008 Rossby Elevation waves in the presence of a critical layer. *Studies in Appl. Maths.* **120**, 35–64.
- CAILLOL, P. & GRIMSHAW, R. H. J. 2012 Internal solitary waves with a weakly stratified critical layer. *Phys. of Fluids* **24** (5), 056602.
- CAILLOL, P. & MASLOWE, S. A. 2007 The small-vorticity nonlinear critical layer for Kelvin modes on a vortex. *Studies in Appl. Maths.* **118**, 221–254.
- CAMPBELL, L. J. 2004 Wave-mean flow interactions in a forced Rossby wave packet critical layer. *Stud. Appl. Math.* **112**, 39–85.
- CHEN, Y., BRUNET, G. & YAU, M. K. 2003 Spiral bands in a simulated hurricane. Part II: Wave activity diagnostics. *J. Atmos. Sci.* **60**, 1239–1256.
- CHEN, Y. & YAU, M. K. 2001 Spiral bands in a simulated hurricane. Part I: Vortex Rossby wave verification. *J. Atmos. Sci.* **58**, 2128–2145.
- CORBOSIERO, K. L., MOLINARI, J. & AIYYER, A. R. 2006 The structure and evolution of Hurricane Elena (1985). Part II: Convective asymmetries and evidence for vortex Rossby waves. *Month. Weather Rev.* **134**, 3073–3091.
- DAVIS, R. E. 1969 On the high Reynolds number flow over a wavy boundary. *J. Fluid Mech.* **36**, 337–346.
- DERZHO, O. & GRIMSHAW, R. 2002 Solitary waves with recirculation zones in axisymmetric rotating flows. *J. Fluid Mech.* **464**, 217–250.

- DIDLAKE, A. C., REASOR, P. D., ROGERS, R. F. & LEE, W. 2018 Dynamics of the transition from spiral rainbands to a secondary eyewall in Hurricane Earl (2010). *J. Atmos. Sci.* p. online.
- EMANUEL, K. A. 1985 An air-sea interaction theory for tropical cyclones. Part I: Steady-state maintenance. *J. Atmos. Sci.* **43**, 585–604.
- GAO, C. & ZHU, P. 2016 Vortex Rossby wave propagation in baroclinic tropical cyclone-like vortices. *Geophys. Res. Lett.* **43** (24), 12578–12589.
- GUINN, T. A. & SCHUBERT, W. H. 1993 Hurricane spiral bands. *J. Atmos. Sci.* **50** (20), 3380–3403.
- HABERMAN, R. 1972 Critical layers in parallel flows. *Stud. Appl. Math.* **51** (2), 139–161.
- HOUZE, R. A., JR, CHEN, S. S., LEE, W., ROGERS, R. F., MOORE, J. A., STOSSMEISTER, G. J., BELL, M. M., CETRONE, J., ZHAO, W. & BRODZIK, S. R. 2006 The hurricane rainband and intensity change experiment: Observations and modeling of Hurricanes Katrina, Ophelia, and Rita. *Bull. Amer. Meteor. Soc.* **87**, 1503–1521.
- HOWARD, L. & GUPTA, A. 1962 On the hydrodynamic and hydromagnetic stability of swirling flows. *J. Fluid Mech.* **14** (3), 463–476.
- JUDT, F. & CHEN, S. S. 2010 Convectively generated potential vorticity in rainbands and formation of the secondary eyewall in Hurricane Rita of 2005. *J. Atmos. Sci.* **129**, 3581–3599.
- KIVSHAR, Y. S. & MALOMED, B. A. 1989 Dynamics of solitons in nearly integrable systems. *Rev. of Mod. Phys.* **61** (4), 763–916.
- LEIBOVICH, S. 1970 Weakly non-linear waves in rotating fluids. *J. Fluid Mech.* **42**, 803–822.
- MALLIER, R. & MASLOWE, S. A. 1999 Weakly nonlinear evolution of a wave packet in a zonal mixing layer. *Stud. Appl. Math.* **102**, 69–85.
- MASLOWE, S. A. 1986 Critical layers in shear flows. *Annu. Rev. Fluid Mech.* **18**, 405–432.
- MOLLER, J. D. & MONTGOMERY, M. T. 1999 Vortex Rossby waves and hurricane intensification in a barotropic model. *J. Atmos. Sci.* **56**, 1674–1687.
- MOLLER, J. D. & MONTGOMERY, M. T. 2000 Tropical cyclone evolution via potential vorticity anomalies in a three-dimensional balance model. *J. Atmos. Sci.* **57**, 3366–3387.
- MONTGOMERY, M. T. & ENAGONIO, J. 1998 Tropical cyclogenesis via convectively forced vortex Rossby waves in a three-dimensional quasigeostrophic model. *J. Atmos. Sci.* **55**, 3176–3206.
- MONTGOMERY, M. T. & KALLENBACH, R. J. 1997 A theory for vortex Rossby-waves and its application to spiral bands and intensity changes in hurricanes. *Q. J. R. Meteorol. Soc.* **123**, 435–465.
- NOLAN, D. S. & FARRELL, B. F. 1999 The intensification of two-dimensional swirling flows by stochastic asymmetric forcing. *J. Atmos. Sci.* **56** (23), 3937–3961.
- QIU, X., TAN, Z. M. & XIAO, Q. 2010 The roles of vortex Rossby waves in hurricane secondary eyewall formation. *Month. Weather Rev.* **138**, 2092–2109.
- REASOR, P. D., EASTIN, M. D. & GAMACHE, J. F. 2009 Rapidly intensifying Hurricane Guillermo (1997). Part I: Low-wavenumber structure and evolution. *Month. Weather Rev.* **137**, 603–631.
- REASOR, P. D., MONTGOMERY, M. T., MARKS, F. D. & GAMACHE, J. F. 2000 Low-wavenumber structure and evolution of the hurricane inner core observed by airborne dual-Doppler radar. *Month. Weather Rev.* **128** (6), 1653–1680.
- RUAN, K., ZHA, Y. & HUANG, H. 2014 Contribution of vortex Rossby wave to spiral rainband formation in tropical cyclones. *J. of Hydro.* **26** (5), 725–733.
- SHAGALOV, S. V., REUTOV, V. P. & RYBUSHKINA, G. V. 2009 The asymptotic theory of the generation of long-wave structures in critical layers of weakly dissipative jet flows. *Izvest. Atm. and Ocean Phys.* **45**, 629–645.
- VELASCO FUENTES, O. U. 2005 Vortex filamentation: its onset and its role on axisymmetrization and merger. *Dyn. of Atmos. and Oceans* **40**, 23–42.
- VORONOVICH, V. V., PELINOVSKY, D. E. & SHRIRA, V. I. 1998a On internal wave-shear flow resonance in shallow water. *J. Fluid Mech.* **354**, 209–237.
- VORONOVICH, V. V., SHRIRA, V. I. & STEPANYANTS, Y. A. 1998b Two-dimensional models for nonlinear vorticity waves in shear flows. *Stud. Appl. Math.* **100**, 1–32.

- WANG, L., KOBLINSKY, C., HOWDEN, S. & BECKLEY, B. 1998 Large-scale Rossby wave in the mid-latitude South Pacific from altimetry data. *Geophys. Res. Lett.* **25** (2), 179–182.
- WANG, T., ZHONG, Z. & WANG, J. 2018 Vortex Rossby waves in asymmetric basic flow of typhoons. *Adv. in Atmos. Sci.* **35**, 531–539.
- WANG, Y. 2002*a* Vortex Rossby waves in a numerically simulated tropical cyclone. Part I: Overall structure, potential vorticity, and kinetic energy budgets. *J. Atmos. Sci.* **59**, 1213–1238.
- WANG, Y. 2002*b* Vortex Rossby waves in a numerically simulated tropical cyclone. Part II: The role in tropical cyclone structure and intensity changes. *J. Atmos. Sci.* **59**, 1239–1262.
- ZHANG, J. A., ROGERS, R. F., NOLAN, D. S. & MARKS JR., F. D. 2011 On the characteristic height scales of the hurricane boundary layer. *Month. Weather Rev.* **139**, 2523–2535.